Correlation between the Mechanical Properties and the Structure of the Equine Osteochondral Interface During Maturation

Technische Universiteit Delft

Emma Boersma
MSc Thesis Biomedical Engineering
Delft University of Technology
March 2022

TU Delft
Delft University of Technology

Erasmus MC
Universitair Medisch Centrum Rotterdam

Correlation between the Mechanical Properties and the Structure of the Equine Osteochondral Interface During Maturation

by

Emma Boersma

A thesis submitted to the Delft University of Technology in partial fulfillment of the requiremenst for the degree of

Master of Science
in Biomedical Engineering

March, 2022

Student number:	4331575	
Supervisors:	Prof. dr. G.J.V.M. van Osch,	Erasmus MC & TU Delft
	dr. M.J.Mirzaali,	TU Delft
Thesis Committee:	Prof. dr. G.J.V.M. van Osch,	Erasmus MC & TU Delft
	dr. M.J.Mirzaali,	TU Delft
	dr. A.C. Akyildiz,	Erasmus MC & TU Delft
	Additional expert members:	
	Prof. Dr. K. S. Stok,	University of Melbourne
	M. Cruz Saldivar,	TU Delft

ABSTRACT

The osteochondral interface is known to smoothly mitigate the stress concentration over the surface area of the subchondral bone, with a structural transition from the cartilage to bone. These sites in the body are exposed to high forces, which makes them prone to failure. To improve the repair strategies, a better understanding of the mechanical property-structure relationship of osteochondral interface is crucial. The aim of this study was to observe the structure and map the stiffness of the equine osteochondral interface during maturation and detect a possible mechanical property-structure relationship.
Osteochondral samples from the metacarpo- and metatarsophalangeal joint of 9 days, 12 days, 7 weeks, 13 months old and three mature horses were investigated in this study. Histology was performed to observe the structure. The local elastic modulus was determined using nanoindentation and the strain distribution with compression tests combined with digital image correlation (DIC).
The cartilage thickness decreased with age and an emerging tidemark was detected in the 13 months old joint, indicating calcification of the cartilage starts at this age. The local elastic modulus showed a clear transitional region between low and high values for the mature interface, indicating the articular cartilage and subchondral bone region was indented, respectively. For the immature samples, a less clear transition was found and in the 9 days and 12 days old interface the entire matrix consisted of low elastic modulus values. The strain distribution from the compression tests over the interface confirmed the decreasing cartilage thickness with age. The transition location from high to low strain decreased with age.
The mechanical transition from cartilage to bone showed significant changes within the interface and during maturation for the local elastic modulus and the strain distribution. These changes can be compared to the structural changes demonstrated in the histology images. The data obtained in this research provides new insights into the maturing osteochondral interface and the mechanical and structural changes within this complex biological tissue.

Keywords: Osteochondral Interface; Maturation; Nanoindentation; Digital Image Correlation; Elastic Modulus.

ACKNOWLEDGEMENTS

With this thesis, I am finalizing my master's degree in Biomedical Engineering at the Delft University of Technology with a specialization in Tissue Biomechanics. This thesis could not have been written without the help and support I received along the way and I would like to thank them through this way.

First, my supervisors, Gerjo van Osch and Mohammad Mirzaali, who provided guidance throughout the project and were always approachable and prepared to help me out right away. I was very comfortable to discuss everything with them, which has made this research project a very educational, pleasant and interesting experience. Furthermore, I would like to thank everyone from the Connective Tissue Repair Lab at Erasmus MC, especially Nicole Kops. Without the help of Nicole, I would not have been able to make any samples and perform any measurements. In addition, the coffee breaks and lunches at Erasmus really helped me along and gave me extra energy during the more lonely times in the summer and the Covid pandemic.
I want to thank Nelda Antonovaite from Optics 11 for all her support, she was always prepared to answer any questions or struggles I had regarding the nanoindenter. For all the measurements performed at the TU Delft, I would like to thank Pedro Diaz Payno, Mauricio Cruz Saldivar and Niko Putra for their help with the machines I used to analyse the samples, their insights and feedback along the way. I also want to thank Kathryn Stok and Pholpat Durongbhan from the University of Melbourne, for the pleasant conversations and who were more than happy to help me out and share their insights on the nanoindentation data, despite the huge time difference.

Lastly, I want to thank my friends and family. My friends from Delft, my roommates from Delft, Rotterdam and The Hague who always helped me to take my mind off work and recharged me after a long day. Most importantly, I want to thank my family, my dad, mom, two sisters and two brothers. No matter what, I could always call for advice and some wise words to get me going again. Pap, Mam, Soph, Mats, Alex and Caat, thanks for being there for me, believing in me and always making me laugh again even during the harder times!

Emma Boersma
The Hague, March 2022

TABLE OF CONTENTS

LIST OF FIGURES

LIST OF TABLES

ACRONYMS

DIC Digital Image Correlation

TBS Tris-Buffered Saline

OA Osteoarthritis

SOC Secondary Ossification Center

HE Haematoxylin and Eosin

GAG Glycosaminoglycan

RGB Red Green Blue

Saf O Safranin O

EDTA Ehtylenediaminetetraacetic acid

MPa Megapascal

GPa Gigapascal

Nano. Nanoindentation

Micro. Microindentation

TPB Three-Point Bending testOP Oliver-Pharr

SEM Scattered Electron Microscopy

HDMS Hexamethyldisiloxane

PC Personal Computer

UV Ultraviolet

AFM Atomic Force Microscopy

1

INTRODUCTION

The structure of the osteochondral interface has always been a subject of great interest. This interface is the connection between bone and the overlaying cartilage layer in the joints. The main function of this attachment is to distribute and mitigate the subjected load over the bone to reduce the stress concentration [5]. The interest in this region is high, due to the strong connection and the slow regeneration rate of these sites. However, a lot still remains unknown, due to the complexity, irregularity and small scale of the structures.

Even though the natural connection is strong, due to the fact that these sites are subjected to high, and in some cases abrupt, forces, these sites are prone to failure. Long-term injuries or osteochondral diseases, like osteoarthritis (OA), are common, especially in elderly. These cases are often accompanied with a high pain sensation, up till the point where one is obstructed from a normal day to day life [6; 7]. Unfortunately, regeneration techniques of these attachments are still limited. Currently, small defects are often relieved by removing the damaged tissue instead of fixing or replacing it. The creation of a microfracture in the joint might cause Mesenchymal Stem Cells (MSCs) from the underlying bone to be attracted and stimulated to start a healing process [8; 9; 10]. In larger defects, the entire joint is often replaced by an implant. The downside to this type of treatment is that it is highly invasive and has a high risk of infections [11]. In addition, the implant has a lifespan of approximately 15 years. Resulting in more surgeries to replace the implants, which is more invasive and can only be performed a few times before the bone is too damaged to hold an implant. For this reason, implants are not recommended and unsuitable for young patients [12; 13].

A recent emerging technique is the field of tissue engineering, which aims to regenerate the osteochondral tissue in the defect. In particular bi-layered scaffolds, which are scaffolds made up of two different materials with differing properties, are emerging for osteochondral defects. This method tries to mimic the difference in mechanical properties of cartilage and bone, as bone is found to have a higher stiffness value than cartilage. However, an artificial connection between a stiff and a soft material often fails to resist the shear forces it encounters [8; 14]. Therefore, it is crucial to know the characteristics of the natural structures and the composition as this could lead to new insights in the connection strength and behaviour. Understanding the development of the original osteochondral interface and how the mechanical properties develop during maturation, could lead to new insights and improvement of the current regeneration methods.[15; 16; 17; 18].

In this study, the aim is to identify the mechanical properties and micro-structural changes over the interface layers during different maturation stages. In this chapter, the general structure of the osteochondral interface will be presented, followed by the maturation process of the attachment. Thereafter, the current knowledge of the relationship between the material properties and structure of the interface will be elaborated and finally, the resulting research questions of this study will be presented.

1.1 THE OSTEOCHONDRAL INTERFACE

The natural mature osteochondral interface can be divided into three distinct layers from the cartilage surface towards the bone: the articular cartilage, the calcified cartilage and the subchondral bone (Figure 1.1).
The articular cartilage consists of mostly collagen type II, proteoglycans, water and chondrocytes [19; 20]. The collagen fibers create a stable structure in the cartilage to increase resistance to the stresses to which it is subjected. The most abundant proteoglycan present, is aggrecan, which contributes to the cartilage structure and withstanding compression loads [21]. Proteoglycans have negatively charged parts called glycosaminoglycans (GAGs), which attract water into the cartilage. This creates the sponge effect of the cartilage, offering a higher resistance against the load it endures [22; 23].
Within the articular cartilage, three structural zones can be identified (Figure 1.1). The most external zone, referred to as the superficial zone, contains a high density of chondrocytes. Together with the collagen fibers, they are organised in a parallel manner to the surface of the articular cartilage. In addition, the highest water concentration is detected within this layer. It was found, that this type of organisation makes the top zone ideal for resisting the tensile forces[23; 24]. Following the superficial zone, is the transitional zone. Here, the density of the chondrocytes has decreased and the fibers are organised randomly. Lastly, the deep zone of the articular cartilage is the zone between the transitional zone and the calcified cartilage. The lowest water concentration of the articular cartilage is found here. In addition, the fibers are organised in a perpendicular manner opposed to the superficial zone, making this layer most ideal for resisting compressive forces[23; 24].
Below the deep zone of the articular cartilage, the calcified cartilage layer emerges. Between the articular cartilage and calcified cartilage, a distinct line can be detected, called a tidemark. In some cases, multiple tidemarks can be identified. This line is thought to be a gathered mineralization line and found to be approximately 10 µm thick [25].

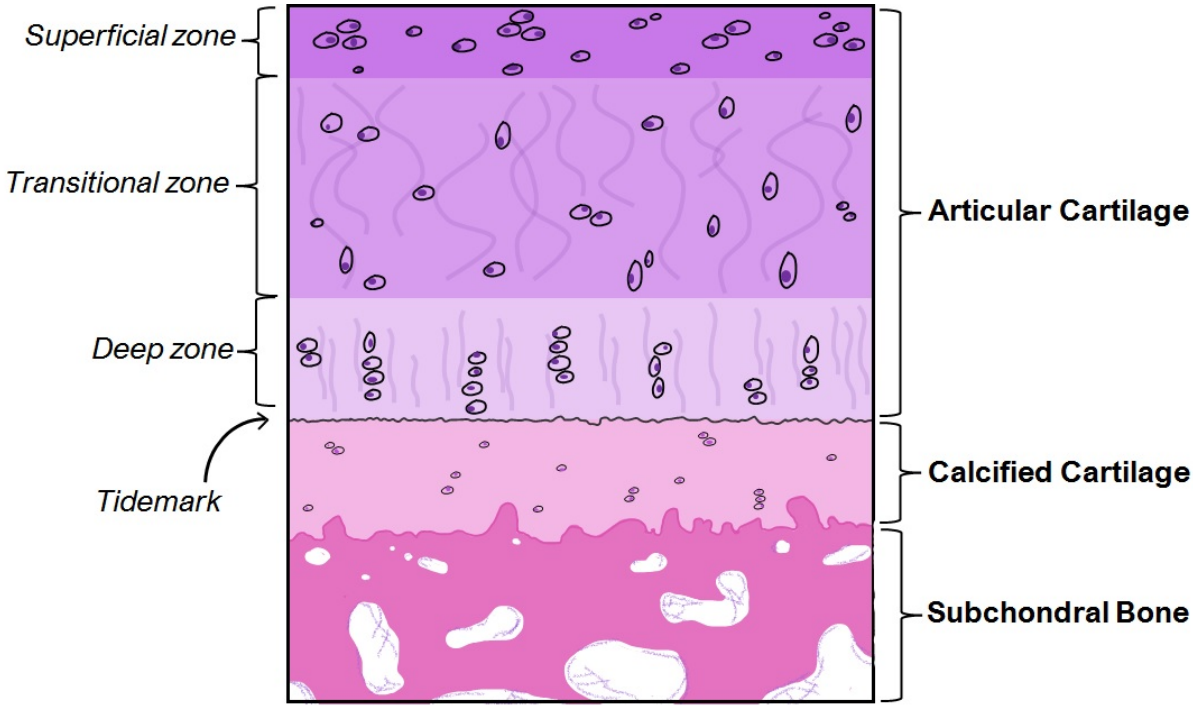

Figure 1.1: Schematic overview of the general identified layers and zones of the mature osteochondral interface.

After this boundary mark, the cartilage starts to contain crystalline hydroxyapatite, which is also abundantly present in bone. The mineralization of the cartilage can be explained by the protein chondrocalcin, which is formed as a result of the degraded collagen type II fibers. This protein is involved in the calcium binding process within bone formation, thus can cause the mineralization of the cartilage[23]. The calcified cartilage can be seen as the connecting layer between the articular cartilage and the subchondral bone. It has been found that the collagen fibrils disperse towards the subchondral bone and anchor themselves, creating a higher contact area to smoothly mitigate the force onto the bone [26]. Within the calcified cartilage, a low cell density of hypertrophic chondrocytes is present[27].
Finally, the subchondral bone layer is reached. The subchondral bone can be divided in two zones: a compact plate followed by a trabecular bone zone. Within the subchondral plate, channels with vessels and nerves are found, which branch out to the calcified cartilage (Figure 1.1). The trabecular subchondral bone contributes highly to the shock absorbing capacity. The inorganic component most abundantly present in this layer, is crystalline hydroxyapatite. The bone matrix also contains calcium, carbonate and phosphate. Furthermore, collagen type I fibers, enzymes, cytokines and growth factors are detected in this layer [23; 28].

1.2 MATURATION OF THE INTERFACE

The timeline of the development of the skeletal system varies between species. In this research, equine joints were investigated. In this species, a rapid infant growth, childhood phase and puberty all occur before the age of three. However, for the human species, these maturation stages happen over the duration of approximately 18 years (Figure 1.2)

[1].

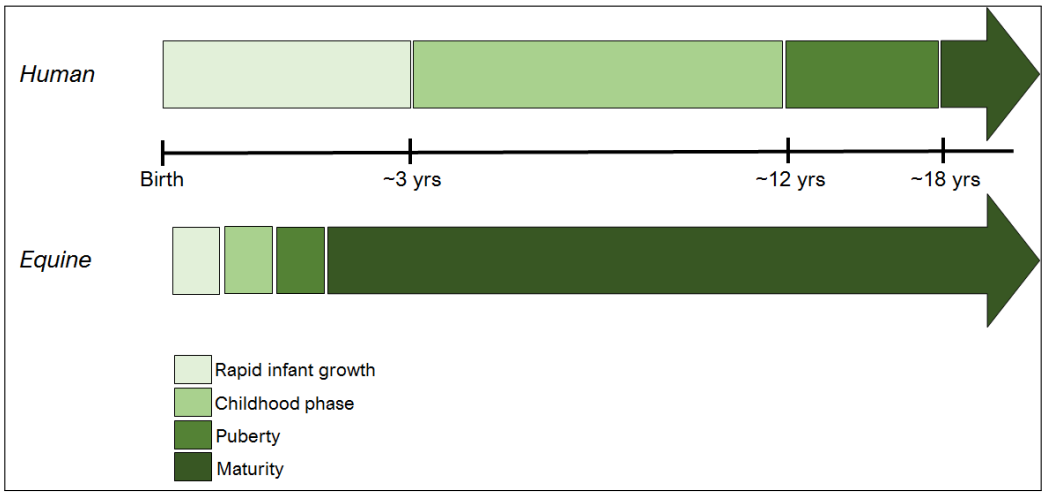

Figure 1.2: Timeline of the human and equine skeletal development [1].

In the skeleton, the formation of long bones exceeds from hyaline cartilage in the primary and secondary ossification centers. The secondary ossification centre (SOC) is located in the center of the epiphysis of long bones and usually emerges in a latest stage of prenatal development. Before the formation of the SOC, the fully cartilaginous epiphysis is invaded by a network of blood vessels. During the late stage of gestation, the SOC develops from these vessels and a growth plate emerges (Figure 1.3). The SOC transforms the hyaline cartilage into bone, which eventually forms into the cartilage-bone interface [29].
Before birth, cartilage canals are abundantly present in the epiphysis. These canals contain blood vessels and connective tissue (Figure 1.4). It is thought that these canals are present for multiple reasons; Firstly, they provide nutrition and eliminate waste products from the growing cartilage. Another reason is that these canals carry mesenchymal cells and therefore might have a contribution to the ossification process. Lastly, the cartilage canals serve as a reservoir for cartilage growth cells. The canals undergo regression and chondrification during the foal stage [30]. At the age of 8-10 weeks the number of canals has decreased and the thickness of the cartilage layer has lowered. At the age of 6 months, the foals have a cartilage layer with the thickness of mature cartilage and all the cartilage canals have been resorbed and replaced by bone [29].

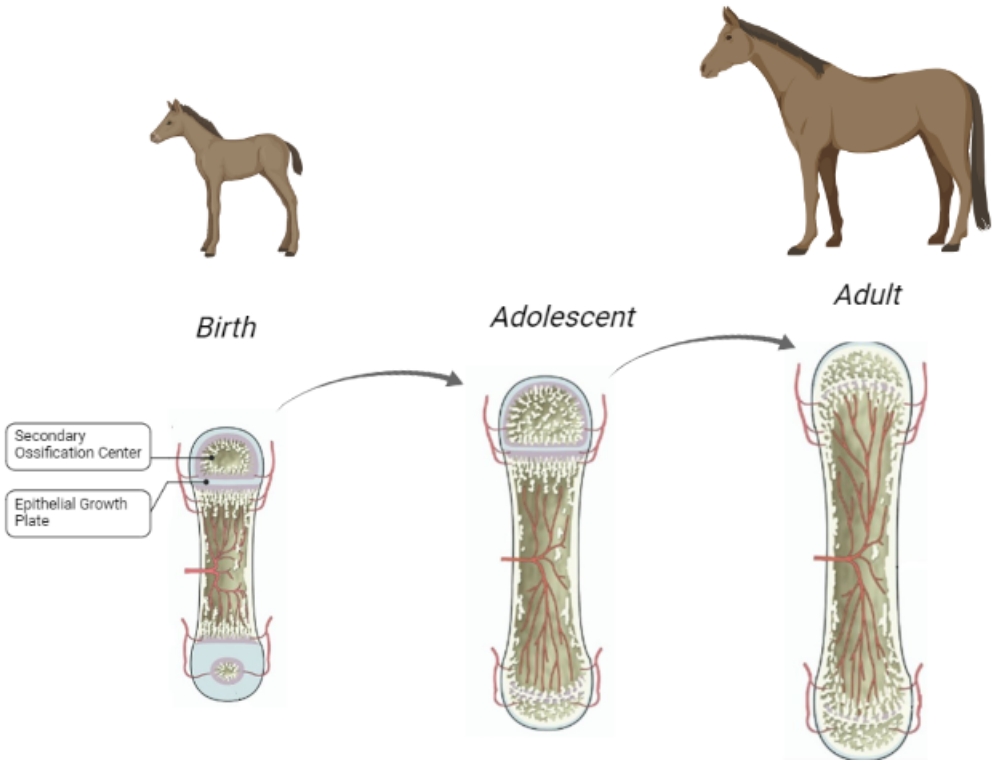

Figure 1.3: Schematic overview of the equine bone growth after birth in long bones. Modified from van Weeren (2006) [2].

From 6 months old, the premature cartilage layer can be divided into three zones, from which the mature cartilage layers, mentioned above, originate. The most superficial zone is the zone with the resting chondrocytes (Figure 1.4). Here, the cells are flattened right beneath the articular surface. The following zone is called the proliferative zone, where the chondrocytes undergo rapid division perpendicular to the long axis of growth. The final zone is called the hypertrophic zone, where the hypertrophic chondrocytes can be found. Their main task is in the cartilage mineralization process to create the calcified cartilage layer during further development (Figure 1.4) [31].

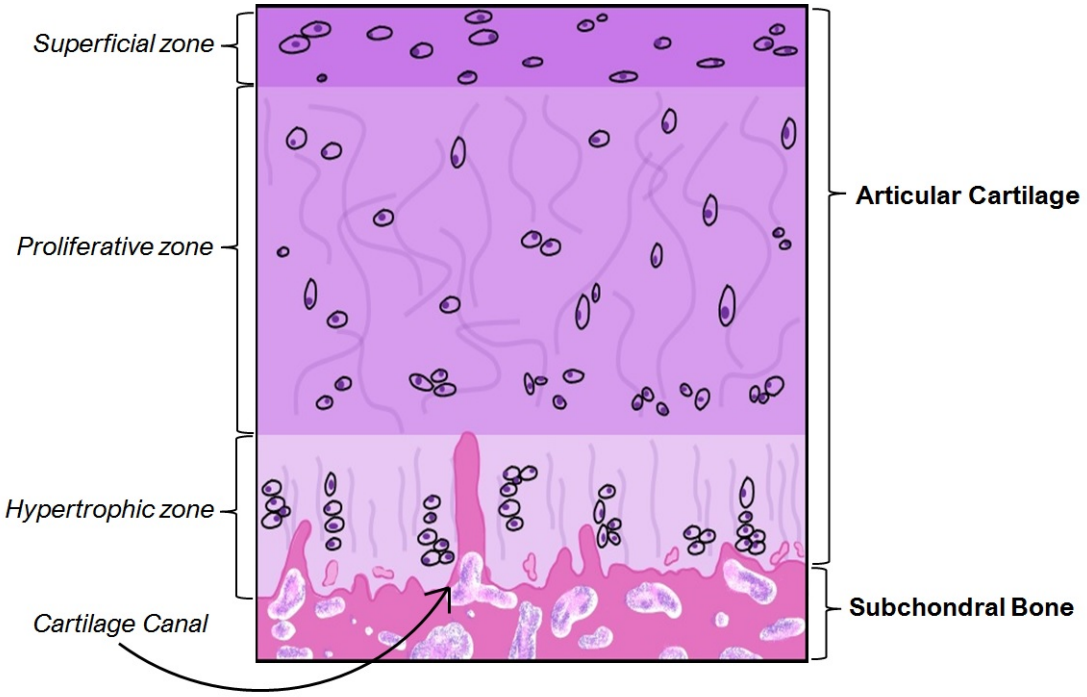

Figure 1.4: Schematic overview of the layers and zones in the immature osteochondral interface.

The composition of the growing interface changes over age. It has been found that collagen type II in the hyaline cartilage of long bones in a maturing foal, is replaced by collagen type I, which is abundantly present in bone. In the subchondral bone, a decrease of water and hydroxylysine was found during the first 5 months after birth. In contrast, the calcium and collagen content highly increased during this period. Interestingly, the mineralization process does not stabilize at all. This suggests that mineralization is an ongoing process [16; 18].
Another remarkable finding in the aging osteochondral interface, is the increasing number of tidemarks. From birth till the adolescent stage, no tidemarks are present at all in the cartilage. They emerge during the mineralization of cartilage. Furthermore, with increasing age, the number of tidemarks increases. It is still debated, however, whether this increase is associated with age or OA, which also has a correlation with aging [32]. Lastly, it is important to note that it is thought that loading has an influence on the ossification and chondrification process [18; 33; 34]. Different loading conditions can affect the architecture of the collagen network and mineral composition [16; 18]. This results in a varying structure of the osteochondral interface amongst different species and anatomical locations, as these all have a different range of body weight and load endurance [33].

1.3 MATERIAL CHARACTERISTICS OF CARTILAGE AND BONE

In order to understand and mimic the interfacial properties, it is crucial to investigate the mechanical characteristics. One way to describe a material mechanically, is by observing and mapping the local elastic moduli. This property describes the resistance of a material to elastic deformation. A higher modulus results in a stiffer material, while a lower modulus indicates a softer material. It is a key property that needs to be considered in the material selection process. Especially, in the body where the damping of forces

depends on the stiffness of the cartilage and interface [35].
In the osteochondral interface, it has been found that the orientation of the collagen fibers and their cross-links contribute to the elastic stiffness of the region. In the superficial layer, the fibers and chondrocytes tend to lay parallel along the articular surface. In addition, the density of the fibers is higher in the superficial layer compared to the deeper layers. In contrast, the density of the calcium particles tends to increase towards the bone [36; 37].
Due to all these structural changes within the cartilage, it has anisotropic properties, meaning that the mechanical properties have different values in every direction. This can be explained by the orientation of the fibers. A parallel structure reacts differently to a parallel or perpendicular load. Thus, the compressive stiffness of the cartilage in the axial direction differs from the compressive stiffness in the transverse direction, for example (Figure 1.5) [38].
Furthermore, the materialistic behaviour of cartilage can be described as viscoelastic behaviour. Viscoelastic materials have a time-dependent property, due to the liquid it contains. If a constant load is applied to a viscoelastic material, the displacement will non-linearly increase over time, due to the movement of the fluid within the material [39; 40]. It has been found, that the amount of collagen cross-links also influences the viscoelasticity of the cartilage. Interestingly, the cross-link concentration of collagen depends on age and gender, which might lead to a difference in elastic modulus and viscoelasticity of the interface over age [41]. Furthermore, the proteoglycan matrix within the articular cartilage is found to be the main contributor to the elastic behaviour of the tissue [37].

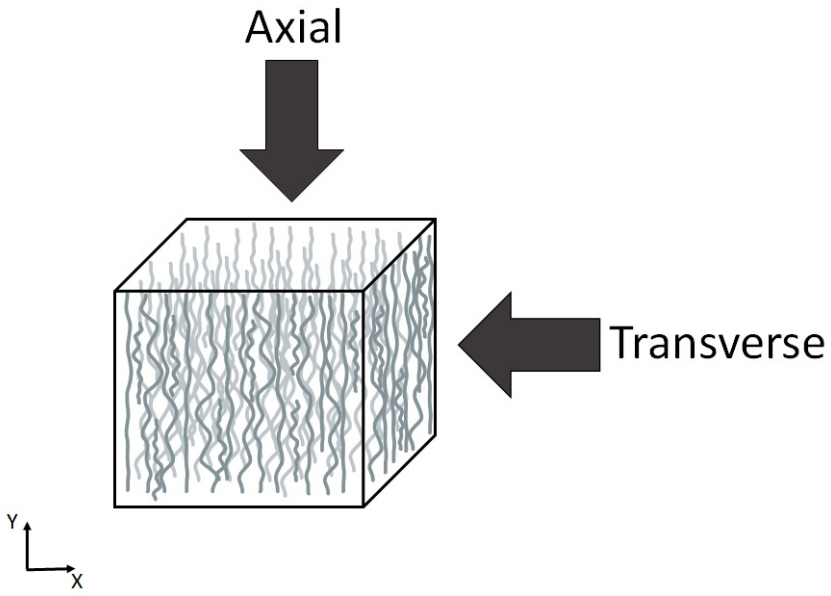

Figure 1.5: The organisation of collagen fibers in cartilage, resulting in different mechanical behaviour in the axial and transverse direction.

The morphology of collagen fibers (i.e., shapes and orientations) are not the only indication for the mechanical characteristics. The degree of mineralization also has an effect on the stiffness of the cartilage and bone. Several studies have investigated the elastic modulus of the osteochondral interface with different measuring techniques [16]. Often it has been found that the value of subchondral bone can be an order of magnitude

higher than that of articular cartilage (Table 1.1) [42; 43]. A higher value has also been measured for the calcified cartilage, compared to the non-calcified cartilage. Confirming, that the mineralization has a contribution to the stiffness values and mechanical properties of the tissue [43; 16; 41]. It is, however, important to realize that different measuring methods result in different values. In addition, the mechanical properties may vary with anatomical location and species. Therefore, it is challenging to determine the the absolute value of the elastic modulus.

Table 1.1: Elastic modulus of the tissue types in the osteochondral interface.

Tissue Type	Study	Method*	Orientation	Elastic Modulus [GPa]
Articular Cartilage	Campbell, 2012	Nano.	Transverse	5
	Gupta, 2005	Nano.	Transverse	5
	Moshtagh, 2016	Nano.	Axial	$1.6 * 10^{-}3$
Calcified Cartilage	Campbell, 2016	Nano.	Transverse	$20 - 25$
	Gupta,2005	Nano.	Transverse	$13 - 25$
	Hargrave-Thomas, 2015	Nano.	Transverse	$6 - 8$
	Hargrave-Thomas, 2015	Micro.	Transverse	$4 - 6$
	Hargrave-Thomas, 2015	TPB	Axial	$0.5 - 1$
	Mente, 1994	TPB	Axial	0.32
Subchondral bone	Campbell, 2016	Nano.	Transverse	$20 - 25$
	Gupta, 2005	Nano.	Transverse	$13 - 25$
	Gardner-Morse, 2010	Micro.	Axial	3.7
	Hargrave-Thomas, 2015	Nano.	Transverse	$10 - 18$
	Hargrave-Thomas, 2015	Micro.	Transverse	$6 - 8$
	Hargrave-Thomas, 2015	TPB	Axial	$4 - 6$
	Mente, 1994	TPB	Axial	5.7

The methods used were Nanoindentation (Nano.), Microindentation (Micro.) and the Three-Point Bending test (TPB).

1.4 RESEARCH QUESTIONS

The osteochondral interface is a complex structure of which the mechanical properties are challenging to determine. Previously, research has been performed on the structure and fiber orientation of the different cartilage layers. However, knowledge is still lacking in the mechanical properties of the different layers and especially the calcified cartilage. In addition, knowledge of the mechanical properties and structural changes during maturation might lead to new insights on the process of formation of the interface. The main objective of this research, is to map the elastic modulus of the different tissue types within the osteochondral interface during maturation. In order to measure this mechanical property locally, the Piuma Nanoindenter (Optics 11, Amsterdam. The Netherlands) will be used and strain distribution will be measured using compression tests with digital image correlation (DIC). Here, the osteochondral interface of equine metacarpo- and metatarsophalangeal joints of different ages will be investigated. This leads to the following research question, which will be answered by several sub-research questions:

What is the property-structure relationship of the equine osteochondral interface and how does that vary during maturation?

- Which protocol should be used for the Piuma nanoindenter to measure the localized mechanical properties?
- What are the differences in elastic stiffness between the osteochondral layers?
- What are the changes in the elastic stiffness of the osteochondral layers during maturation?
- What are the changes in the (micro-)structure of the osteochondral layers during maturation and how does it associate to the elastic stiffness measurements?

These questions will be answered by creating a protocol to measure the local elastic moduli across the bone-cartilage interface and observing the structure with histology stainings. In the following chapter, the materials and methods will be presented. Followed by the results and the discussion and, lastly, the conclusion of this research.

2

MATERIALS AND METHODS

Specific dimensions and restrictions were required for the samples to be able to perform the mechanical tests. The joints were sectioned in such a way, that their surfaces were flat and smooth, for nanoindentation, and had a thickness large enough to resist failure during compression tests. Before testing the equine joints, different sectioning techniques, polishing trials and nanoindentation profiles were performed on bovine metacarpophalangeal joints (Appendix I). The equine metacarpo- and metatarsophalangeal joints were sampled and after sectioning, nanoindentation was performed on all the mechanical testing samples and histology stainings on the histology samples. Furthermore, compression tests were executed with cameras with Digital Image Correlation (DIC) software.

2.1 TISSUE SAMPLING

The joints used in this study were from horses with the age of 9 days, 12 days, 7 weeks, 13 weeks old and three fully mature horses, of which the exact age was unknown. The biological material was provided by the Faculty of Veterinary Medicine at the University of Utrecht in the Netherlands. After death, the lower legs were separated from the tarsus or carpus down till the hoof. From each horse, one lower leg was used in this study. After separation, they were stored at -20 °C till further processing.
The next step was to section the joints into samples for mechanical testing and histology. The legs were thawed overnight at 4 °C, and the metacarpo- or metatarsophalangeal joint was freed from the surrounding skin and subcutaneous tissues. The joint was opened up and inspected visually to confirm the absence of degenerative changes. The proximal part of the joint was used for further analysis. The joint was freed from the proximal phalanx bone at the neck of the bone by using a bench vice and a handsaw, while keeping the head of the joint intact. Subsequently, the lateral and medial sides of the head of the proximal phalanx were sliced off using the handsaw. The anterior and posterior sides were cropped off for optimal clamping in the circular saw (Proxxon Micromot, Fohren, Germany).
A diamond blade was used to create a straight, smooth surface. The samples were constantly cooled by dripping distilled water onto the sample with a pipette to prevent high temperatures and burning the the tissue during cutting.
The mature joints were larger than the immature joints; thus, approximately four samples for mechanical testing were obtained from the mature joints, while for the immature joints, two mechanical samples per joint. From every joint, two samples were cut for histology, one from the medial side and one from the lateral side (Figure 2.1). This method resulted in 21 samples for mechanical testing and 14 samples for histological analysis (Table 6.1). The dimensions of all the mechanical samples were similar and they were measured with a caliper (Appendix II).

The histology samples were cut as separate samples, as the samples undergoing mechanical could get damaged during testing. Furthermore, it would save time due to the long decalcification process for larger samples. After sectioning, all the samples were stored in histological cassettes and labeled. The mechanical samples were stored at −20 °C till further use, and the histology samples were immediately processed.
The samples were all labeled according to the age and position of the samples within the joint. The immature samples were indicated with a 'Y', the mature samples with an 'A', followed by the age and an 'L' for the lateral side or 'M' for the medial side of the joint. For the mature and 13 months old joint a 'D' or 'P' was added to the label, for the distal or proximal sample of the medial or lateral side of the joint (Figure 2.2 and Appendix II).

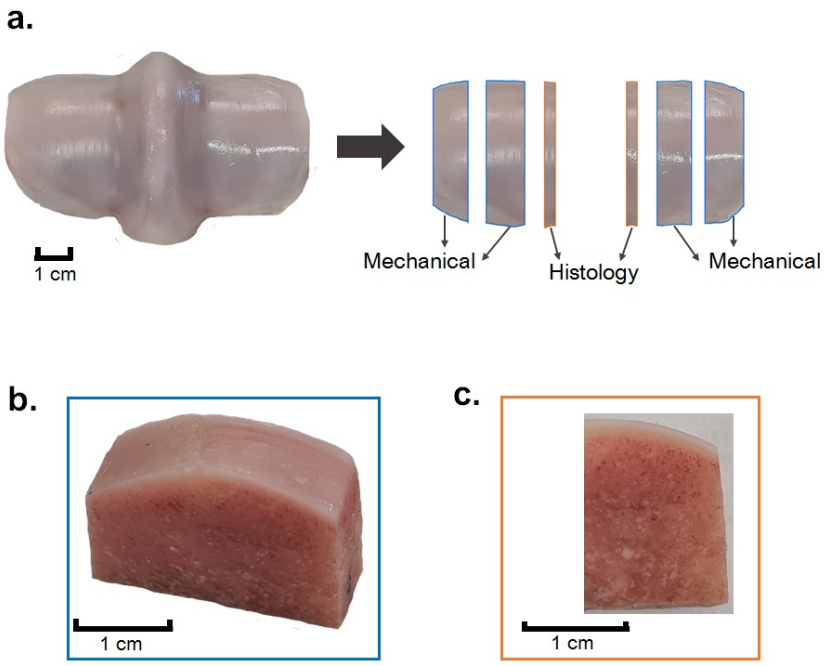

Figure 2.1: Sectioning of the proximal part of the joint. (a.) Sectioning of the mature and 13 months old sample. For the younger samples, only two mechanical samples were sectioned per joint. (b.) A sample for mechanical testing. (c.) A histology sample.

Table 2.1: Age, number of joints and number of samples used in this research

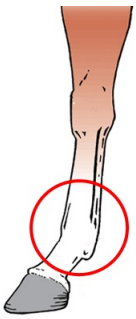

Age	Number of Joints	Mechanical Samples	Histology Samples
9 Days	1	2	2
12 Days	1	2	2
7 Weeks	1	2	2
13 Months	1	4	2
Mature	3	11	6
Total	**7**	**21**	**14**

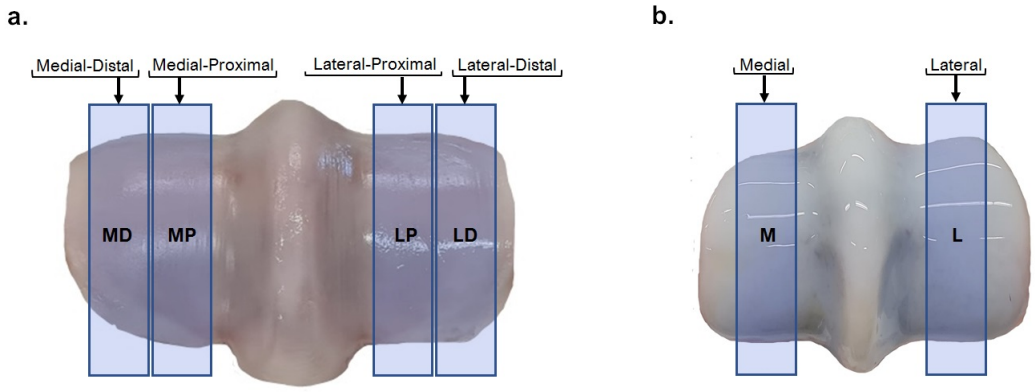

Figure 2.2: Labelling of the samples.(a.) Labels for the mature and 13 months old joints. (b.) Labels for the 7 weeks, 12 days and 9 days old joints

2.2 HISTOLOGY

The samples destined for histology were fixed in 4% formalin for 2 days. After that, the samples were decalcified in 10% formic acid for approximately 14 days. The formic acid was refreshed every 2-4 days. After decalcification, all the histology samples were embedded in paraffin.
From each joint, one sample was sliced into 6 µm sections with a microtome (Leica, Nussloch, Germany) at different depths. After that, one slide with three coupers was made per joint for every staining. Three histological staining procedures were performed. First, all the slides were deparaffinized with xylene, ethanol series (100%, 96%, and 70%) and lastly rinsed with distilled water. Thereaftes, the step-by-step protocols for the individual histology stainings were performed (Appendix III).

2.2.1 *Haematoxylin & Eosin staining*

Haematoxylin and Eosin staining (HE) was performed to observe the overall structure. The slides were first immersed in Haematoxylin Gill's (Sigma-Aaldrich, Saint Louis, U.S.A.) for 5 minutes and then carefully rinsed under running tap water. After that, the slides were immersed in Eosin (Merck, Darmstadt, Germany) for 45 seconds. Following, the slides were dehydrated in a series of ethanol and xylene, after which they were mounted with Depex (Merck) and dried overnight at 37 °C.

2.2.2 *RGB staining*

RGB-trichrome staining was used to show a distinct difference between the uncalcified and calcified zones in the tissue. Here, the blue color represents the GAG density, the red color the collagen fibers, and the green the calcified tissue [44]. After deparaffinization, the slides were immersed in Alcian Blue solution with a pH of 2.5 (Sigma-Aaldrich) for 20 minutes, carefully rinsed with tap water, and then immersed in Fast Green solution (Sigma-Aaldrich) for 20 minutes. Lastly, the slides were rinsed with tap water again and immersed in Picro Sirius Red (Sigma-Aaldrich) solution for 30 minutes, followed by a quick rinse with 1% acetic acid solution. After the staining procedure, the slides were dehydrated in ethanol series, mounted with Depex, and dried overnight at 37 °C.

2.2.3 *Safranin O staining*

In order to observe the cartilage area and the GAG distribution in the interface, Safranin O (Honeywell Fluka, Charlotte, U.S.A.) staining was used with a counterstaining of Light Green (Honeywell Fluka). The slides were first immersed in Light Green solution for 8 minutes and quickly rinsed with 1% acetic acid. Subsequently, the slides were immersed in Safranin O solution for 12 minutes, rinsed with 96% ethanol, and dehydrated in 100% ethanol and xylene. Finally, the slides were mounted with Depex and dried overnight at 37 °C.

After histology staining, the samples were analyzed and images were obtained with a microscope (Olympus, Tokyo, Japan). To obtain images of the complete section with a higher resolution, a Nanozoomer (ND.view2, Hamamatsu, Japan) was used on the HE stained samples. From these images, the thickness of the articular cartilage and calcified cartilage layer, if present, was determined (Appendix II). Histology was performed either on the samples of the medial or lateral side of the joint.

2.3 NANOINDENTATION

The local elastic modulus of the osteochondral interface was measured with a displacement-controlled nanoindentation machine (Piuma, Optics 11, Amsterdam, Netherlands). This device used a micro-scale spherical probe attached to a cantilever connected to an optical fiber (Figure 2.3 a.). Within the nanoindenter, a piezoelectric sensor was used to detect the force and displacement of the probe. When an indentation was made, the cantilever bent, and deflection was measured as the tip's displacement. In addition, the force it generated was tracked, which resulted in a force-displacement curve for every indentation. The elastic modulus was calculated from this curve by analyzing the slope.

2.3.1 *Sample Preparation*

The samples were thawed overnight in 4 °C in a plastic petri dish, while immersed in 1X TBS solution with protease inhibitors (EDTA-free inhibitor cocktail tablets, complete Roche, Basel, Switzerland). The solution was prepared by dissolving two protease inhibitor tablets in 100 mL 1x TBS. The solution was stored and reused for a maximum of 3 days. After this time, it was disposed and new solution was prepared for the next samples. The protease inhibitors were EDTA-free to prevent possible decalcification and maintain the mechanical stability and composition [45].
Just before measuring, the thawed sample was fixed to a plastic petri-dish with superglue (Pattex, Düsseldorf, Germany). It was important that only very little was used, and only at the bone end, to maintain the mechanical properties of the osteochondral interface and prevent damage when pulling the sample off the dish after testing. As soon as the glue had dried, the protease inhibitor solution was poured back in the petri dish till the sample was fully immersed. Lastly, the sample was observed from the side to check which measuring direction would be best for the probe. Some samples were cut in a slight angle and thus directing the probe from a lower level to higher surface would cause it to collide into the sample and break while moving along the matrix.

2.3.2 *Probe Selection*

For the probe selection, it was important to consider the stiffness of the cantilever and the radius of the tip of the probe. For a stiff material, a stiffer cantilever was required ($\sim$ 250 N/m) to generate a force high enough to perform an indentation. For a softer material, a less stiff probe was needed. If a softer material was indented with a stiff cantilever, the cantilever would likely not bend during indentation, and thus not record any deflection (Figure 2.3 b.). As for the tip size, a softer material required a larger tip ($\sim$ 50 µm), while for a stiffer material a smaller radius ($\sim$ 8 µm) was preferable. In addition, the pores of the material were taken under consideration. The probe tip had to be larger than the pores or defects on the surface of the sample. In the case of the osteochondral interface, the preference was a stiff probe with a large radius, as the pores of subchondral bone could reach a radius of 10 µm to 200 µm. However, the stiff probes were only manufactured with a small radius.
Furthermore, in order to select an appropriate probe, some indication of the stiffness of the measured material was necessary. For cartilage it was found to be in the range of 1-4 MPa and for subchondral bone it could range from 1 to 25 GPa, with different measuring methods [46; 43; 42]. To keep the measurements consistent, the same probe was used to measure the cartilage and subchondral bone. For that reason, stiff probes with a small radius were used. It is important to mention that the probes were highly sensitive to external environmental factors. Consequently, multiple probes were used to have a back up in case one broke or would have trouble calibrating (Table 2.2). The range of stiffness of the probes was similar. To evaluate whether the difference could be negligible, indentations with different probes were made on pure cartilage of the same sample. It was chosen to indent the cartilage, instead of the bone, because bone had larger pores and a more heterogeneous structure. An overview of which probe was used for each sample is presented in Appendix V.

Table 2.2: Probe properties used in this research

Probe Label	Stiffness [N/m]	Radius [µm]
P_1	249	8.5
P_2	254	9.5
P_3	261	8.0
P_4	283	9.0

2.3.3 *Calibration and Indentation Profile*

The calibration of the probe was performed in 1X TBS solution by pouring some droplets on a glass microscope slide with a plastic pipette and lowering the probe into the liquid. The step-by-step protocol for nanoindentation is provided in Appendix V. The indentations were performed perpendicular to the articular cartilage surface and the natural loading direction, so that all the transitional zones could be measured (Figure 2.3a). The placement of the probe was done in such a way that all the transitional regions of the interface were captured. For that reason, the starting point of the probe was set in the transitional zone of the articular cartilage. From that point, the matrix was performed in the direction of the subchondral bone. As soon as the starting point and direction had been defined, an indentation matrix of 6x12 indentations was set. Six

indentations along the cartilage and 12 over the osteochondral interface. Due to time, the matrix dimensions were limited to this amount. The space between indentations in the x-direction was 100 µm and 80 µm in the y-direction (Figure 2.3 c.). These values were chosen to ensure enough distance between indentations. As the thickness of the calcified cartilage was found to vary between 130 to 220 µm in the equine osteochondral interface, the y-direction had a smaller value to make sure the calcified cartilage was indented at least once [47].
The indentation depth was 5 µm and the indentation time frame was based on a previous study, which investigated indentations in the articular cartilage by Moshtagh (2016)[46]. A load time of 0.83 seconds, holding time of 5.83 seconds and unloading time of 16.67 seconds was applied (Figure 2.3 d.). The time duration of a complete single indentation matrix was approximately 1.5 hours. In order to collect more data on the local elastic modulus, the indentation matrix was performed three times in the same location. Immediately after the completion of a matrix, the probe was set to the initial starting point with the software for two more matrices.

a.

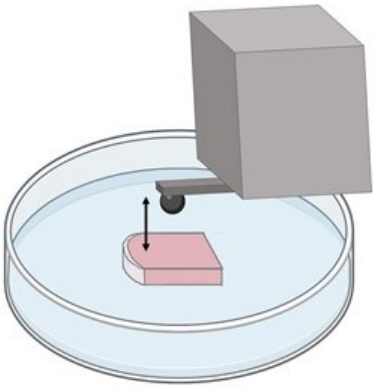

b.

Sample Young's modulus	Advised cantilever stiffness range
10 Pa – 1 kPa	0.025 N/m
1 kPa – 500 kPa	0.25 N/m
500 kPa – 10 MPa	5 N/m
10 MPa – 100 MPa	50 N/m
100 MPa – 1 GPa	500 N/m

c.

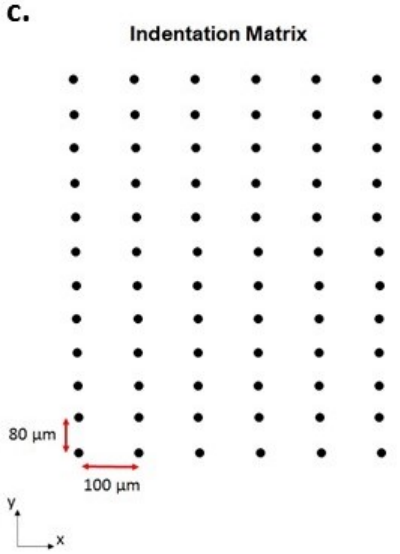

d.

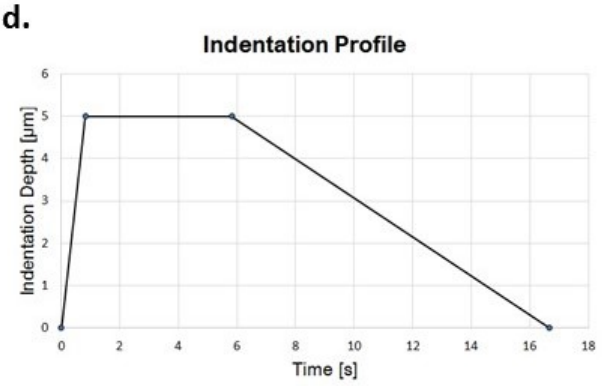

e.

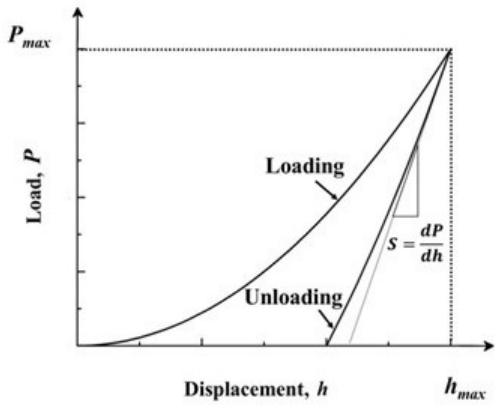

f.

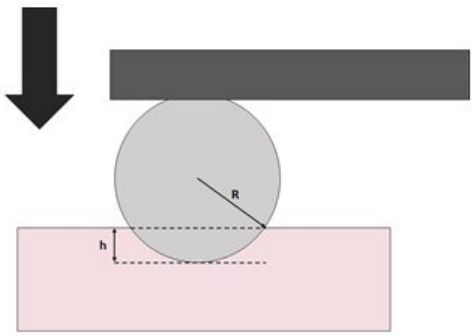

Figure 2.3: The nanoindentation profile and procedure with a schematic overview of the indenter and the sample (a.). (b.) The probe stiffness selection guide according to Optics 11 [3].(c.) The indentation matrix and spacings between indentations. (d.) The indentation profile over time for every indentation. (e.)The force-displacement curve resulting from an indentation, showing the analysis of the unloading curve. S represents the stiffness and the derivative of the load over the displacement [4]. (f.) A close up of the probe indentation, where R is the probe radius and h the maximum displacement.

2.3.4 *Data Analysis*

Cartilage and bone can be defined as materials with viscoelastic behavior [48; 49]. Multiple nanoindentation analysis methods exist for different types of materials. However, implementing the viscoelastic material properties remains challenging due to the time-dependent property of the material. Therefore, the analysis method used in this study was the Oliver-Pharr (OP) method. This method is based on elastic-plastic material properties and modified so that the viscoelastic characteristics can be neglected from further analysis.
The OP-method has shown to be very effective and robust for elastic-plastic materials. Here, the unloading curve of the indentation profile is analysed (Figure 2.3 e.). This method will, however, most likely overestimate the elastic modulus if viscoelastic properties are ignored. If unloading of the indentation occurs immediately after loading, the viscoelastic material will not follow the displacement with the decreasing force. This phenomenon could lead to an increased unloading curve or a negative slope, causing the overestimation [50]. The material requires time to reach an equilibrium with a constant load to prevent the overestimation of the elastic modulus. A holding time of 5-10 seconds has been demonstrated to be sufficient enough to eliminate the viscoelastic creep [51; 52]. The analysis of the unloading curve was performed between 70-95% of the load. This top limit was chosen to ensure the unloading had started. In addition, the lower limit was chosen to maintain in the linear region of the curve [53; 54]. A MATLAB code was set up to implement the OP-method for this nanoindentation data (Appendix VI).

The OP-method is based on research performed by Sneddon[55], who derived general a relationship between the load, displacement and contact area for any indentation metric,

$$P = \alpha * h^m \tag{2.1}$$

Where P is the indentation load, h is the displacement of the probe, and α and m are constants. The value for m depends on the probe geometry. For a spherical probe, it typically was found to be 1.5 [54]. α is determined by the fit of the curve to the indentation data. From equation 2.1, the unloading curve was described by the following power-law,

$$P = \alpha * (h_c)^m \tag{2.2}$$

Where h_c is the contact depth, which was defined by,

$$h_c = h_{max} - h_f \tag{2.3}$$

Where h_{max} is the maximum indentation depth and h_f the indentation depth where the load, during unloading, has reached 0 N again [53]. The contact radius, a, was then calculated from the contact depth of the probe,

$$a = \sqrt{(2Rh_c - h_c^2)} \tag{2.4}$$

Where R is the probe radius (Figure 2.3 f.). From this contact radius, the contact area, A, was retrieved, which was required for calculating the elastic modulus,

$$A = \pi * a^2 \tag{2.5}$$

The stiffness and elastic modulus were then obtained, using the following equations,

$$S = \frac{dP}{dh} = m * \alpha (h_{max} - h_f)^{(m-1)} \tag{2.6}$$

$$E = \frac{S\sqrt{\pi}}{2\sqrt{A}} * (1 - \nu^2) \tag{2.7}$$

Where ν is the Poisson's ratio of the material and S the slope and stiffness of the initial part of the unloading curve. Equation 2.1 was used to obtain the derivative of the load, P. The Poisson's ratio for articular cartilage was assumed to range from 0.3 to 0.5. The difference in methods, location, and species make it challenging to determine an absolute value [56; 57]. In subchondral bone a Poisson's ratio between 0.28 and 0.33 was found [57; 58]. For this reason, a Poisson ratio of 0.3 was used to obtain the elastic modulus for all indentations in the matrix.
For every indentation matrix, heatmaps were created to observe the indented surface. All the single indentation curves were inspected to see if the OP-method fit the data. If it did not fit or if an error occurred during indentation, that indentation point was eliminated from further data analysis. The eliminated data points were then referred to as NaN and visualized as black boxes in the matrix.
Lastly, a Gaussian filter was applied to every matrix to identify the general regions of the different interface layers. A sigma of 0.5 was applied to the filter, which generates a kernel of $3x3$. A higher value for sigma would result in a greater kernel, which leads to a higher chance of eliminating the distinction of the thinner tissue layers. As mentioned before, the mineralized cartilage layer is thin. A higher sigma would possibly fade out the measured mechanical properties of this layer. The possible NaN values in a matrix were excluded from the Gaussian filter analysis in the MATLAB code (Appendix VI).

2.3.5 *Probe dependency*

Multiple probes were used in this research. It was assumed that the difference in the elastic modulus due to the varying probe properties would be negligible. To validate this assumption, pure cartilage of the same sample was indented by two probes with different stiffness properties and probe tips. Identical indentation profiles, similar to the previous indentations, were applied in a matrix of 4x4 indentations with 50 µm spacing between indentations in both directions (Figure 2.4) . Probes P1 (249 N/m, 8.5 µm) and P2 (254 N/m, 9.5 µm) were used as comparison, P3 (261 N/m, 8.0 µm) and P4 (283 N/m, 9 µm) had broken in the process of previous indentations. After indentations, the raw data was run through the MATLAB code with an OP-method analysis. The mean and standard deviation of all the indentations in the two matrices were retrieved and compared.

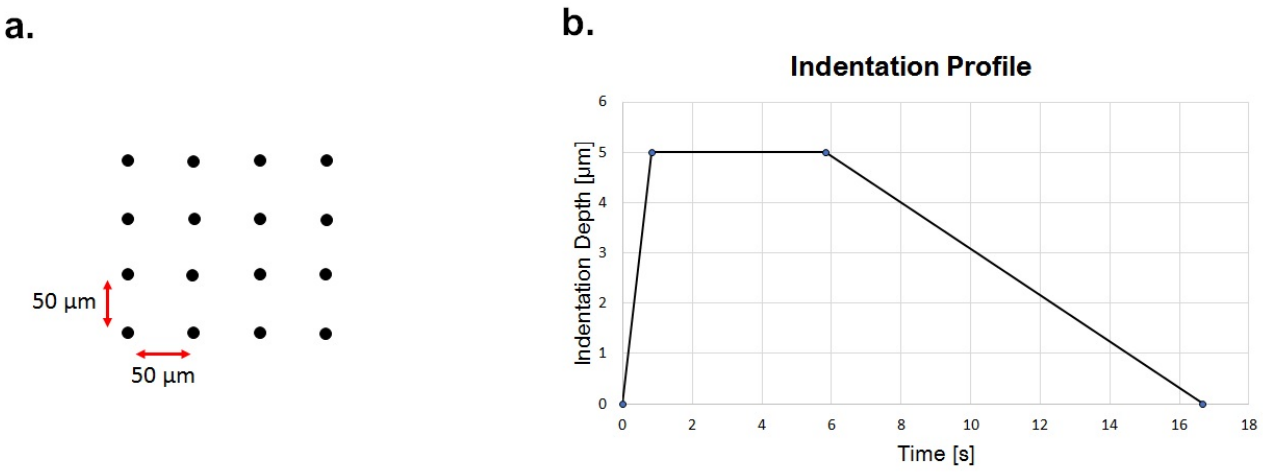

Figure 2.4: The indentation matrix and profile for the probe dependency tests. a.) The indentation matrix with 50 µm spacing between indentations. b.) The indentation time and depth profile.

2.3.6 *Plastic deformation*

The force-displacement curve generated by the nanoindenter cannot demonstrate plastic deformation, due to the viscoelastic behaviour of the tissue. In this research, three indentation matrices were performed at the same location. For that reason, it was important to know if the indentations left any damage for the following matrices. To investigate this, indentations were performed on a mature sample and analyzed with scattered electron microscopy (SEM, JEOL JSM-IT100, Tokyo, Japan). The mature sample was thawed in 1X TBS with protease inhibitors overnight at 4 °C in a plastic petri dish. The indentations were performed in a 4x8 matrix with 250 µm spacing in between to ensure indentations were made in the bone region. After indentation, the sample was dehydrated by immersing it in ethanol series and hexamethyldisiloxane (HDMS) for 15 hours each. Finally, the sample was left in the recirculation cabinet overnight and stored in a closed plastic petri-petridish at 4 °C. The day of testing, the sample was allowed to reach room temperature. Following, the sample was retrieved from the dish and coated with a thin gold layer, to improve electrical conductivity. Thereafter, the sample was placed in the microscope and images of the indented area were made with a electron beam energy of 10 kV and a working distance of 10 mm.

2.4 COMPRESSION WITH DIGITAL IMAGE CORRELATION

In this study, a novel method has been used to characterize the mechanical properties of the osteochondral interface. Compression tests were performed on the samples with Digital Image Correlation (DIC) analysis (Limess, Krefeld, Germany). This technique made use of two high resolution cameras, which tracked the the strain in a certain region of interest. From this, the strain distribution over the interface was determined.

2.4.1 *Sample Preparation*

For the compression tests, three samples from every age group were used, which had also been used for nanoindentation previously. The samples were required to have

a constant height over the thickness of the sample so that the the contact area could be determined. For this reason, the samples with the least curves were selected for these tests. The selected samples were A-1-LP, A-2-L, A-3-MD, Y-13M-MD, Y-13M-MP, Y-13M-LD, Y-7W-L, Y-12D-L, Y-9D-M. Before testing, the samples were thawed in 1X TBS with protease inhibitors solution overnight at 4°C. In order to ensure strain observation, a random speckle pattern was created on the surface. The pattern was applied by an airbrush and the use of white and black acrylic primer paint. This paint had hyperelastic properties, thus behaved elastically to the deformation. First, the white paint was applied over the entire surface, thereafter the black speckles were applied. After the paint had dried, the samples were placed on the compression plate for testing one after another (Appendix V).

2.4.2 *Compression Test*

The cameras were positioned as close to the sample as possible and calibrated. After calibration, the compression tests were executed. The set-up for the DIC consisted of a Lloyd LR5K compression machine with a 5 kN load cell. In addition, two high resolution cameras, connected to a PC, and an UV-light source, were focused on the sample (Figure 2.5). The samples were subjected to a single compression deformation of 1-2 mm, till the entire osteochondral interface was subjected to strain, with a compression speed of 1 mm/min. After testing, a mark was left on the samples from the compression plate. This area was measured and assumed as contact area of the plate. Thereafter, the samples were stored at -20 °C for possible further observation.

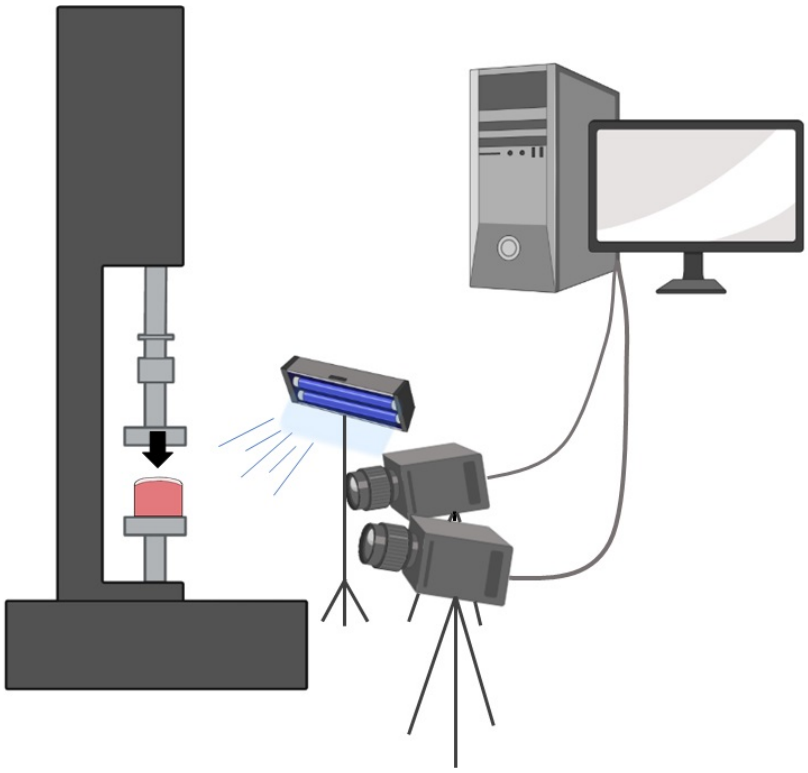

Figure 2.5: Digital Image Correlation Experimental Set-up

2.4.3 *Data Analysis*

The strain distribution was determined using Istra4D software. In the force-time curve a clear linear region was detected. A time-step within this linear region was selected for further analysis (Appendix IV). The selected step was where the force was high to ensure that deformation of the entire interface had been reached. At this step, five strain lines with the length of the distance of the osteochondral interface were created per sample (Figure 2.6). From these five strain lines, the true principal strain in the compression direction was determined over the length. Lastly, the mean of the strain distribution of the five curves was obtained per sample.

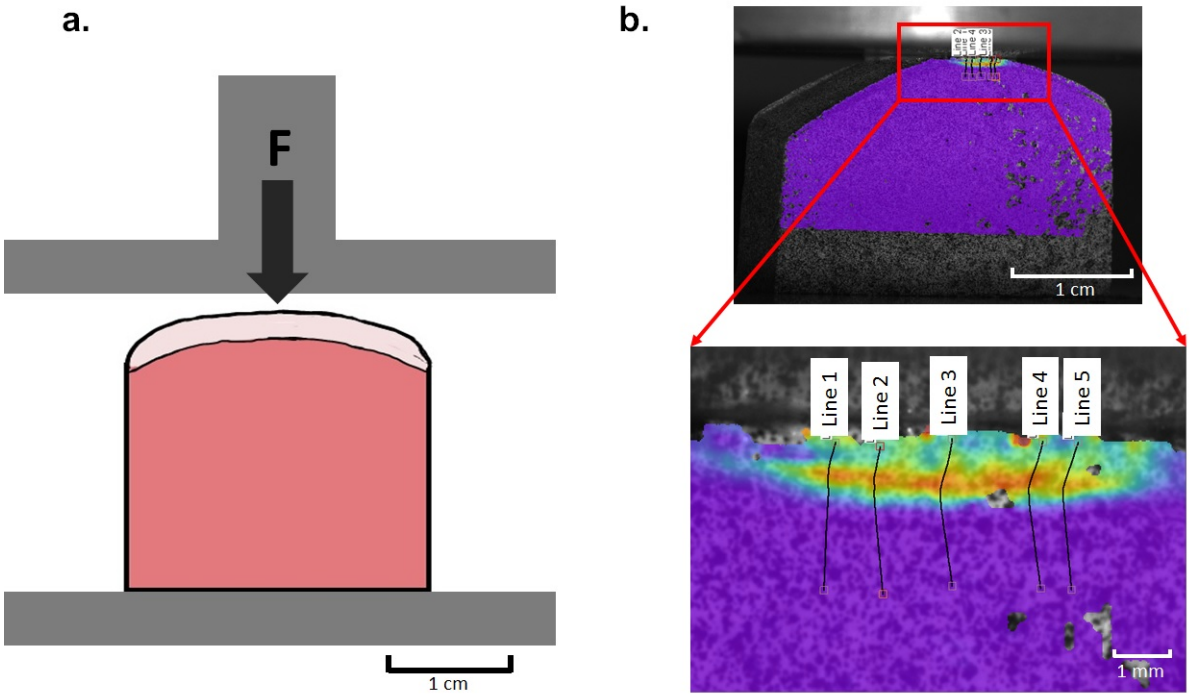

Figure 2.6: DIC data analysise. (a.) Schematic overview of the sample on the compression plates, where F is the constant compression force applied on the sample. (b.) An example of a sample during compression, where the five analysis lines have been selected at a certain time step.

3

RESULTS

3.1 STRUCTURAL DEVELOPMENT OF THE OSTEOCHONDRAL INTERFACE

To visualize the structure of the osteochondral interface of the different joints at a microscopic level, the HE staining was used to identify the different tissue types and the chondrocyte pattern, the RGB staining to identify the calcified zones within the different layers and the Saf O to visualize the proteoglycan distribution in the articular cartilage (Figure 3.1). The cartilage layer of the sample from the 9 days old joint, was thicker than the 13 months old and mature cartilage. In addition, cartilage canals were present in the immature cartilage, marked as an intersection of a vessel in the deep zone of the cartilage. Furthermore, in the 9 days old subchondral bone, the structure was highly porous and no clear border mark was detected between the two types of tissue. In addition, a high density of hypertrophic chondrocytes could be found in the deep zone of the articular cartilage (Figure 3.1). This also applied to the histology images obtained for the 12 days and 7 weeks old interface (Appendix IV).
The interface of the 13 months old interface, showed a reduction in cartilage thickness and compact subchondral bone layer with an emerging border between the articular cartilage and bone. In the mature interface, the different layers and zones are highly defined. A clear calcified cartilage layer was present, including tidemarks, in all the mature interface stainings. In these images, the deep zone of the articular cartilage clearly showed a column structure of chondrocytes compared to the more superficial layers (Figure 3.1). Furthermore, histology demonstrated that the cell density in the interface decreased with increasing age.
For all the samples, the superficial layer of the cartilage contained the highest density of chondrocytes and collagen fibres as visible on the RGB staining (Figure 3.1). The Saf O stains demonstrated that the deep zone of the cartilage was darker red than the transitional and superficial zone for all the samples. This indicated that the proteoglycan density was highest in the deep zone of the articular cartilage.

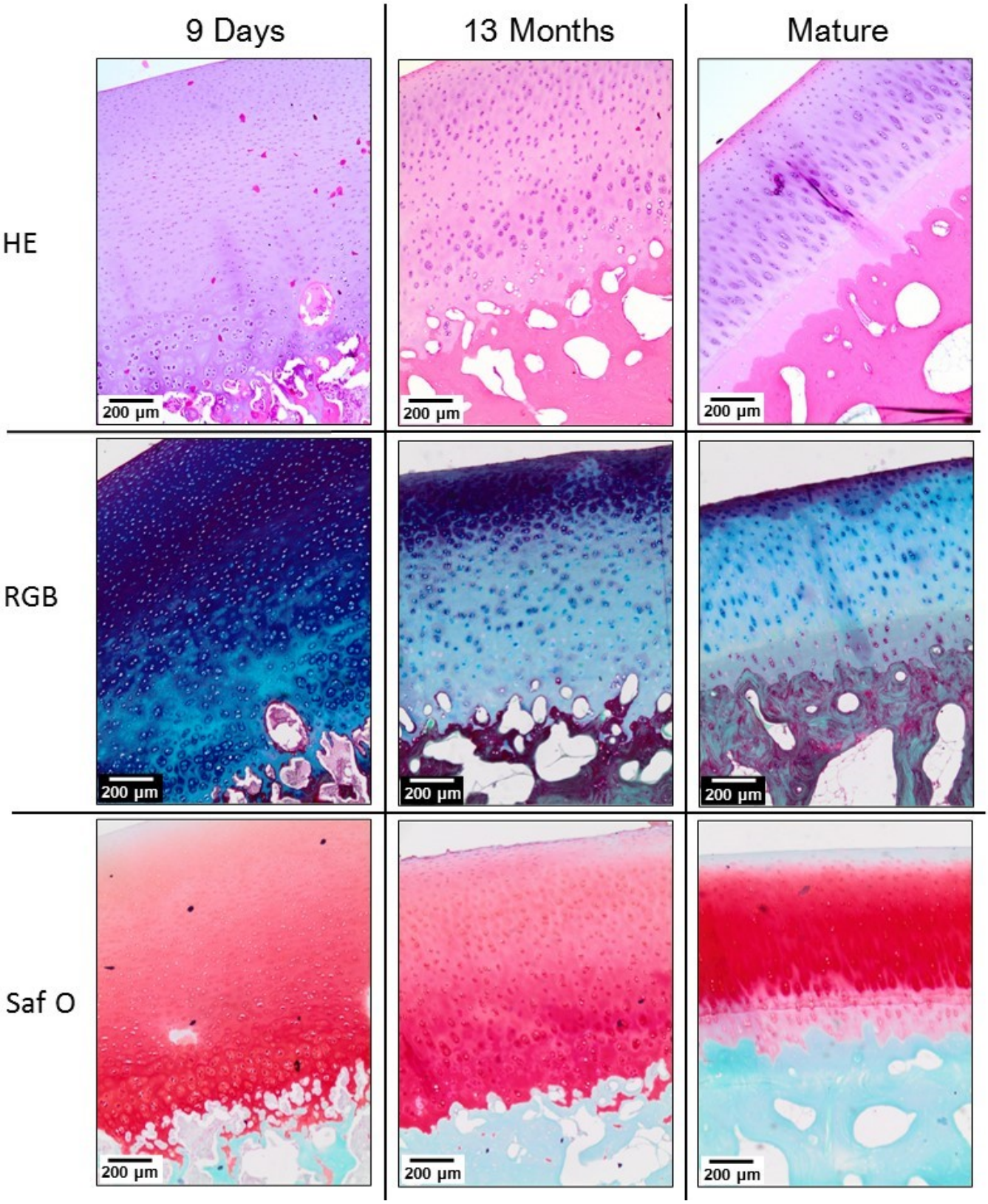

Figure 3.1: Histology of the osteochondral interface. Samples of the 9 days old, 13 months old and a mature joints are presented from left to right for HE, RGB and Saf O staining. In the RGB stain, the bright blue represents the proteoglycan density, calcified cartilage turns pink-green and mineralized bone green. For the Saf O stain, the intensity of the stain refers to the proteoglycan density in the tissue.

As mentioned above, the tidemarks were clearly visible in the mature samples. These tidemarks were a clear border between the articular and calcified cartilage. In all the samples of the mature interface, multiple tidemarks were detected (Figure 3.2 and Appendix IV). The 9 days old osteochondral interface did not show any tidemarks or presence of calcification in the deepest zone of the cartilage, this also applied for the other young interfaces (Appendix IV). The 13 months old interface, however, demonstrated a potential, extremely light, tidemark border line (Figure 3.3 a.). The HE staining images were observed closely along the deep zone of the interface and the arrows indicate a light change in colour along a border.
The calcification of the subchondral bone during maturation was demonstrated with the RGB staining (Figure 3.3 b.). In the 9 days old subchondral bone, some green stains were detected in the deeper parts of the bone, indicating calcification. While in the 13 months old subchondral bone, a clear increase of green staining was observed, thus an increase in calcification. In the mature sample, the subchondral bone was fully calcified especially towards the osteochondral interface.

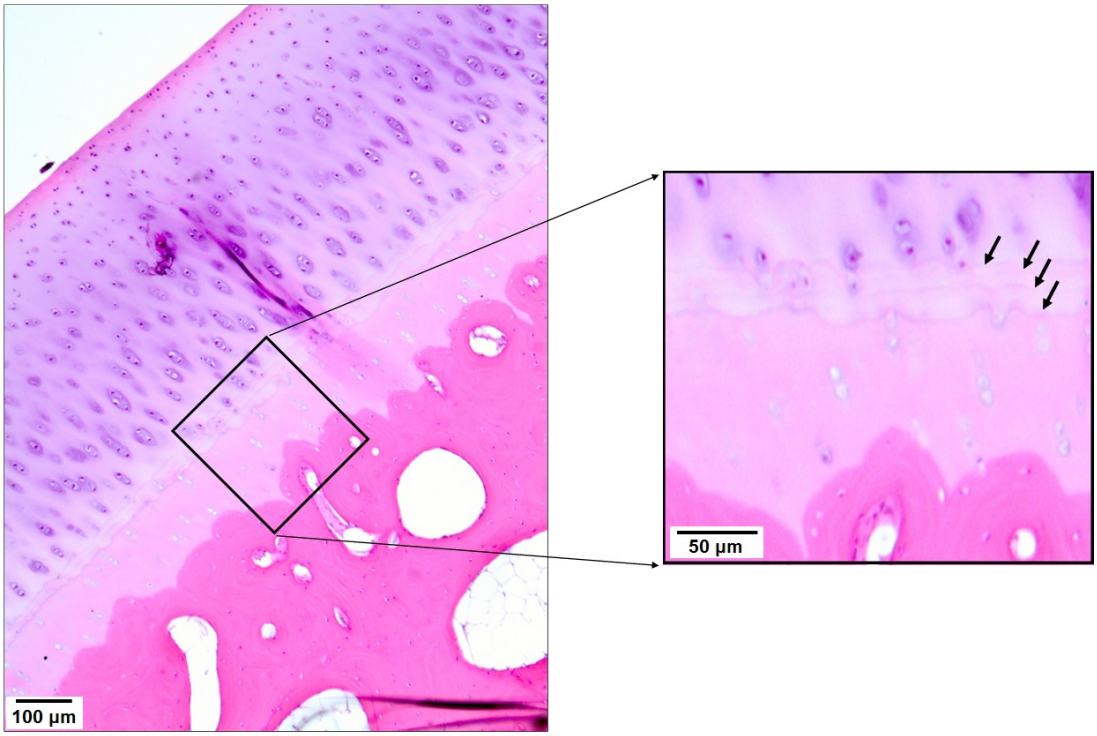

Figure 3.2: Multiple tidemarks between the calcified cartilage and articular cartilage in the mature interface. The tidemarks are indicated with the black arrows in the zoomed image (right).

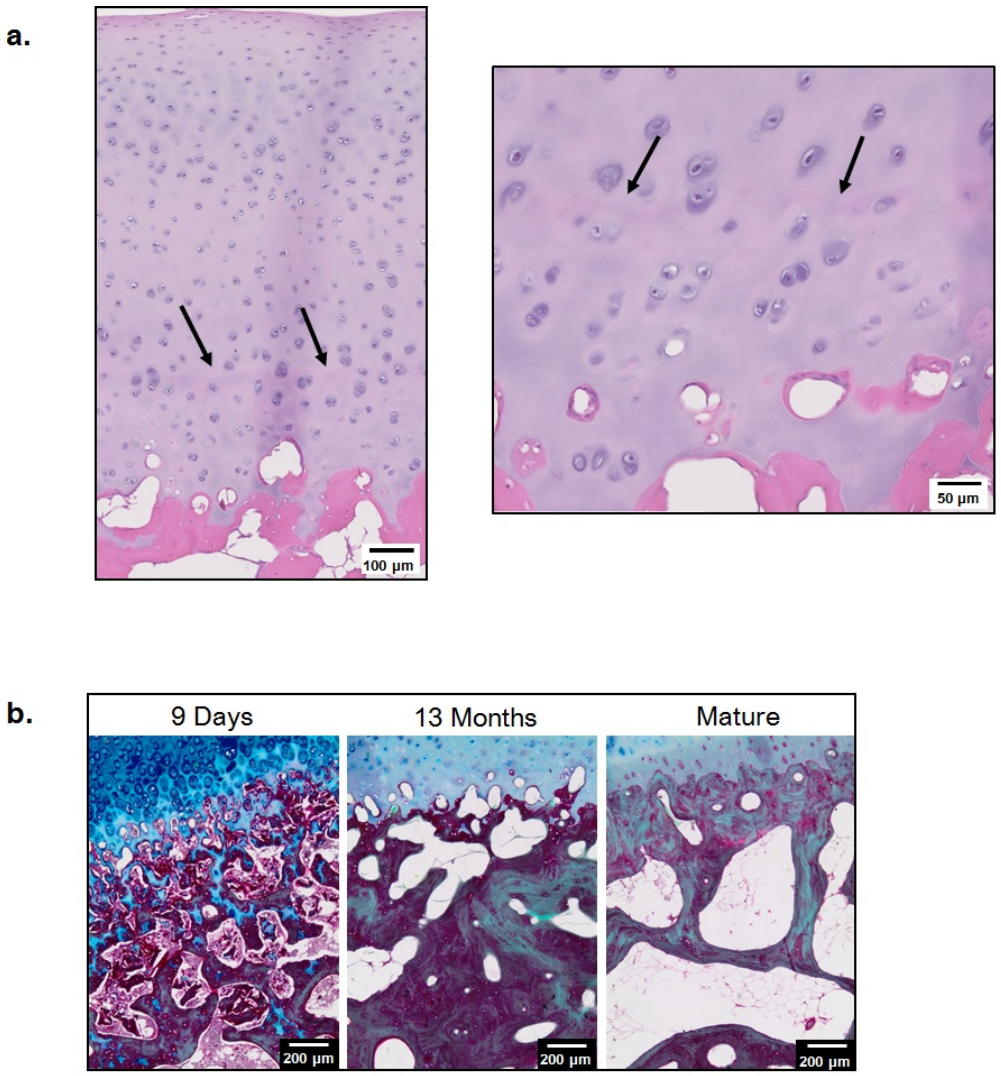

Figure 3.3: The calcification of the cartilage. a.) The RGB staining of the subchondral bone for the 9 days old, 13 months old and mature joints, where the calcification is indicated by a green stain. b.) Emerging tidemark in the HE staining of the 13 months old joint, indicated by black arrows (left) and a zoomed in images of the emerging tidemark (right).

3.2 THE LOCAL ELASTIC MODULUS

A nanoindentation matrix measurement was performed on every sample to locally measure the elastic stiffness of the natural tissue interfaces, which was repeated three times for every sample. Due to the uncertainty of the plastic deformation and the spatial resolution of the nanoindenter machine, the first matrix of every sample was used for further analysis. In this section, the main results obtained from nanoindentation will be presented. A complete overview of all the heatmaps for all the samples was included in Appendix IV.

3.2.1 *Scale of Indentations*

The heatmaps presented in this chapter showed each indentation by a blue coloured square. However, it is important to note that the indentations were made with a certain

space between each indentation. Therefore, the histology images were used to create a scaled indentation matrix to show the true distribution of indentations (Figure 3.4). It should be noted, that these scaled indentations are merely an indication. These are not the true indentation locations as this could not be seen with the nanoindenter. Therefore, the comparison between the histology image and the heatmap is to show how the indentations are translated and not the exact indentation locations.

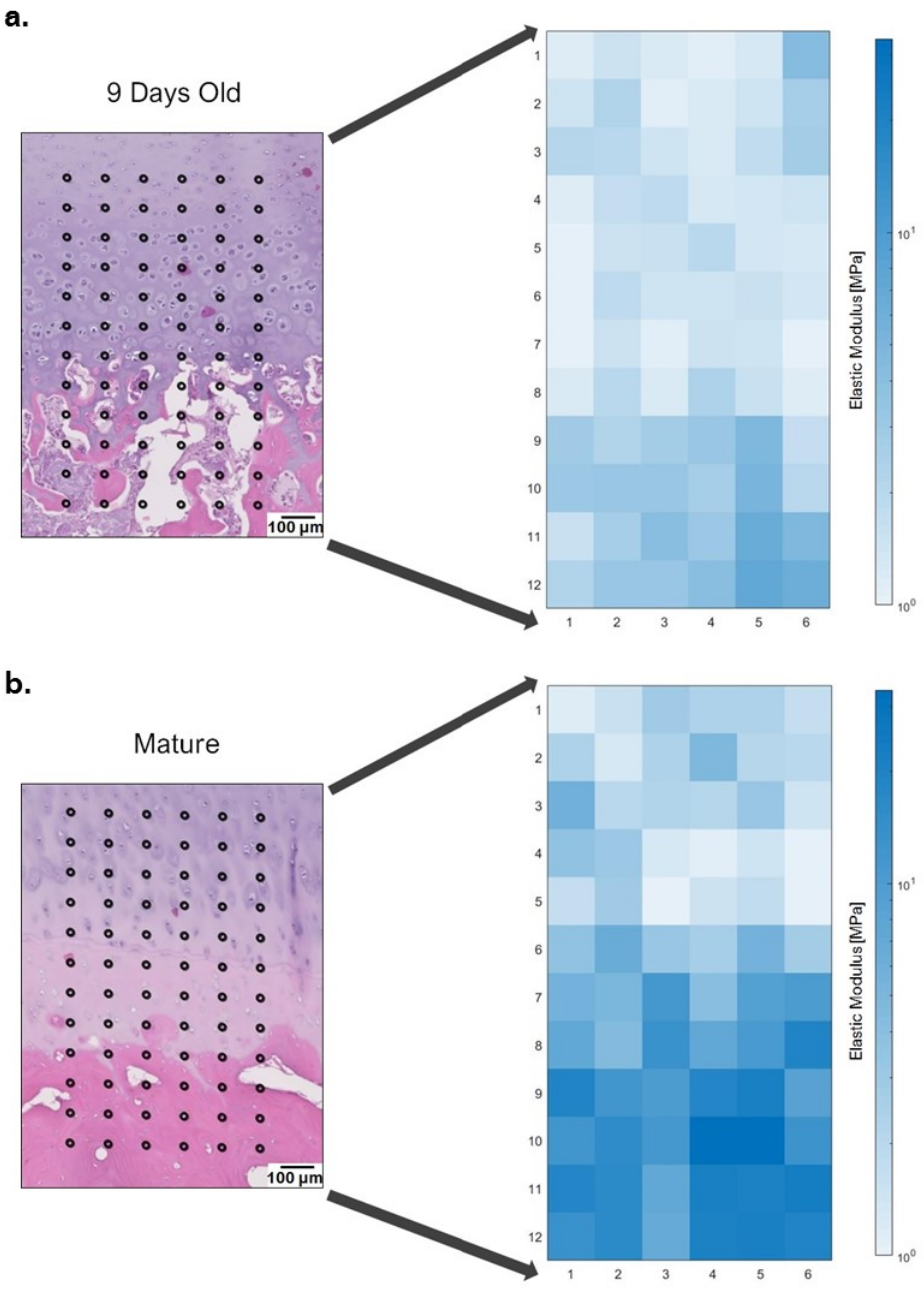

Figure 3.4: An indication of the location of the indentations in the matrix translated to the heatmap. The indentations were scaled to the histology image by use of the Nanozoomer. a.) The indentation matrix of a 9 days old interface and b.) of a mature interface.

3.2.2 *The Mature Interface*

For all the samples of the mature interface, a clear transition from a low to a higher elastic modulus value could be detected (Figure 3.5 and Appendix IV). Since the indentation matrix was positioned manually, the interface was not positioned at the exact same location within the heatmaps of the samples of the joint. Therefore, the heatmaps were arranged in such a way that the transitional region of the elastic modulus values were aligned. The rows of the heatmap define the distance over the osteochondral interface. From 400 µm deep, darker regions, thus higher values, emerged. Below this region a heterogeneous pattern was found of lower and higher values of the elastic modulus.
The alignment was performed for all the mature joints and from the transitional region, the mean and corresponding standard deviation of the elastic modulus were calculated (Figure 3.6). For the first to indentations for each joints, the pure articular cartilage was indented and the values remained similar to each other. The mean value of the articular cartilage was approximately 2.82 ± 1.03 MPa. From 150 µm distance from the starting point, the values started to increase. The increase in Adult 1 was more gradual compared to Adult 2. In addition, Adult 3 showed a slight increase at 150 µm, however, showed a large increase from 600 µm. The maximum value found for each joint was 37.58 ± 17.30 MPa for Adult 1, 36.88 ± 20.21 MPa for Adult 2 and 124.43 ± 111.01 for Adult 3. Lastly, the standard deviation increases with the distance over the interface.

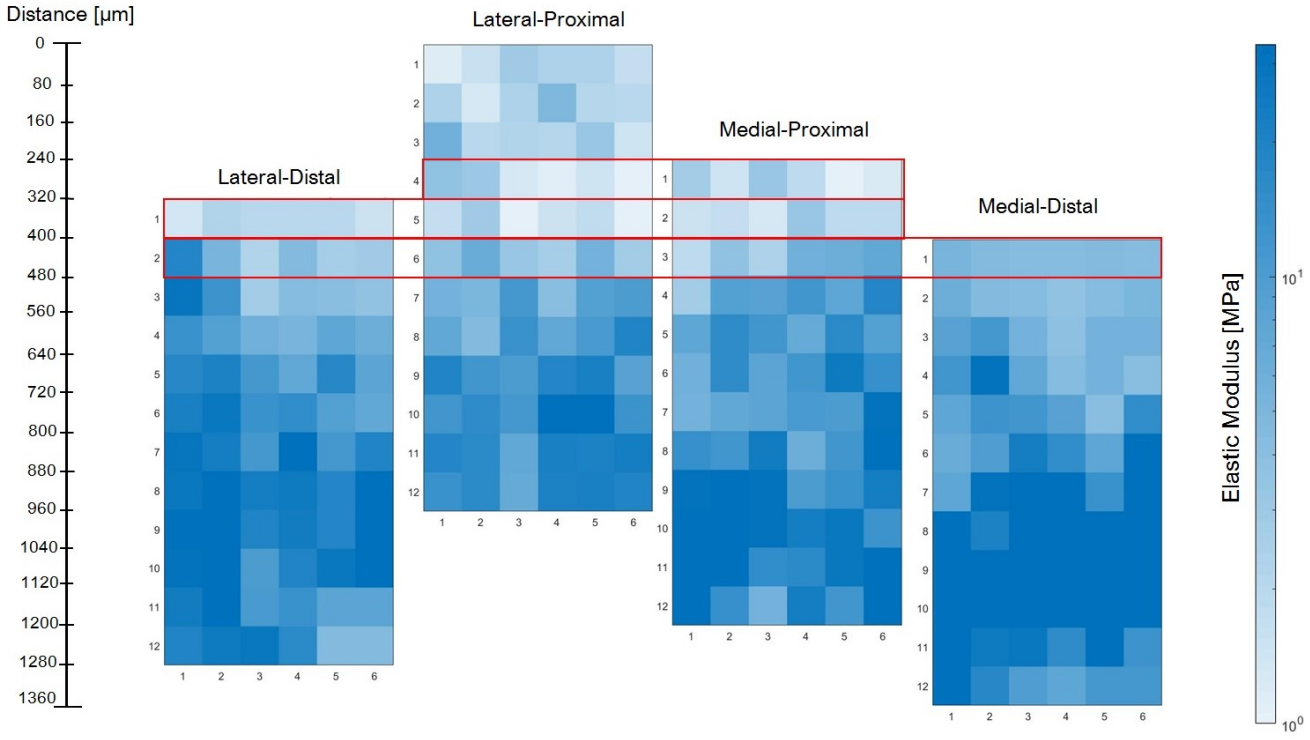

Figure 3.5: An example of heatmap alignment of the samples of the Adult 1 osteochondral interface. The red boxes show the values based alignment. The logarithmic scale bar indicates the value of the elastic modulus in the heatmap. The titles of the heatmaps are to specify the location of the sample in the joint. The distance (left) shows the length of the indentation matrix over the interface.

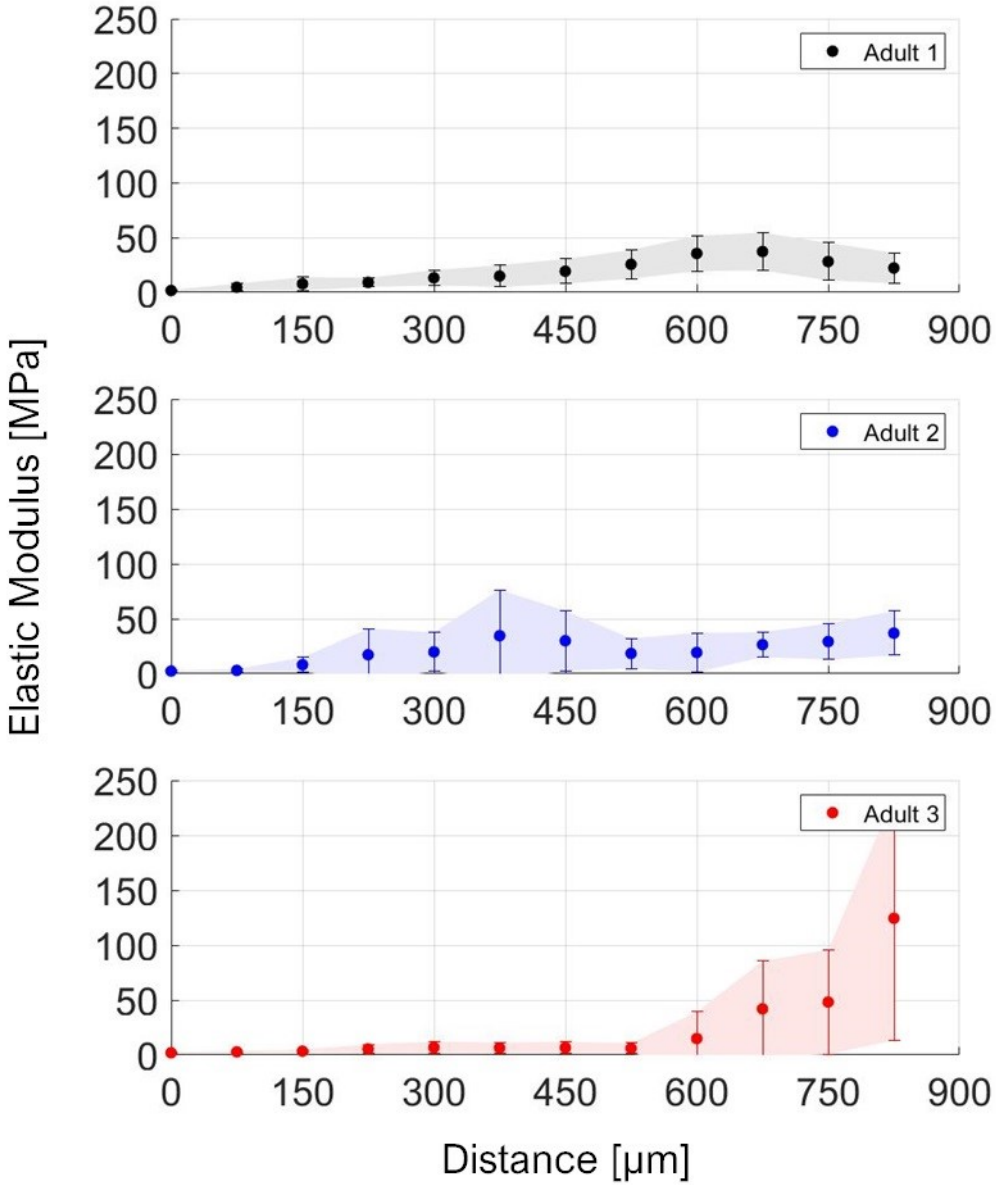

Figure 3.6: The average elastic modulus distribution over mature interface of the joints of Adult 1 (top), Adult 2 (middle) and Adult 3 (low).The distance is the distance over the transitional region of the interface. The standard deviation is shown with the coloured patch.

3.2.3 *The 13 Months Old Interface*

For the 13 months old joint, the separate heatmaps showed a high variation between samples (Figure 3.7). For that reason, the heatmaps could not be aligned to obtain an average over the interface layers in the matrix. The Lateral-Distal and Medial-Proximal sample showed a transition from a low elastic modulus to higher values for the subchondral bone region. In the Medial-Proximal sample, a higher value of elastic modulus at 560 µm was followed by a lower region again between 640 and 800 µm, showing the heterogeneity of the subchondral bone region. The Lateral-Proximal sample, however, showed a completely random distribution, where high values were found distributed

over the entire matrix (Figure 3.7). The Medial-Distal sample showed a homogeneous heatmap of lower values for the elastic modulus. However, in the deeper region of this matrix, higher values started to emerge.

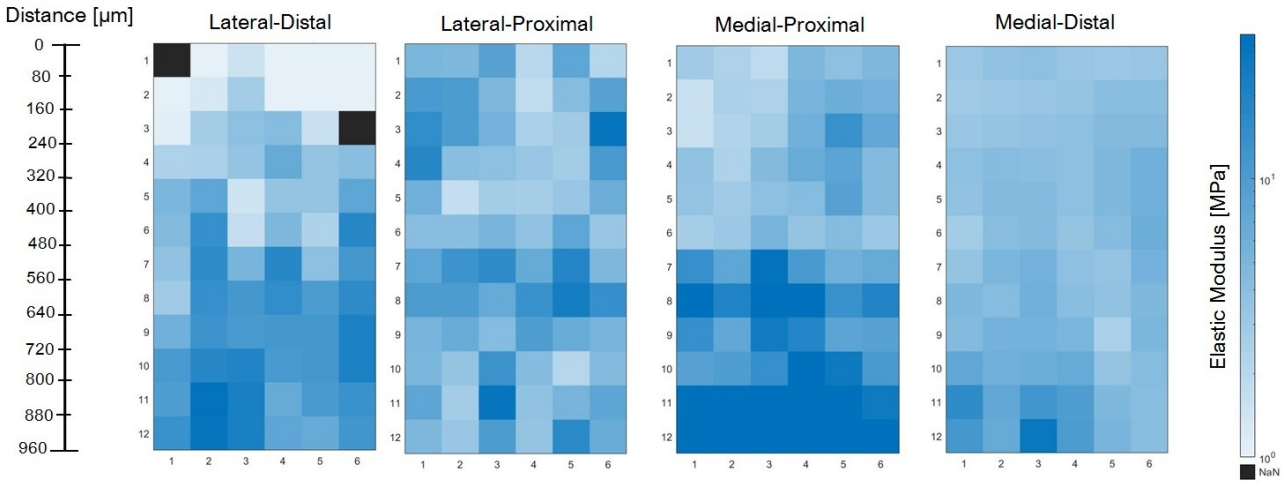

Figure 3.7: The heatmaps of the indentation matrix for every sample from the 13 months old joint. The logarithmic scale bar indicates the value of the elastic modulus in the heatmap. The titles of the heatmap are to specify the location of the sample in the joint. The distance (left) shows the length of the indentation matrix over the interface. The NaN-values in the Lateral-Distal heatmap represented eliminated data points.

3.2.4 *Youngest Interfaces*

The heatmaps of the 7 weeks, 12 days and 9 days old interfaces showed similar patterns of the elastic modulus distribution. A slight increase could be found towards the subchondral bone, thus the heatmaps were aligned according to this transitional region (Figure 3.8). In the heatmap of the lateral sample of the 7 weeks old joint a more defined transitional region could be found. The medial samples of the 7 weeks old interface was eliminated from further data analysis, due to the large amount of NaN-values, this also accounts for the medial sample of the 12 days old interface. In the 12 days and 9 days old interface, the heatmaps mainly consisted of low values for the elastic modulus over the entire region (Appendix IV).
The mean value and standard deviation over the heatmaps of all the youngest joints was determined (Figure 3.9). The value of the articular cartilage was in a similar range for all the joints up to 300 µm, which was approximately 1.58 ± 0.13 MPa. For the 7 weeks old joint, the values started to increase from this distance to a maximum of 10.28 ± 5.91 MPa. In the 12 days old and 9 days old joints, the values increased minimally. However, the standard deviation was found to be higher in the subchondral bone region of these interfaces. The maximum value of the elastic modulus for the 12 days old joint was 3.58 ± 2.78 MPa and for the 9 days old interface 4.48 ± 3.43 MPa (Figure 3.9).

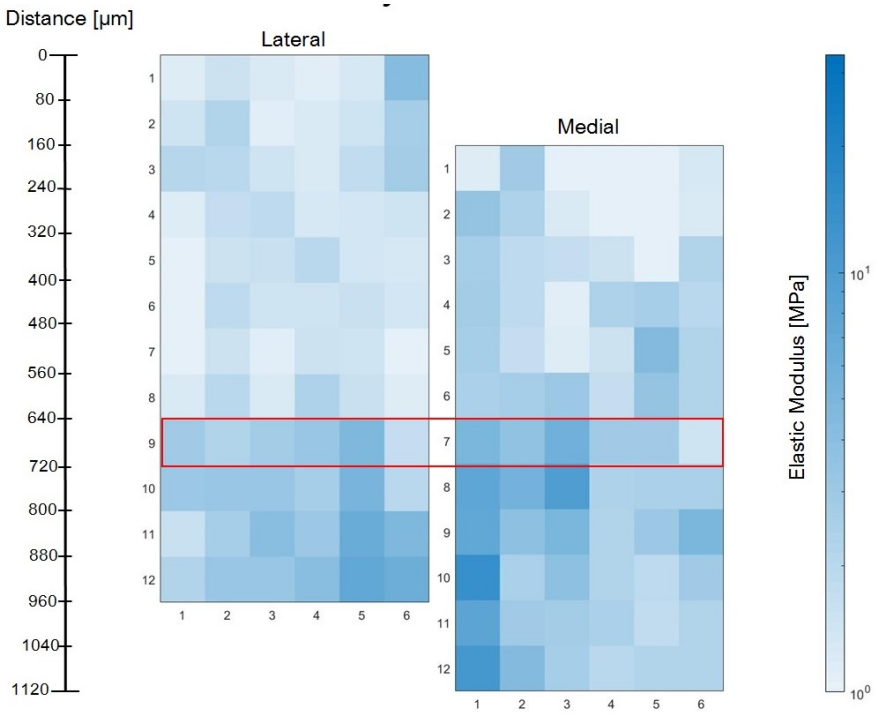

Figure 3.8: An example of heatmap alignment of the samples of the 9 days old osteochondral interface. The red box shows the values based alignment. The logarithmic scale bar indicates the value of the elastic modulus in the heatmap. The titles of the heatmaps are to specify the location of the sample in the joint. The distance (left) shows the length of the indentation matrix over the interface.

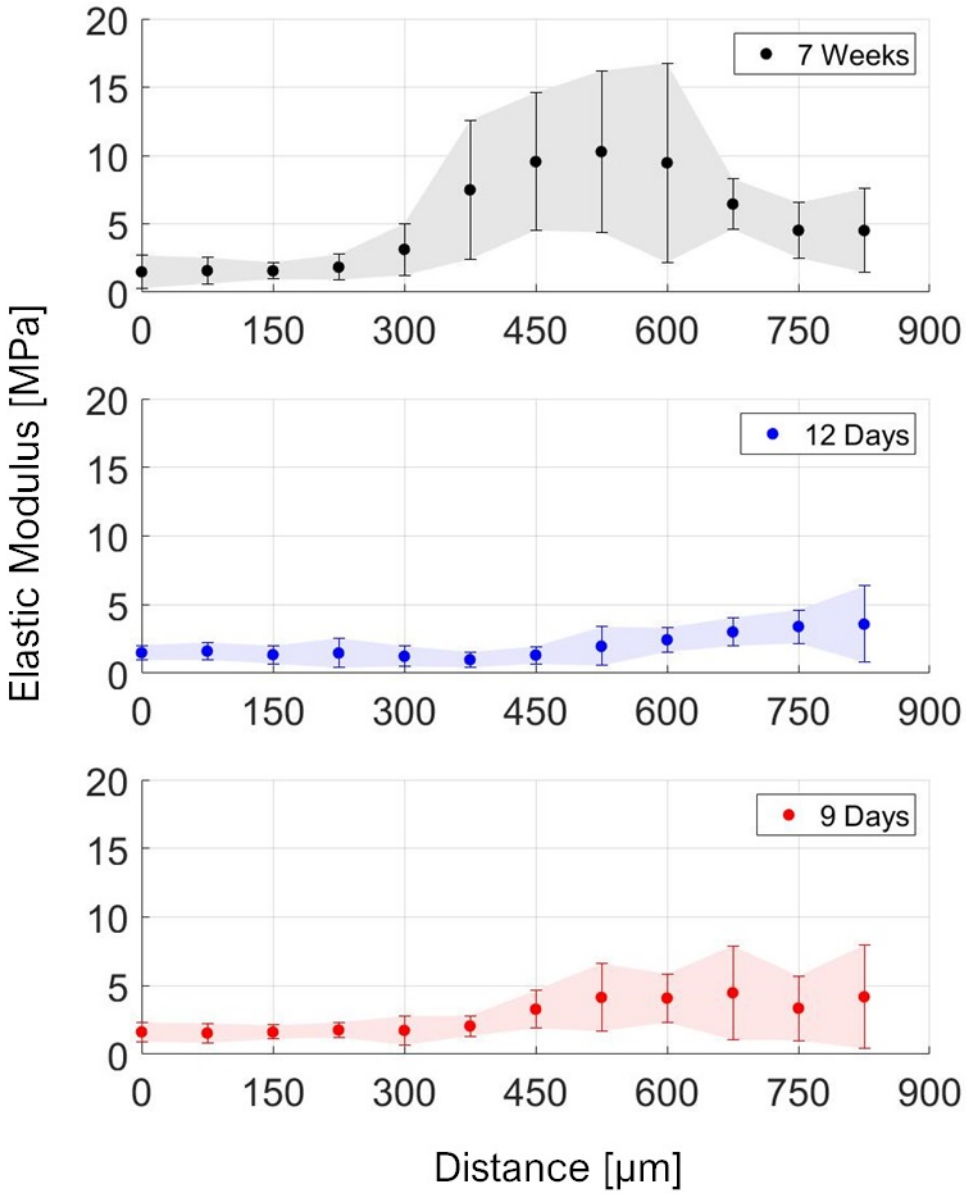

Figure 3.9: The average elastic modulus distribution over immature interface for the 7 weeks old (top), 12 days old (middle) and 9 days old (low) joints.The distance is the distance over the transitional region of the interface. The standard deviation is shown with the coloured patch.

3.2.5 *Probe dependency*

The probes used for the Piuma nanoindenter were highly sensitive and fragile, thus broke easily. For that reason, multiple probes were used during the measurements. Pure cartilage was evaluated with two different probes to obtain more knowledge of the possible effect of the probe properties on the resulting elastic modulus. The mean of the elastic modulus and the corresponding standard deviation were determined per probe 3.1. The two probes tested were P1 (249 N/m, 8.5 µm) and P2 (254 N/m, 9.5 µm). The values of the elastic modulus remained in a similar range. Thus, the effect of the

difference in probe properties was considered negligible for further analysis.

Table 3.1: Influence of different probe stiffness

Probe	Elastic Modulus [MPa]
P1	2.51 ± 1.01 (N=16)
P2	2.18 ± 0.85 (N=16)

3.2.6 *Plastic Deformation*

A sample of a mature joint was observed with SEM to observe if any plastic deformation was caused by the probe during indentation. The interface showed a high rate of damage and over the entire sample, due to the crosscut saw (Figure 3.10). As a consequence of all these dents, a clear mark of the indentation matrix could not be detected in the indented region. In addition, the geometry of the probe was spherical, thus the shape of the plastic deformed dent was challenging to recognize. For that reason, the plastic deformation was assumed negligible for the nanoindentation data analysis.

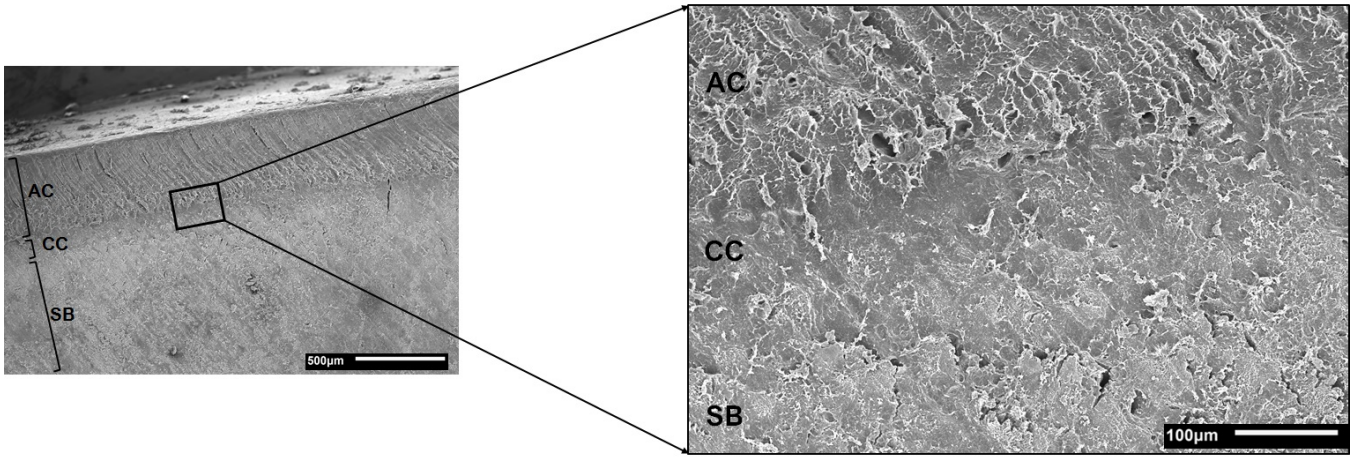

Figure 3.10: SEM images of the indented area on the mature osteochondral interface. The regions visible were the articular cartilage (AC), calcified cartilage (CC) and the subchondral bone (SB). One image is zoomed in 50x (left) the other 200x (right).

3.3 INTERFACE STRAIN DISTRIBUTION

Uniaxial quasi-static compression tests were performed to determine the strain distribution over the interface with the DIC method. The distributions were analyzed by age group (Figure 3.11 and Appendix IV). The interface of Adult 2 and Adult 3 showed a low strain value over the entire distance, thus a clear transitional region of this mechanical property could not be detected (Figure 3.11 a.). In contrast, the sample from the joint of Adult 1 showed the highest strain value for the articular cartilage of all the samples in total. However, a corresponding high standard deviation was visible in the articular cartilage region.
In the strain distribution of the 13 months old interface samples, a transitional region of the strain values could be clearly detected (Figure 3.11 b.). At 0.5 mm distance from the superficial cartilage layer the strain was approaching 0. In addition, the strain value was higher than most of the mature samples, indicating that it was less stiff than the mature articular cartilage.
The strain in the cartilage region of the 7 weeks old interface was higher compared to the 12 months old interface (Figure 3.11 c.). In addition, the transition to a lower strain occurred at 0.5 mm, while for the 12 months old interface this started at 1 mm. A higher standard deviation was found in the transitional region compared to the other regions in the strain distribution. For the three different groups, the interface distance varied (Figure 3.11). The transition distance was largest for the youngest samples and decreased with age. This is due to the fact that the cartilage thickness decreased with age (Appendix II, Table 6.3).

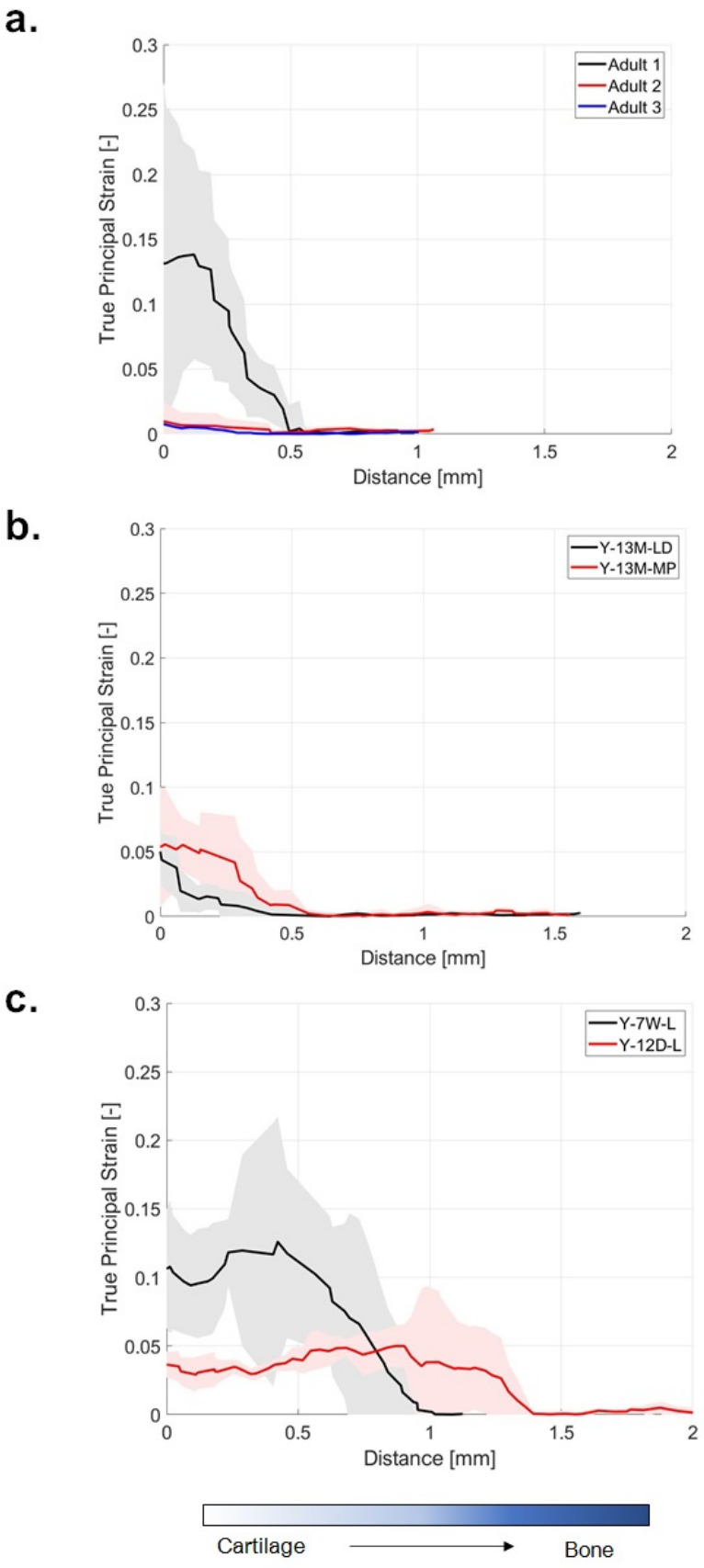

Figure 3.11: The averaged true principal strain along the interface, where the distance is from the superficial layer of the cartilage to the subchondral bone. The strains are presented in the different age groups. a.) Strain distribution of the three mature interfaces, b.) the distribution of two samples of the 13 months old interface and c.) the distribution over the 7 weeks and 12 days old interface. All distributions show a corresponding standard deviation.

4

DISCUSSION

The aim of this research was to characterize the structural and mechanical properties of the osteochondral interface during maturation. The structure and organization of the interface was visualized by use of histology. Nanoindentation and compression tests with DIC were used to obtain the stiffness of the different tissue types over the interface.

4.1 TISSUE SAMPLING

The nanoindenter used in this study, has not been used to perform indentation measurements over the complete interface before. Therefore, it was crucial to create samples that provided a smooth surface and had a clear visual transition from cartilage to bone. The joints provided in this study, were equine metacarpo- and metatarsophalangeal joints, which have a thick cartilage layer. As stated before, it is important to consider the difference in tissue configuration between different anatomical sites. Furthermore, the difference in loading conditions for the different areas of the joint itself should be considered. Thus, all the results obtained in this study are only applicable for this type of osteochondral interface.
The mechanical samples were retrieved from the lateral and medial condyle of the cannon bone. However, due to the thickness of the samples, it was challenging to obtain samples with a complete straight top surface, indicating that it included a section of the condyle on which less force was submitted during life than other parts of the sample. As mentioned before, the formation of the structural organisation of cartilage and the interface is, amongst other things, stimulated by mechanical force. Resulting in a possible difference in structure and stiffness within the samples.
Another important note, is the fact that the exact age of the mature joints was unknown. In addition, the cause of death had not been specified for any of the horses. Macroscopic inspections revealed no damage of the immature joints. However, for the adult joints, some wear marks could be detected, indicating signs of osteoarthritis. The stiffness of the interface has found to increase in joints with osteoarthritis, thus this could have had an effect on the results obtained in this research [59; 60; 61].
To section the samples for histology, separate samples had to be made since the mechanical tests could damage the samples. The assumption made in this study, is that the distribution of the different tissue types remains constant over the condyles of the joint, while in reality this could vary by several micrometer and, as mentioned before, have structural variations [16; 18; 62].

4.2 HISTOLOGY

Three different stainings were used to observe the structure, proteoglycan distribution and observe the calcification. Multiple tidemarks were detected in the mature joint. This could suggest that the horse was older of age, since the amount of tidemarks increases with age [63]. However, an increase in tidemarks could also be an indication of osteoarthritis [32; 64]. The tidemark is caused by the mineralization of the cartilage, which happens in both aging and osteoarthritis. Thus, both causes should be considered when analyzing these histology images.
For the joint of 13 months old, a light tidemark could be detected. It was found that horses can obtain tidemarks in the femoral condyle from the age of 12 months [15]. For this reason, it was thought that the slight line detected in the histology, can be considered as an emerging tidemark.

4.3 NANOINDENTATION

In the nanoindentation matrix for the mature interface, a clear difference could be detected between the different stiffness regions. This was assumed to be an indication for the different tissue types, articular cartilage, calcified cartilage and subchondral bone. From the heatmaps, it could be strongly suggested that the lower values in the top rows are in the non-calcified cartilage region.
As soon as the regions started to show higher values for the elastic modulus, the calcified cartilage or the subchondral bone region could have been entered. The space between indentations should have confirmed to indent at least one matrix row in the calcified cartilage. However, due to the uncertainty of the angle of placement of the sample and the exact indentation location it could have skipped the calcified cartilage. In addition, it could be that a pure cell was hit instead of the extra-cellular matrix. The radius of the probe is found to be smaller than the average chondrocyte [65]. Anything smaller than 8 µm in the tissue could not be indented fully, thus would result in a stiffness measurement of the surrounding tissue. Furthermore, a Gaussian filter was applied to the nanoindentation data. The kernel was selected in such a way that the elastic modulus of the calcified cartilage layer would not be completely blurred out. However, it cannot be guaranteed that this was the case. Lastly, it cannot be excluded that the calcified cartilage might have had similar mechanical property values as the subchondral bone. This would explain the absence of a distinct difference in values between the subchondral bone and the calcified cartilage [43; 61]. However, it should be mentioned that this has been measured with different equipment and set-ups than used in this study. The main limitation is the lack in knowledge of the location of indentation, which makes it challenging to clearly assess the single indentation results. A Hysitron Nanoindenter (Bruker, Billerica, U.S.A.) , for example, could indent a specimen with higher location precision and environmental factors are of less influence as the indenter can be completely covered by the machine [66; 67; 61]. Another alternative measurement equipment is Atomic Force Microscopy (AFM). This technique performs indentations on nano-scale and makes use of a microscope, thus the indentation location can be defined [43; 68].

For the non-calcified cartilage region, the values for the elastic modulus demonstrated a low variation. The main explanation for this was the homogeneous structure. Towards the subchondral bone, an increased standard deviation was found. This results from the

distribution of low to high values in the subchondral bone region. This suggests that obtaining the average over the horizontal indentations, would not lead to an accurate end result of the exact elastic modulus for the interface layers beneath the non-calcified cartilage. The average of the horizontal indentations can generate an indication in which region the indentations were made, however it cannot be used to determine the elastic modulus value of the heterogeneous subchondral bone layer.
The matrices for the different samples from the same joint can be aligned well for the mature horses. The difference in matrix location on the interface can be explained by the lack of visionary aid during the placement of the sample in the nanoindenter machine. Every sample is placed manually, thus variance in placement of the starting point is inevitable.
As mentioned above, the higher values, and thus dark blue squares in the heatmap, suggest it is indenting subchondral bone. Surrounding the darker points are squares of a lighter shade, suggesting it hit a pore filled with soft tissue. These lighter blue colours were also present in the transitional area between the subchondral bone and non-calcified cartilage, this could suggest that the calcified cartilage was indented in that region. However, it did not clearly present itself in a clear line, as it did in the histology images.
The heatmaps of the 13 months old joint were inconsistent with each other. An obvious value difference was found in the soft and stiff tissue, however, a transitional region could only be detected in two of the samples. One could argue that the different probes used could cause this difference, however, the validation of the probe dependency in this research showed that this had little effect on the elastic modulus of the non-calcified cartilage. It could, however, have an effect on a stiffer material, the subchondral bone in this case, which has not been tested in this research. Lastly, the bone region seemed more compact in the histology images for the 13 months old interface, which could be seen in the higher values present in some of the heatmaps.
The youngest interfaces in this study, the 9 days and 12 days old, were clearly different from the older interfaces. The values of the these heatmaps remained low over the entire interface and little to no detection of high values were found within the subchondral bone. The value for the immature cartilage was slightly lower compared to the values found for mature non-calcified cartilage. However, they remained in the same range. Some darker, and thus higher, values were detected deeper into these young interfaces, indicating that the subchondral bone had been indented. An explanation for the low values for the entire immature interface could the absence of calcification. Mineralization of the tissue occurs in a later stadium of maturation and results in a stiffer material [59; 42].In addition, the subchondral bone in the immature interface was highly porous and the chance that the probe indented bone was lower than in the older interfaces.
Overall, the values found for the non-calcified cartilage were in line with the values found in previous research performed with the Piuma Nanoindenter [46]. It must be said, however, that the measurements in Moshtagh (2016) were performed axially on the articular cartilage and not in the transverse direction [46]. Cartilage can be described as an anisotropic material, thus it was expected that different values would appear for different measuring directions [38]. The similar values can be explained due to the scale of the measuring method. Bundled collagen fibres have an effect on the mechanical properties, while a single or a few fibres could have little effect on these properties in the nano-scale.
The values for the subchondral bone found in this research, cannot be validated by previous research with this method. The Piuma Nanoindenter has not been used before

to perform measurements on subchondral bone and every measuring technique results in a different outcome. For that reason, it was challenging to find an absolute value for the stiffness of this tissue type. The elastic modulus is a property that can be measured with several methods on different scales all resulting in a different stiffness values [61]. In this study, conclusions on the elastic modulus were made from the values relatively to each other instead of comparison with results from previous research with other measuring techniques.

It is important to comment on the fact that the squares in the heatmaps represent the indentation matrix. The indentations were made with 80 µm in between them. The squares that represent the indentations were connected in the heatmaps, however, in reality the indentations had some space between them. In between the indentations small pores or variety in the structure could be present, thus the heatmaps should not be considered to be a complete overview of the matrix area.
A limitation in this study, as mentioned above, was the use of different probes for the different samples. Due to the sensitivity, multiple probes broke during indentation, thus different probes were used, albeit in the same range of 249 to 283 N/m cantilever stiffness and 8 to 9.5 µm for the tip radius. The difference between two different probes was tested on articular cartilage. Unfortunately, not all the probes could be tested due to damage, limiting the probe dependency validation. In addition, the probes were only tested on a softer tissue and not on the stiffer tissue due to the homogeneous properties of cartilage. For this reason, we cannot completely exclude a slight difference in elastic modulus due to the difference in probe properties. Furthermore, due to the high sensitivity of the probes, environmental factors, like disturbance movement in the lab, could also have had an effect on the results. However, these effects were considered to be negligible as the movement in the lab was minimized during indentations. In addition, the calibration factor was never exactly the same for every calibration, which could also have minimal effect on the force-displacement curves. Lastly, the surface roughness was of great importance for nanoindentation [69; 70]. A high surface roughness could have been created by cutting the samples with a circular saw. Bovine osteochondral test samples were cut with the circular saw and polished with a Dremel (Dremel, Racine, U.S.A.) to determine if polishing the interface would decrease surface roughness (Appendix I). However, polishing the surface after cutting created a higher surface roughness for the articular cartilage. The Dremel was used manually with the smoothest polishing stone available. For future research, higher smoothness might be achieved with a diamond wheel point. In this research, the diamond blade in the circular saw without polishing was the best way to create a flat a surface as possible .
Another factor to consider, is the piezo-sensor within the probe. Piezo sensors are known to wear out over a certain amount of time and require recharging. It was noted that the calibration of the probe was more challenging if the same probe was used two days in a row. While, a week later, the probe would calibrate properly again. This phenomenon could result in a stretched out sensor and therefore record an inaccurate and lower force with the corresponding indentation, resulting in an underestimation of the elastic modulus. For that reason, the aim was to not use the same probe if calibration errors started to occur. The probe was only used if the calibration factor was within the correct region according to the protocol (Appendix V).
The movement of the platform on which the sample was placed, is also a point for discussion. The platform was navigated by using the Piuma software. However, the movement resolution was unknown. It seemed that it was showing backlash, which is an occurring

phenomenon in mechanical machines [71]. Meaning, there is a mechanical kickback in both directions when it is moving to the next point. The effect on the indentations itself was negligible, however, it did result in an even less accurate knowledge of the indentation location and the precise matrix sizes. In addition, if one would want to indent the same matrix at the same location twice, the location of the second matrix would not indent at the exact same location. For that reason, only the first matrices were used for further analysis as it was not possible to perform identical indentation matrices with the Piuma nanoindenter.
The method used for post-processing the nanoindentation data, was the Oliver-Pharr method. Here, the unloading curve was analyzed and the elastic modulus was calculated from the slope of this curve. It has been stated, that this method is not optimal for viscoelastic materials [72; 73]. The Oliver-Pharr method is mainly used for elastic-plastic materials. Viscoelastic materials do not show a clear presence of plastic deformation due to the time dependency of the material to retract to its original shape [48; 74]. This results in an uncertainty regarding the probe contact area, leading to an overestimation of the elastic modulus [75]. However, if a slow unloading time is applied to the nanoindentation, this method could be used for viscoelastic materials [51]. For that reason, an unloading time of 16.67 seconds was selected for these measurements.
As mentioned before, the Gaussian filter was applied to all the indentation matrices to create a better visualization of the different tissue regions. The NaN-values were excluded from the filter. However, if NaN-values were abundantly present in a heatmap, some kernels would exist only of NaN-values. This resulted in an inaccurate replacement of the elastic modulus value by the filter. Thus, if NaN-values were present in a large amount, the heatmap was excluded from further analysis. In this study this applied for the 7 weeks old medial sample and the 12 days old medial sample.
To validate if plastic deformation occurred due to nanoindentation in the interface, SEM images were analyzed. However, the surface roughness was high and marks of indentations could not be detected. In previous research on nanoindentation in bone, permanent deformation was detected with a Berkovich tip and 100 nm indentation depth [76]. However, when a spherical tip was used with a low indentation depth, plastic deformation often was prevented [48]. The SEM images do not exclude plastic deformation of the interface, however it can be assumed that it is negligible due to the highly damaged surface on the nano-scale.
Lastly, the same indentation protocol was used for the cartilage measurements as well as for the subchondral bone measurements. While, it was required to have a separate protocol for nanoindentation for every type of material [3]. It was chosen to use the same protocol so that all the results of the interface could be compared to each other. If a different protocol was used for every layer, the difference in results could have been influenced by the indentation time and depth. Except for the similar protocol, similar probes were used for the different tissue types. It was advised to use a probe with a less stiff cantilever for cartilage and a stiffer cantilever for bone indentations. If a stiff cantilever is used for a softer material, an underestimation of the elastic modulus will take place. The cantilever will deform less, detecting a lower force, which leads to a lower elastic modulus compared to an indentation with a probe with a less stiff cantilever. However, as mentioned above, using different probes would make it impossible to compare the results for the different regions, thus the same probe was used for the entire interface.
The high amount of assumptions and considerations for nanoindentation in this research, made it challenging to obtain useful results. However, if all these limitations are

considered, the results obtained in this study can be used for further research in this field.

4.4 DIC

The analysis of the osteochondral interface by use of compression tests with DIC, was a novel technique to observe the strain patterns of this biological tissue. A clear transitional region was detected in most of the samples from cartilage to bone. The higher strain rate of the 7 weeks old interface compared to the 12 days old interface, can be explained by the selected time step. The time step chosen for the 7 weeks old interface, had a corresponding compression force of 256.07 N. For the 12 days old interface, that force was 204.132 N. The maximum time step possible was chosen in order to track as much deformation as possible in the deeper layers. However, this resulted in varying forces with the corresponding strain distribution. In addition, the cameras had a high sensitivity to environmental factors which could have influenced the results by tracking a strain inaccurately. It was expected that the 7 weeks old cartilage had a high strain value in the cartilage region, however, not much higher than the 12 days old cartilage.
The two samples from the 13 months old joint, showed similar curves with the similar strain values at the superficial layer of the cartilage. The transition to a lower strain value was at a shorter distance from the superficial cartilage layer compared to the younger interfaces. This can be explained by the thickness difference of the cartilage, which reduced with increasing age.
For the mature joint, the Adult 2 and Adult 3 samples showed a low strain value across the entire interface. This suggested that the entire interface was stiffer than in the samples of the immature joints. The Adult 1 sample, however, showed the highest strain value in the cartilage compared to all the other samples. It was expected that the strain would be lower for the samples of the mature joints, due to the mineralization. An explanation for this highest strain value could be the that the sample was slightly curved, thus that the observed cartilage surface was not fully resting on underlying bone and hanging over the bone, resulting in a quicker deformation.
One of the limitations in this method was the geometry of the samples used. The samples were assumed to be firm enough to withstand the compression force without failing. However, the samples were first also used for nanoindentation, thus could not be too thick, as a higher thickness, would obstruct the sample from getting immersed in liquid for nanoindentation. This resulted in blocks, where the superficial layer was curved in both directions. This created an uneven contact area for the compression plate. In addition, due to the previous testing with nanoindentation, the samples contained some superglue at the bone end. This might have effected the mechanical properties of that part of the sample. This part of the sample is not within the region of interest, however, with the uniaxial compression should be considered. Lastly, the nanoindenter could have applied some plastic deformation to the matrix region which could weaken that part of the interface. The SEM images did not detect plastic deformation due to indentation, however, they did show damage on the surface due to the cutting technique. It is unlikely that it would cause any effect on the measured strain, as the point of data observation was before the sample failed. Thus, this possible effect was considered to be minimal on failure during compression.
Another limitation within this mechanical method, is that the samples could not be tested in liquid. This could have lead to dehydration of the sample during measurements, which affects the mechanical properties in such a way that they become stiffer and brittle [77; 78].

The samples were dry for a limited amount of time, however it would be preferable to keep them hydrated. Lastly, folding of the cartilage on the observed surface occurred during the compression of some samples (Figure 4.1). It mostly took place in the young samples, which had a thicker and a slightly softer cartilage layer. Furthermore, the chance of folding occurring also depended on the geometry of the samples. A slight angle of the sample surface, could have lead to a higher chance of the cartilage folding over the subchondral bone. This phenomenon limits the region of interest and data analysis. In these situations, a lower time step and force was selected. This method and data analysis is highly complex for biological materials with varying tissue types. Thus it is of great importance that the assumptions and limitations are carefully considered during these measurements.

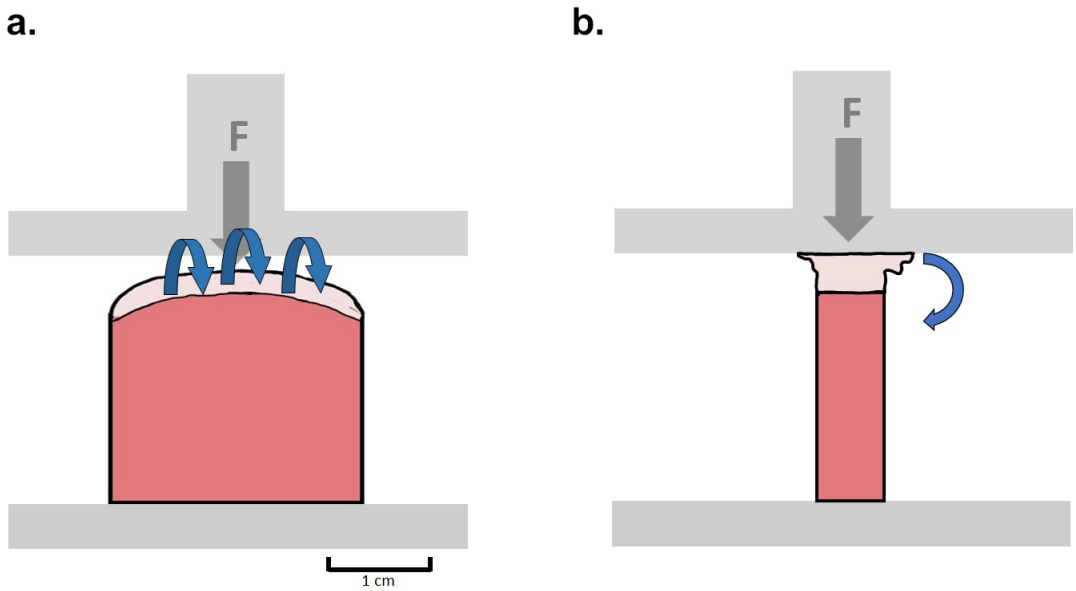

Figure 4.1: Folding phenomenon of the cartilage during compression.a.) The front view of the sample, which is the surface the DIC cameras tracked. b.) Side view with a schematic of the cartilage layer folding due to high force.

4.5 RECOMMENDATIONS

For future research, it is recommended to use a nanoindenter machine where the indenting location can be accurately visualized. In that case, the indentation locations can be retrieved and determined with a higher. If, however, the Piuma nanoindenter is used for further analysis, the resolution of the movement through the software of the nanoindenter should be investigated and validated.
Within this research, multiple indentation matrices were performed on one sample. Due to the uncertainty of indentation location and plastic deformation, only the first matrix was analyzed. It could be interesting to investigate and register the three matrices performed per sample, so that more data can be analysed.
It is advised to set up a protocol for the tissue sampling for the compression tests. The geometry should be optimized in order to obtain the corresponding contact area and to prevent folding of the cartilage. Furthermore, an analysis method should be designed to obtain the elastic modulus from this data. This could lead to more insights in the

different measuring methods and the stiffness of the transitional layers from cartilage to bone.
Following from these optimizations, novel research can be performed on the osteochondral or tendon-to-bone interface of different species and anatomical location. This could lead to a better understanding of the mechanical properties of the interface and improved regeneration techniques.

5

CONCLUSION

This study aimed to characterize the property-structure relationship of the maturing equine osteochondral interface. A nanoindentation protocol was developed, which could measure the elastic modulus of the cartilage and subchondral bone, with a slow unloading time and an indentation depth of 5 µm to ensure indentation in the inconsistent surfaces. Stiff probes had to be used to so that indentations could be made and compared in both soft and stiff materials.

This protocol resulted in matrices of local elastic modulus values for all the samples. The local elastic modulus varied per location, however, a clear transition between regions of low values and high values was found in the mature interfaces, in some 13 months old samples and a light transition in the younger samples. The region with low values indicated that indentations were made in the articular cartilage. The higher values were approximately 10 times higher than the region with lower values, suggesting that the subchondral bone and possibly the calcified cartilage region was indented in that area. Within the subchondral bone region, a high variation of values was detected, most likely due to the pores and trabeculae found in this tissue type.

The value for the articular cartilage in the immature interfaces was slightly lower compared to the mature articular cartilage, however within the same range. The subchondral bone in the immature interfaces, did not show any high values for the elastic modulus. The mature subchondral bone was highly compact compared to the immature subchondral bone, resulting in lower values over the entire interface for the immature samples. At the age of 13 months, higher values were detected in the indentation matrix. Indicating that the calcification process of the bone and cartilage was occurring at this stage of maturation.

The histology images revealed a clear overview of the differences between immature and mature osteochondral interface. The immature cartilage had a higher thickness, which decreased with age, and did not consist of a calcified cartilage layer. The subchondral bone was highly porous, compared to the 13 months old and mature samples, which was also shown in the elastic modulus matrix for these samples.

At 13 months, a light tidemark could be detected, which indicated calcification and compact subchondral bone was emerging, which could be seen in the corresponding heatmaps. The mature interfaces demonstrated clear layers and tidemarks in the histology images. The indentation matrices for these interfaces showed a clear transition, however not a highly defined calcified cartilage area.

The strain distributions demonstrated a clear difference in cartilage thickness for different ages. The transitional zone between low and high strain values of the immature interface occurred at a higher distance from the superficial layer compared to the mature interfaces. This confirmed that a clear mechanical difference between cartilage and subchondral bone was present.

The main limitations in this research, were the lack of knowledge of indentation location

for measurements of the local elastic modulus matrices and the lack of knowledge of the structure and sample geometry during compression tests. Therefore, assumptions had to be made on the values within the different regions and for the data analysis of the DIC method.
This study provides new insights in measuring techniques for the mechanical properties of the osteochondral interface. Furthermore, an overview was provided of the local elastic moduli and compared with the structure during the maturation of the equine interface. However, in order to obtain more knowledge on the specific layers in this interface, more studies are required where the indentation location can be clearly defined. This could lead to new insights and repair strategies of this highly complex natural structure.

BIBLIOGRAPHY

[1] C. Rogers, E. Gee, and K. Fittmer, "Growth and bone development in the horse: When is a horse skeletally mature?," *Animals*, vol. 11, no. 3402, 2021.

[2] P. Van Weeren, "Etiology, diagnosis and treatment of oc(d)," *Clinical Techniques in Equine Practice*, vol. 5, pp. 248–258, 2006.

[3] O. 11, *User manual Piuma Nanoindenter*. Optics 11, Amsterdam, 2020.

[4] H. Zhang, X. Li, Q. Wenjie, J. Zhu, B. Chen, J. Yang, and Y. Xia, "Characterization of mechanical properties of epoxy/nanohybrid composites by nanoindentation," *Nanotechnology Reviews*, vol. 9, pp. 28–40, 2020.

[5] A. Di Luca, C. Van Blitterswijk, and L. Moroni, "The osteochondral interface as a gradient tissue: From development to the fabrication of gradient scaffolds for regenerative medicine," *Birth Defects Research (Part C)*, vol. 105, pp. 34–52, 2015.

[6] A. Shane Anderson and R. Loeser, "Why is osteoarthritis an age-related disease," *Best Pract Res Clin Rheumatol*, vol. 24, no. 1, 2010.

[7] M. Ding, A. Odgaard, and I. Hvid, "Changes in the three-dimensional microstructure of human tibial cancellous bone in early osteoarthritis," *The Journal of Bone Joint Surgery*, vol. 85, no. 6, pp. 906–912, 2003.

[8] S. Nukavarapu and D. Dorcemus, "Osteochondral tissue engineering: Current strategies and challenges," *Biotechnology Advances*, vol. 31, pp. 706–721, 2013.

[9] H. Upmeier, B. Brueggenjuergen, A. Weiler, C. Flamme, H. Laprell, and S. Willich, "Follow-up costs up to 5 years after conventional treatments in patients with cartilage lesions of the knee," *Knee Surg Sports Traumatol Arthtosc.*, vol. 15, 2007.

[10] J. Harris, R. Brophy, R. Siston, and D. Flanigan, "Treatment of chondral defects in the athlete's knee," *Arthoscopy*, vol. 26, 2010.

[11] P. Aglietti and *et al*, "The intsall-burstein total knee replacement in osteoarthitis," *The Journal of Arthroplasty*, vol. 14, no. 5, pp. 560–565, 1999.

[12] L. Bayliss, D. Culliford, A. Monk, S. Glyn-Jones, D. Prieto-Alhambra, A. Judge, C. Cooper, A. Carr, N. K. Arden, D. Beard, and A. Price, "The effect of patient age at intervention on risk of implant revision after total replacement of the hip or knee: a population-based cohort study," *The Lancet*, vol. 389, no. 10077, pp. 1424–1430, 2017.

[13] A. Marino, E. Pontikaki, M. Truzzi, A. Menon, C. Artusi, M. Di Marco, P. Randelli, R. Cimaz, and R. Vigano, "Early joint replacement in juvenile odiopathic arthritis: Trend over time and factors influencing implant survival," *Arthritis Care Research*, vol. 73, no. 9, pp. 1275–1281, 2020.

[14] M. Mirzaali, A. Herranz de la Nava, D. Gunashekar, M. Nouri-Goushki, E. Doubrovski, and A. Zadpoor, "Fracture behaviour of bio-inspired functionally graded soft-hard composites made by multi-material 3d printing: The case of colinear cracks," *Materials*, vol. 12, no. 7, pp. 1–13, 2019.

[15] T. Lemirre, E. Santschi, C. Girard, U. Fogarty, L. Chapuis, H. Richard, G. Beauchamp, and S. Laverty, "Maturation of the ewuine medial femoral condyle osteochondral unit," *Osteoarthitis and Cartilage Open*, vol. 2, no. 1, p. 100029, 2020.

[16] J. Holopainen, P. Brana, E. Halmesmaki, T. Harjula, J. Tuukkanen, P. van Weeren, H. Helminen, and M. Hyttinen, "Changes in subchondral bone mineral density and collagen matrix organization in growing horses," *Bone*, vol. 43, no. 6, pp. 1108–1114, 2008.

[17] J. Rieppo, M. Hytinnen, E. Halmesmaki, H. Ruotsalainen, A. Vasara, I. Kiviranta, J. Jurvelin, and H. Helminen, "Changes in the spatial collagen content and collagen network architecture in porcine articular cartilage during growth and maturation," *Osteoarthitis and Cartilage*, vol. 17, no. 4, pp. 448–455, 2009.

[18] M. Hyttinen, J. Holopainen, P. van Weeren, E. Firth, H. Helminen, and P. Brama, "Changes in collagen fibril network organization nd proteoglycan distribution in equine articular cartilage during maturation and growth," *Journal of Anatomy*, vol. 215, no. 5, pp. 584–591, 2009.

[19] O. Armitage and M. Oyen, *Engineering Mineralized and Load Bearing Tissues: Chapter 11*. Springer Publishing, 2015.

[20] K. Moffat, W. Sun, P. Pena, N. Chahine, S. Doty, A. G.A., C. Hung, and H. Lu, "Characterization of the structure-function relationship at the ligament-to-bone interface," *The National Academy of Sciences of the USA*, vol. 105, no. 23, pp. 7947–7952, 2008.

[21] C. Kiani, L. Chen, Y. Wu, A. Yee, and B. Yang, "Structure and function of aggrecan," *Cell Research*, vol. 12, no. 1, pp. 19–32, 2002.

[22] N. Broom and A. Thambyah, *The Soft-Hard Tissue Junction*. Cambridge University Press, 2019.

[23] M. Oliveira Silva, J. Gregory, N. Ansari, and K. Stok, "Molecular signaling interactions and transport at the osteochondral interface: A review," *Fron. Cell. Dev. Biol.*, vol. 8, no. 750, 2020.

[24] A. Fox, A. Bedi, and S. Rodeo, "The basic science of articular cartilage: Structure, composition, and function," *Sports Health*, vol. 1, no. 6, pp. 461–468, 2009.

[25] T. Lyons, R. Stoddart, S. McClure, and J. McClure, "The tidemark of the chondro-osseous junction of the normal human knee joint," *Journal of Molecular History*, vol. 36, no. 3, pp. 207–215, 2005.

[26] M. Boi, G. Marchiori, M. Berni, A. Gambardella, F. Salamanna, A. Visani, M. Bianchi, M. Fini, and G. Filardo, "Nanoindentation: An advanced procedure to investigate osteochondral engineered tissues," *Journal of the Mechanical Behaviour of Biomedical Materials*, vol. 96, no. April, pp. 79–87, 2019.

[27] J. Martel-Pelletier, C. Boileau, and P. Pelletier, J. a jnd Roughley, "Cartilage in normal and osteoarthritis conditions," *Best Practice Research Clinical Rheumatology*, vol. 22, no. 2, pp. 351–384, 2008.

[28] G. Li, J. Yin, J. Gao, T. Cheng, N. Pavlos, C. Zhang, and M. Zheng, "Subchondral bone in osteoarthritis: insight into risk factors and microstructural changes," *Arthritis Research Therapy*, vol. 15, no. 223, 2013.

[29] W. Shingleton, E. Mackie, T. Cawston, and L. Jeffcot, "Cartilage canals in equine articular/epiphyseal growth cartilage and a possible association with dyschondroplasia," *Equine veterinary journal*, vol. 29, no. 5, pp. 360–364, 1997.

[30] M. Blumer, S. Longato, and H. Fritsch, "Structure, formation and role of cartilage canals in the developing bone," *Annals of Anatomy*, vol. 190, pp. 305–325, 2008.

[31] L. Jeffcott and F. Henson, "Studies on growth cartilage in the horse and their application to aetiopathogenesis of dyschondroplasia (osteochondrosis)," *The veterinary journal*, vol. 156, no. 3, pp. 177–192, 1998.

[32] F. Hontoir, R. Pirson, V. Simon, P. Clegg, J. Nisolle, N. Kirschvink, and J. Vandeweerd, "Age-related morphometric changes of the tidemark in the ovine stifle," *Anat Histol Embryol.*, vol. 48, pp. 366–374, 2019.

[33] M. van der Harst, C. van de Lest, J. Degroot, G. Kiers, P. Brama, and P. van Weeren, "Study of cartilage and bone layers of the bearing surface of the equine metacarpophalangeal joint relative to different timescales of maturation," *Equine Veterinary Journal*, vol. 37, pp. 200–206, 2005.

[34] F. Verschooten, B. van Waerebeek, and J. Verbeeck, "The ossification of cartilages of the distal phalanx in the horse: An anatomical experimental radiographic and clinical study," *Journal of Equine Veterinary Science*, vol. 16, no. 7, pp. 291–305, 1996.

[35] D. Jones and M. Ashby, *Engineering materials 1*. Elsevier, 2019.

[36] C. Eriksen, D. Kaylon, and H. Wang, "Viscoelastic and biomechanical properties of osteochondral tissue constructs generated from graded polycaprolactone and beta-tricalcium phosphate composites," *Journal of Biomedical Engineering*, vol. 132, p. 091013, 2010.

[37] L. Li and W. Herzog, "The role of viscoelasticity of collagen fibers in articular cartilage: Theory and numerical formulation," *Biorheology*, vol. 41, pp. 181–194, 2004.

[38] J. Jurvelin, M. Buschmann, and E. Hunziker, "Mechanical anisotropy of the human knee articular cartilage in compression," *Proceedings of the Institution of Mechanical Engineers*, vol. 217, pp. 215–219, 2003.

[39] M. Oyen, "Nanoindentation of biological and biomimetic materials," *Experimental Techniques*, vol. 37, pp. 73–78, 2013.

[40] B. Lawless, H. Sadeghi, D. Temple, H. Dhaliwal, D. Espino, and D. Hukins, "Viscoelasticity of articular cartilage: Analysing the effect of induced stress and the restraint of bone in dynamic environment," *Journal of Mechanical Behaviour of Materials*, vol. 75, pp. 293–301, 2017.

[41] Z. Wu, T. Ovaert, and G. Niebur, "Viscoelastic properties of human cortical bone tissue depend on gender and elastic modulus," *Journal of Orthopaedic Research*, vol. 30, no. 5, pp. 693–699, 2013.

[42] H. Gupta, S. Schratter, W. Tesch, P. Roschger, A. Berzlanovich, T. Schoeberl, K. Klaushofer, and P. Fratzl, "Two different correlations between nanoindentation modulus and mineral content in the bone-cartilage interface," *Journal of Structural Biology*, vol. 149, no. 2, pp. 138–148, 2005.

[43] S. Campbell, V. Ferguson, and D. Hurley, "Nanomechanical mapping of the osteochondral interface with contact resonance force microscopy and nanoindentation," *Acta Biomaterialia*, vol. 8, no. 12, pp. 4389–4396, 2012.

[44] F. Gaytan, C. Morales, C. Reymundo, and M. Tena-Sempere, "A novel rgb-trichome staining method for routine histological analysis of musculoskeletal tissues," *Nature*, vol. 10, p. 16659, 2020.

[45] Roche, *The complete guide for protease inhibition*. Roche Diagnostics GmHb, Germany, 2004.

[46] P. Moshtagh, B. Pouran, N. Korthagen, A. Zapoor, and H. Weinans, "Guidelines for an optimized indentation protocol for measurement of cartilage stiffness: The effects of spatial variation and indentation parameters.," *Journal of Biomechanics*, vol. 49, pp. 3602–3607, 2016.

[47] A. Chevrier, A. Kuoao, G. Picard, M. Hurtig, and M. Buschmann, "Interspecies comparison of subchondral bone properties important for cartilage repair," *Journal of Orthopaedic Research*, vol. 33, no. 1, pp. 63–70, 2015.

[48] N. Rodriguez-Florez, M. Oyen, and S. Shefelbine, "Insight into differences in nanoindentation properties of bone," *Journal of Mechanical Behaviour of Biomedical Materials*, vol. 18, pp. 90–99, 2013.

[49] S. Mountcastle, P. Allen, B. Mellors, B. Lawless, M. Cooke, C. Laveccha, N. Fell, D. Epsino, S. Jones, and S. Cox, "Dynamic viscoelastic characterisation of human osteochondral tissue: understanding the effect of the cartilage bone interface," *BMC Musculoskeletal Disorders*, vol. 20, pp. 575–588, 2013.

[50] A. Sadr, Y. Shimada, H. Lu, and J. Tagami, "The viscoelastic behavior of dental adhesives: a nanoindetation study," *Dental Materials*, vol. 25, pp. 13–19, 2009.

[51] B. Han, H. Nia, C. Wang, P. Chandrasekaran, Q. Li, D. Chery, H. Li, A. Grodzinsky, and L. Han, "Afm-nanomechanical test: An interdisciplinary tool that links the understanding of cartilage and meniscus biomchecanics, osteoarthritis degeneration and tissue engineering," *ACS Biomaterials Science Engineering*, vol. 3, no. 9, pp. 2033–2049, 2017.

[52] T. Chudoba and F. Richter, "Investigation of creep behaviour under load during indentation experiments and its influence on hardness and modulus results," *Surface and Coatings Technology*, vol. 148, no. 2, pp. 191–198, 2001.

[53] J. Kohn and D. Ebenstein, "Eliminating adhesion errors in nanoindentation of compliant polymers and hydrogels," *Journal of the mechanical behavior of biomedical materials*, vol. 20, pp. 316–326, 2013.

[54] W. Oliver and G. Pharr, "An improved technique for determining hardness and elastic modulus using load and displacement sensing indentation experiments," *Journal of Material Research*, vol. 7, no. 6, pp. 1564–1583, 1992.

[55] I. Sneddon, "The relation between load and penetration in the axisummetric boussinesq problem for a punch of arbitrary profile," *International Journal of Engineering Science*, vol. 3, no. 1, pp. 47–57, 1965.

[56] H. Jin and J. Lewis, "Determination of poisson's ratio of articular cartilage by indentation using different-sized indenters," *Journal of Biomechanical Engineering*, vol. 126, no. 2, pp. 138–145, 2004.

[57] F. Malekipour, R. Whitton, and P. Lee, "Distribution of mechanical strin in equine distal metacarpal subchondral bone: A microct-based finite element model," *Medicine in Novel Technology and Devices*, vol. 6, 2020.

[58] K. Hauch, M. Oyen, G. Odegard, and T. Haut Donahue, "Nanoindentation of the insertional zones of human meniscal attachments into underlying bone," *Journal of Mechanical Behaviour of Biomedical Materials*, vol. 2, no. 4, pp. 339–347, 2009.

[59] L. Zhang, J.and Liao and J. Zhu, "Osteochondral interface stiffening in mandibular condylar osteoarthritis," *Journal of Dental Research*, vol. 97, no. 5, 2018.

[60] A. Peters, R. Akhtar, E. Comerford, and K. Bates, "The effect of ageing and osteoarthritis on the mechanical properties of cartilage and bone in the human knee joint," *Nature*, vol. 8, p. 5931, 2018.

[61] E. Hargrave-Thomas, F. van Sloun, M. Dickinson, N. Broom, and A. Thambyah, "Multi-scalar mechanical testing of the calcified cartilage and subchondral bone comparing healthy vs early degenerative states.," *Osteoarthritis and Cartilage*, vol. 23, no. 10, pp. 1755–1762, 2015.

[62] H. Brommer, P. Brama, M. Laasanen, H. Helminen, P. van Weeren, and S. Jurvelin, "Functional adaptation of articular cartilage from birth to maturity under the influence of loading: a biochemical analysis," *Equine Veterinary Journal*, vol. 37, no. 2, pp. 148–154, 2010.

[63] L. Lane and P. Bullough, "Age-related changes in the thickness of the calcified zone and the number of tidemarks in adult human articular cartilage," *The Journal of Bone and Joint Surgery*, vol. 62-B, no. 3, pp. 372–375, 1980.

[64] T. Oegema, R. Carpenter, F. Hofmeister, and R. Thompson, "The interaction of the zone of calcified cartilage and subchondral bone in osteoarthritis," *Microscopy research and technique*, vol. 37, pp. 324–332, 1997.

[65] E. Hunziker, T. Quinn, and H. Hauselmann, "Quantative structural organization of normal adult human articular cartilage.," *Osteoarthritis Cartilage*, vol. 10, no. 7, pp. 564–572, 2002.

[66] Bruker, "Hysitron ti 90 nanoindenter."

[67] S. Gourian-Arsiquaud, J. Burket, L. Havill, E. DiCarlo, S. Doty, R. Mendelsohn, M. van der Meulen, and A. Boskey, "Spatial variation in osteonal bone properties relative to tissue and animal age," *Journal of Bone and Mineral Research*, vol. 24, no. 7, 2009.

[68] Y. Zhu, Z. Dong, U. Wejinya, S. Jin, and K. Ye, "Determination of mechanical properties of soft tissue scaffolds by atomic force microscopy nanoindentation," *Journal of Biomechanics*, vol. 44, pp. 2356–2361, 2011.

[69] Y. Xia, M. Bigerelle, J. Marteau, P. Mazeran, S. Bouvier, and A. Iost, "Effect of surface roughness in the determination of the mechanical properties of material using nanoindentation test," *Scanning*, vol. 36, pp. 134–149, 2014.

[70] J. Kim, J. Lee, Y. Lee, J. Jang, and D. Kwon, "Surface roughess effect in instrumented indentation: a simple contact depth model and its verification," *Journal of Materials Research*, vol. 21, no. 12, pp. 1975–2978, 2006.

[71] M. Dang, T. Dao, N. Chau, and H. Le, "Effective hybrud algorithm of taguchi method, fem, rsm and teaching learning-based optimization of multiobjective optimization design of a compliant rotary positioning stage for nanoindentation tester.," *Mathematical Problems in Engineering*, vol. 2019, 2019.

[72] C. Liu, S. Lee, L. Sung, and T. Nguyen, "Load-displacement relations for nanoindentation of viscoelastic materials," *Journal of applied physics*, vol. 100, 2006.

[73] Y. Cheng and C. Cheng, "Relationships between initial unloading slope, contact depth, and mechanical properties for spherical indentation in linear viscoelastic solids," *Materials Science and Engineering:A*, vol. 409, no. 1-2, pp. 93–99, 2005.

[74] D. Ebenstein, "Nano-jkr method eliminates adhesion errors in nanoindentation of compliant polymers and hydrogels," *TechConnect Briefs*, 2018.

[75] J. Kaufman and C. M. Klapperich, "Surface detection errors cause overestimation of the modulus in nanoindentation on soft materials," *Journal of the mechanical behaviour of biomedical materials 2*, pp. 312–317, 2009.

[76] J. Thompson, J. Kindt, B. Drake, H. Hansma, D. Morse, and P. Hansma, "Bone indentation recovery time correlates with bone reforming time," *Nature*, vol. 414, pp. 773–776, 2001.

[77] J. Nyman, A. Roy, X. Shen, R. Acuna, J. Tyler, and X. Wang, "The influence of water removal on the strength and toughness of cortical bone," *Journal of Biomechanics*, vol. 39, no. 5, pp. 931–938, 2007.

[78] Q. Wang, Y. Yand, H. Niu, W. Zhang, Q. Feng, and W. Chen, "An ultrasound study of altered hydration behaviour of proteoglycan-degraded articular cartilage," *BMC Musculoskeletal Disorders*, vol. 14, no. 289, 2013.

6

APPENDIX

Appendix I: Bovine Polishing Histology & Trial Indentation Profiles

Figure 6.1: A comparison between a polished and unpolished bovine sample. An HE staining was performed to observe the difference in structure on the surfaces. The polished sample shows a damaged surface, while the unpolished sample a has smooth cartilage surface.

Table 6.1: Indentation trials on bovine osteochondral samples

Trial No.	Probe (Stiffness, Radius)	Loading Time [s]*	Depth [µm]	Comments
Nano-01	60 N/m, 50 µm	Calibration practice	-	-
Nano-02	283 N/m, 9 µm	1 - 7 - 20 s	8	Probe got stuck at bone, try larger probe
Nano-03	60 N/m, 50 µm 48.1 N/m, 45 µm	1 - 7 - 20 s	8	Probe stuck at bone and broke, one probe would not calibrate
Nano-04	48.1 N/m, 45 µm	Calibration	-	-
Nano-05	197 N/m, 8 µm	1-7-20 s 5-1-5 s 2-1-2 s 10-1-10 s	8	Polished surface, probes did not get stuck
Nano-06	283 N/m, 9 µm & 197 N/m, 8 µm	1 - 7 - 20 s	8	Only cartilage measurements to compare with literature
Nano-07	197 N/m, 8 µm	-	-	Find surface error
Nano-08	197 N/m, 8 µm	1-7-20 s 5-1-5 s	8	Additional polishing, generated faulty curves
Nano-09	197 N/m, 8 µm	1-7-20 s	8	Additional polishing, no stiffness gradient (All cartilage values)
Nano-10	197 N/m, 8 µm	1-7-20 s	4	New sample, freshly polished. Lower indentation depth, still got stuck. Probe broke
Nano-11	270 N/m, 10.5 µm	1-7-20 s	1.6	New probe, theoretical maximum indentation depth, only few indentations made.
Nano-12	270 N/m, 10.5 µm	1-7-20 s	1.6	Validatation previous measurements
Nano-13	270 N/m, 10.5 µm	1-7-20 s 8-1-8 s 6-1-6 s	1.6 5	Cortical bone measurements to check if machine can measure high stiffness, results gave higher valies than cartilage
Nano-14	270 N/m, 10.5 µm	8-1-8 s	5	Polymer sample, measured previously, for validation machine measurements according to Mirzaali (2019) [14].
Nano-15	270 N/m, 10.5 µm	8-1-8 s	5	Additional measurements to Nano-14

*The loading time represents the time for loading-holding-unloading. All procedures and conclusions are recorded in the labbook of this study.

Appendix II: Sample Dimensions & Sample Images

Table 6.2: Dimensions of samples determined with a caliper.

Joint	Label	Width [cm]	Height [cm]	Length [cm]
Adult 1	A-1-LD	0.55	1.35	2.05
Adult 1	A-1-LP	0.70	1.50	2.05
Adult 1	A-1-MP	0.90	1.50	2.70
Adult 1	A-1-MD	1.10	1.60	2.70
Adult 2	A-2-L	0.80	1.45	2.60
Adult 2	A-2-MP	0.80	1.40	2.40
Adult 2	A-2-MD	0.70	1.40	2.40
Adult 3	A-3-LD	1.00	1.70	3.10
Adult 3	A-3-LP	0.85	1.50	3.00
Adult 3	A-3-MP	0.85	1.45	2.90
Adult 3	A-3-MD	0.90	1.75	3.10
13 Months	Y-13M-LD	0.90	1.65	1.65
13 Months	Y-13M-LP	0.75	1.50	1.65
13 Months	Y-13M-MP	0.75	1.75	2.05
13 Months	Y-13M-MD	0.65	1.60	2.00
7 Weeks	Y-7W-L	1.00	1.70	1.60
7 Weeks	Y-7W-M	1.20	1.60	1.90
12 Days	Y-12D-L	1.05	1.50	1.85
12 Days	Y-12D-M	1.00	1.60	1.70
9 Days	Y-9*D*-L	1.10	1.75	1.80
9 Days	Y-9*D*-M	0.90	1.70	1.70

Table 6.3: Thickness of the articular cartilage and calcified cartilage for each joint.

Joint	Articular Cartilage [µm]	Calcified Cartilage [µm]
Adult 1	689.7 ± 28.2	165.6 ± 35.1
Adult 2	833.7 ± 35.9	241.3 ± 33.7
Adult 3	567.3 ± 42.5	169.7 ± 39.4
13 Months	1166.0 ± 60.2	N/A
7 Weeks	1242.0 ± 48.7	N/A
12 Days	1498.0 ± 55.5	N/A
9 Days	1506 ± 77.7	N/A

The thickness was determined with NDP.view2 software (Hamamatsu, Tokyo, Japan). For each region ten measurements were performed, as the border between layers is not a clear straight line, and the measurements were averaged. N/A means was no clear defined calcified cartilage layer was present.

Images Joints and Mechanical Samples

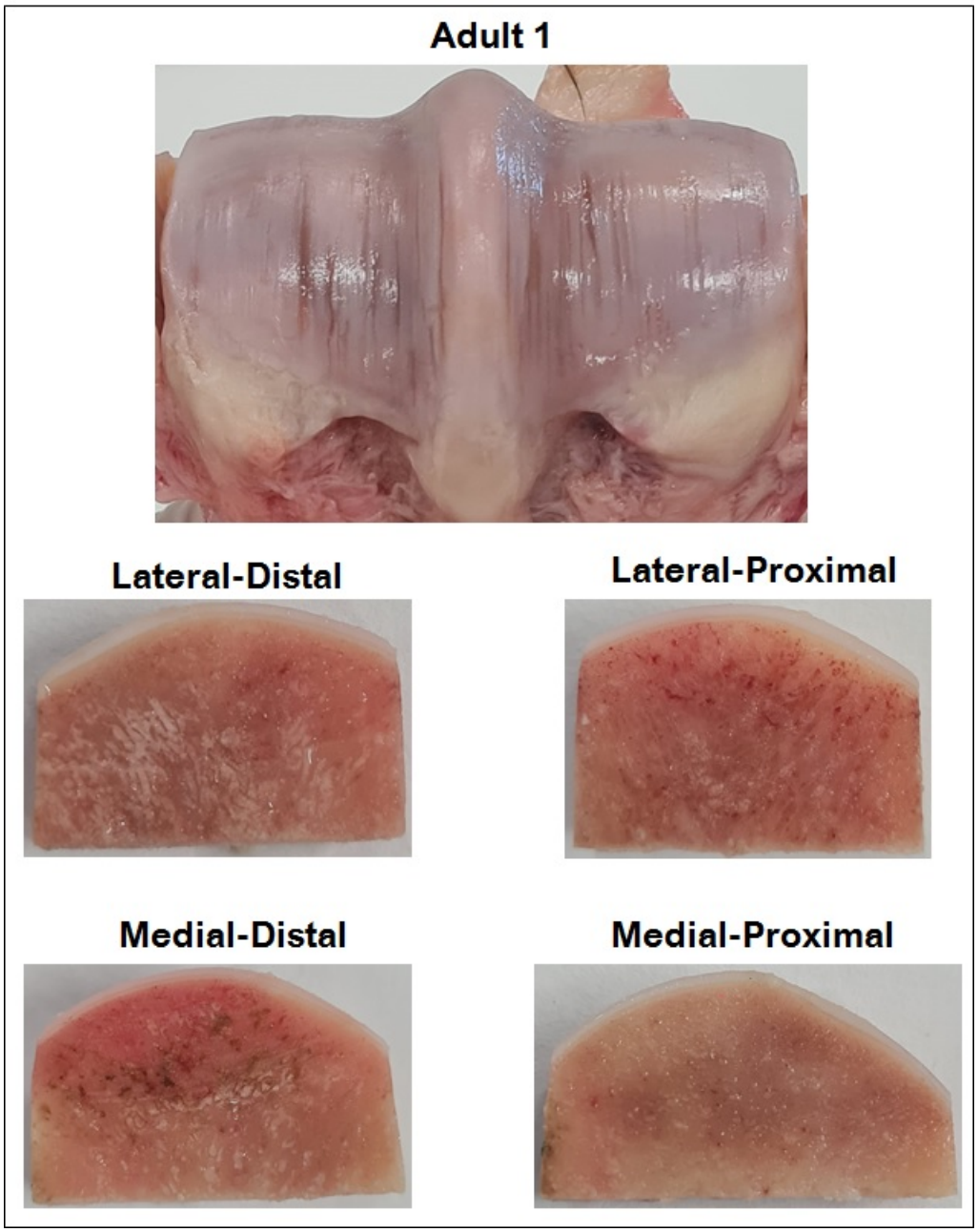

Figure 6.2: Joint and mechanical samples of Adult 1

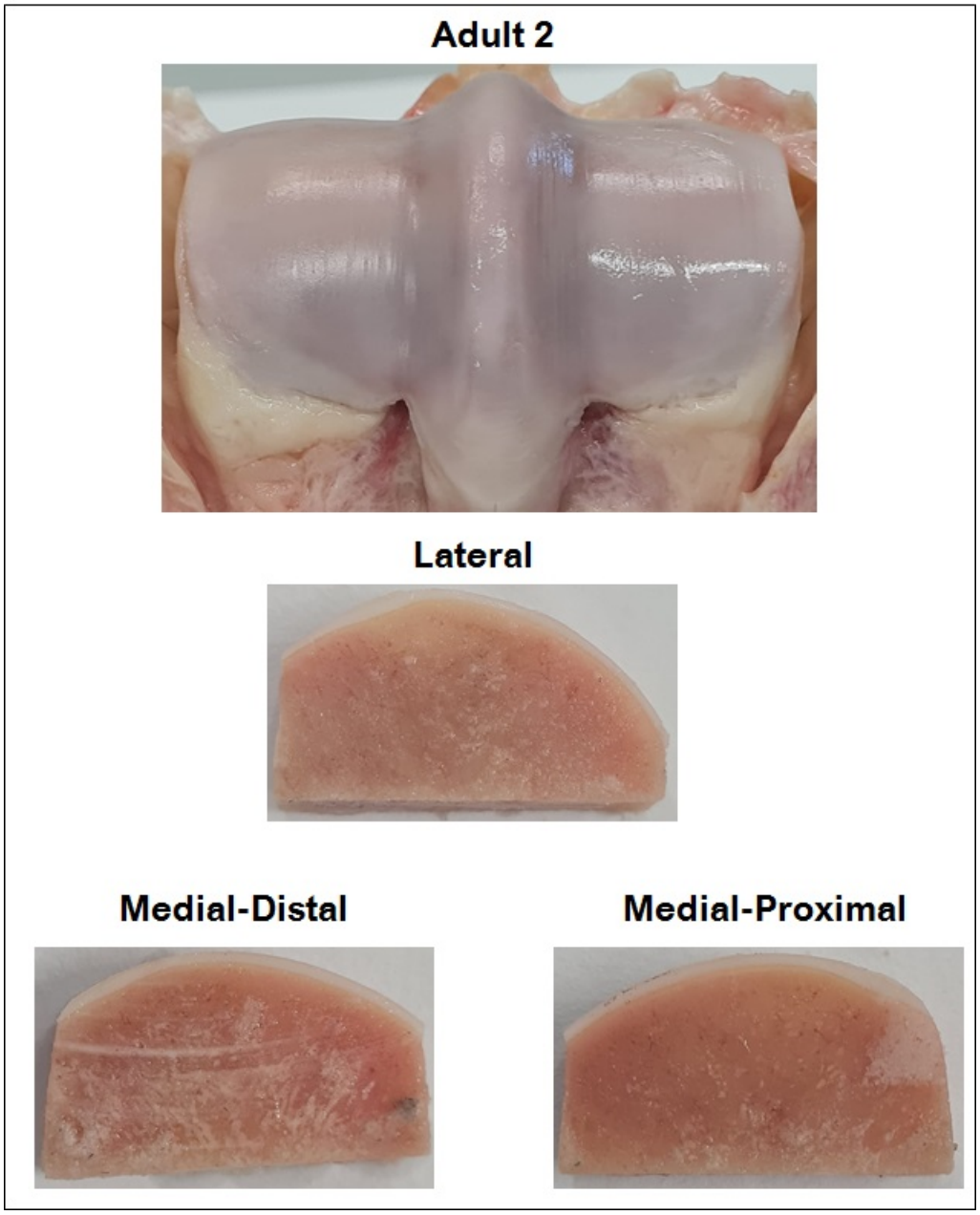

Figure 6.3: Joint and mechanical samples of Adult 2

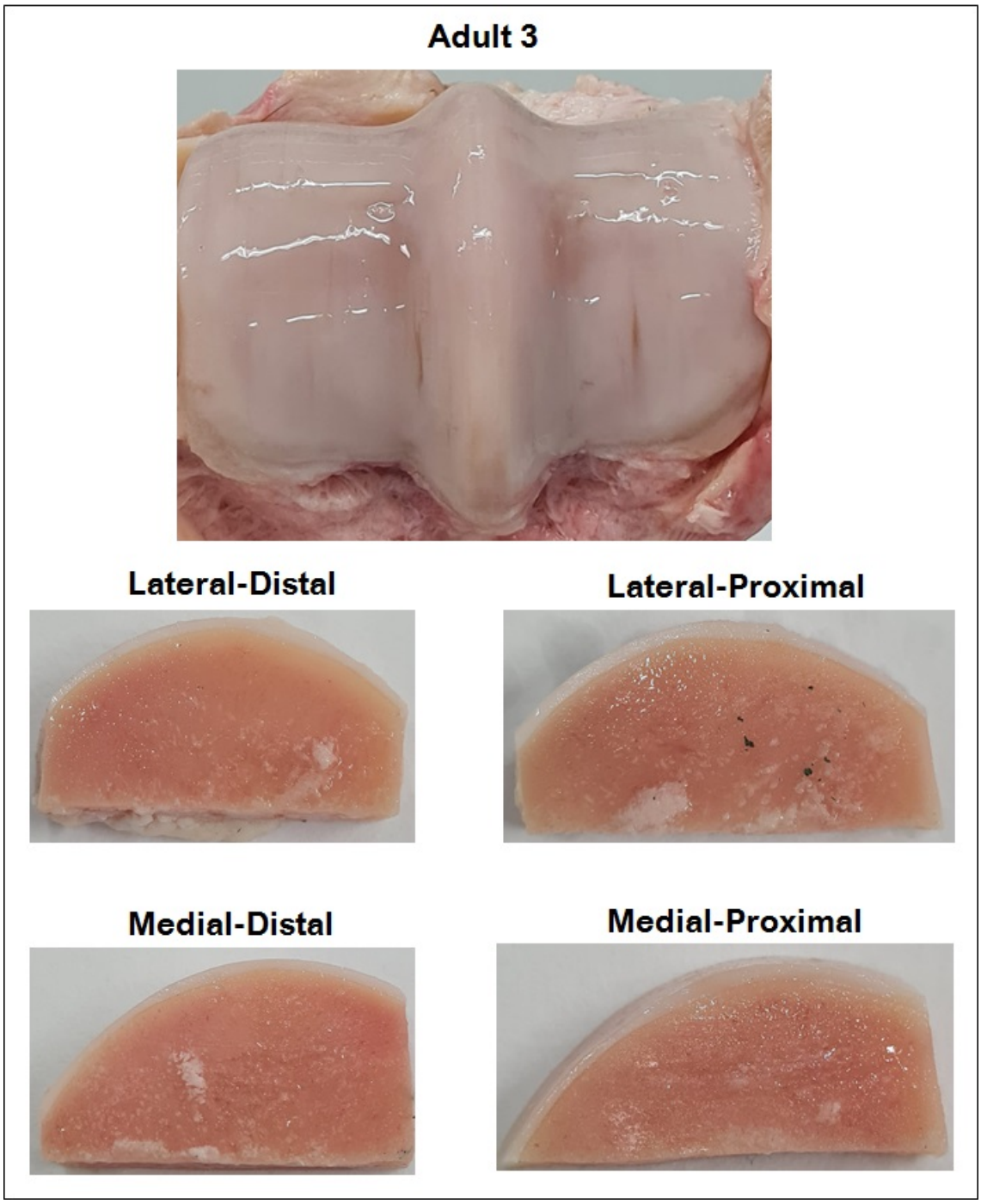

Figure 6.4: Joint and mechanical samples of Adult 3

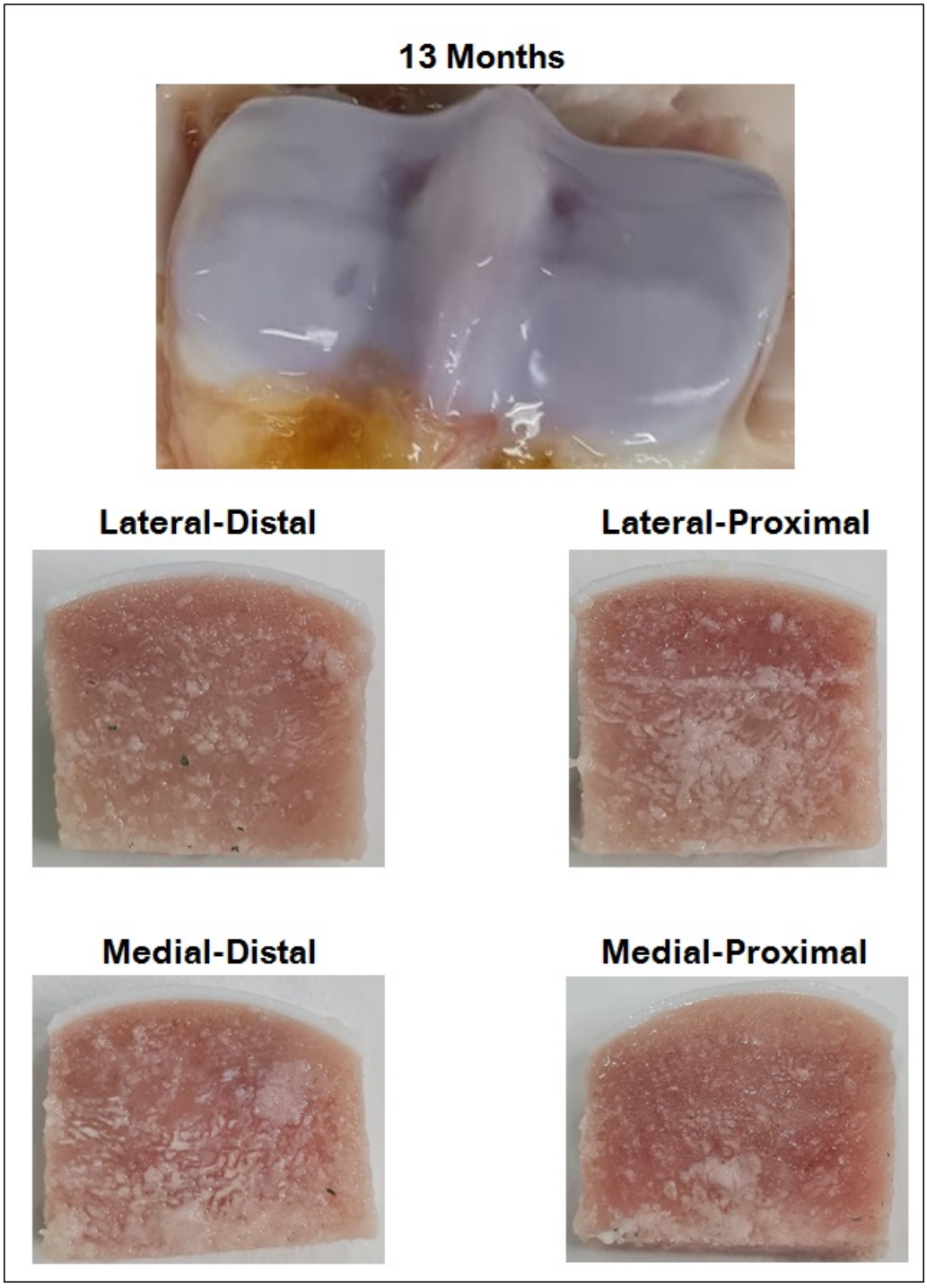

Figure 6.5: Joint and mechanical samples of 13 months old

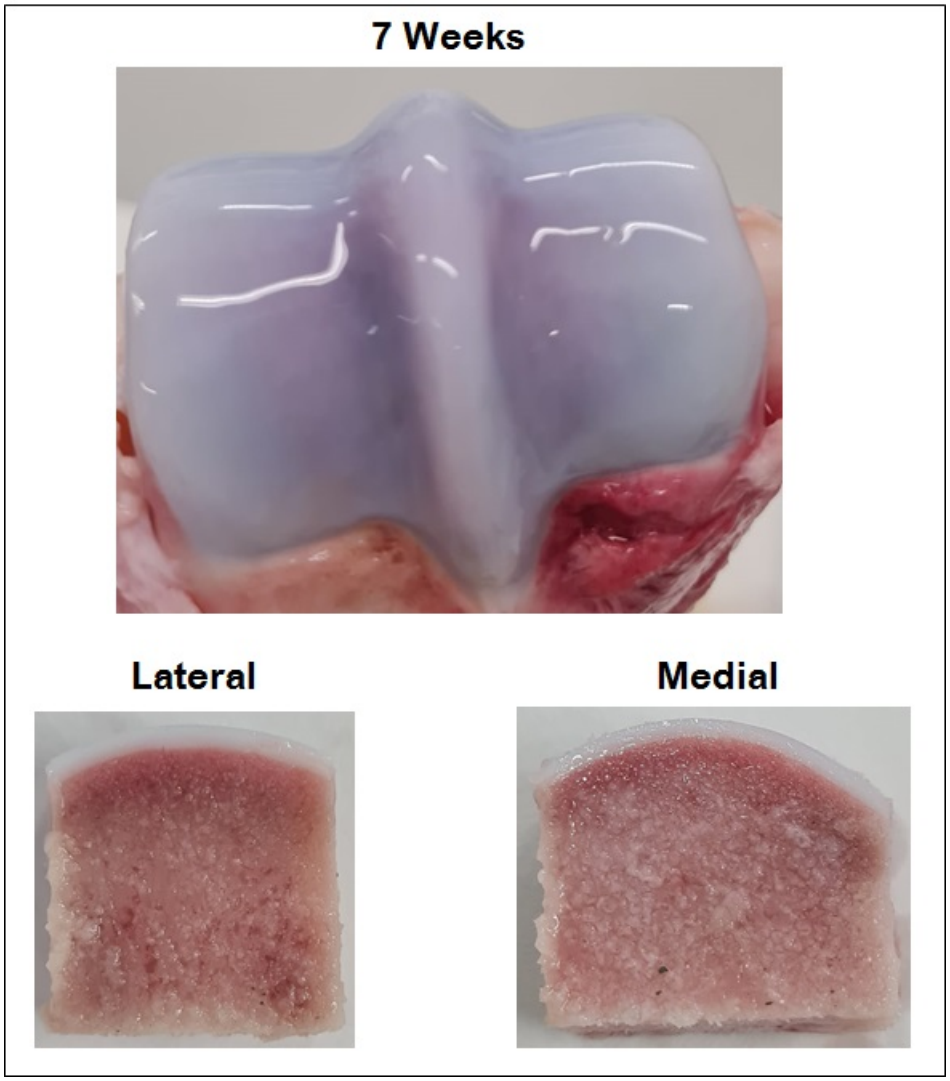

Figure 6.6: Joint and mechanical samples of 7 weeks old

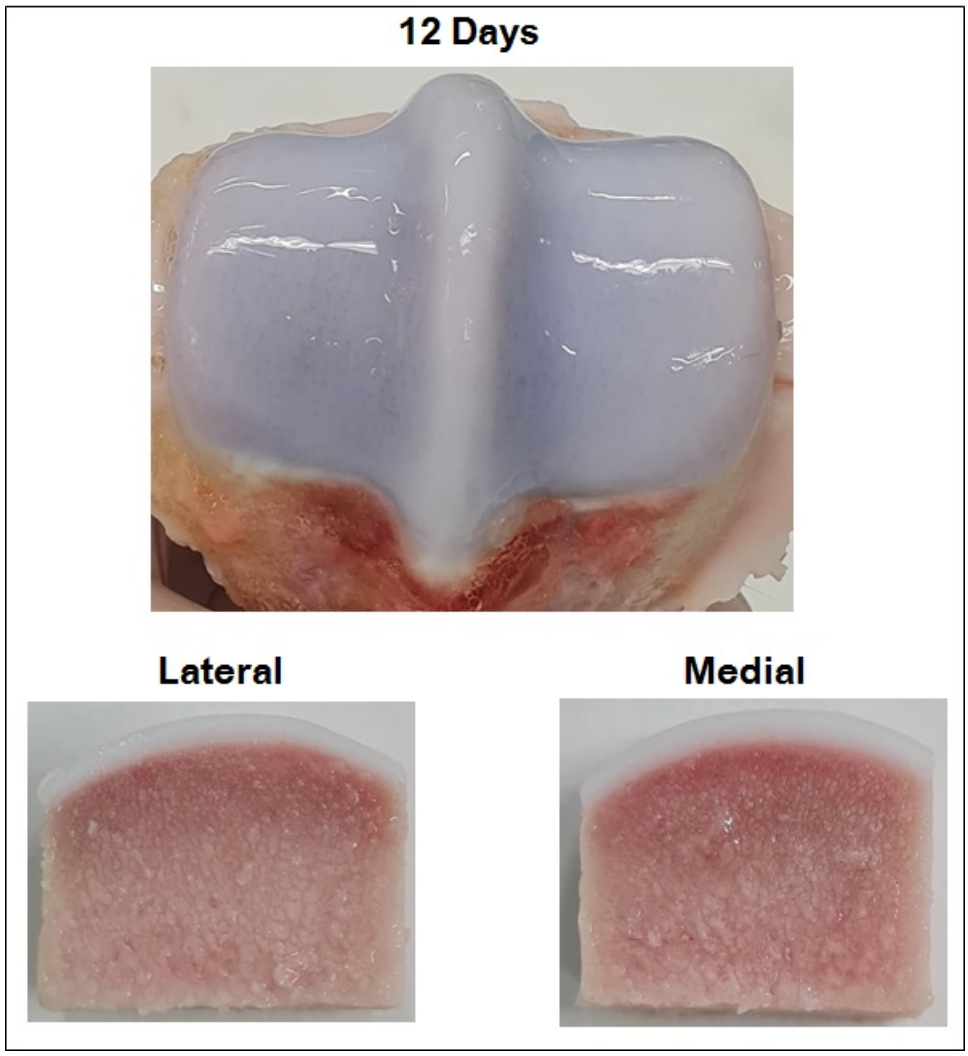

Figure 6.7: Joint and mechanical samples of 12 days old

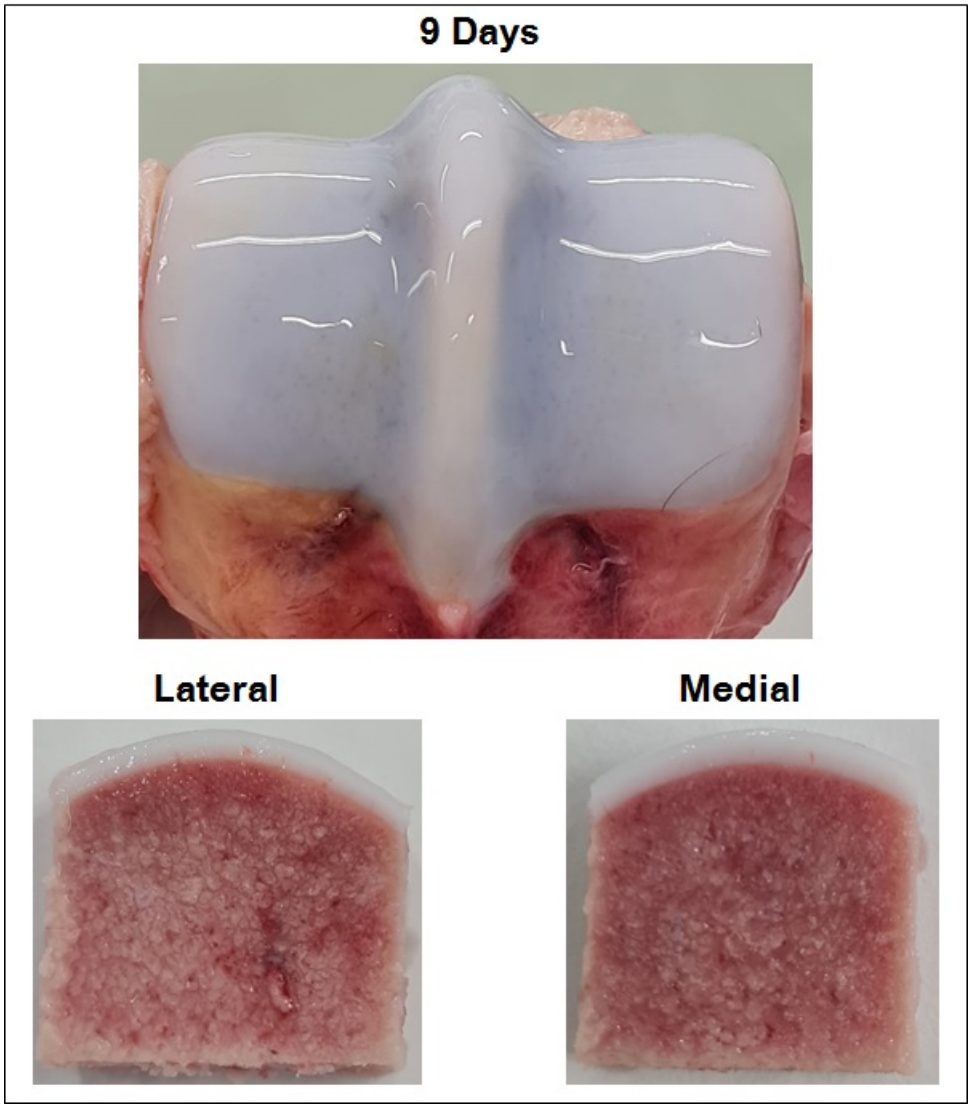

Figure 6.8: Joint and mechanical samples of 9 days old

Sample	Label	Probe
Adult 1 Medial-Proximal	A-1-MP	P3
Adult 1 Medial-Distal	A-1-MD	P3
Adult 1 Lateral-Proximal	A-1-LP	P3
Adult 1 Lateral-Distal	A-1-LD	P3
Adult 2 Medial-Proximal	A-2-MP	P3
Adult 2 Medial-Distal	A-2-MD	P3
Adult 2 Lateral	A-2-L	P1
Adult 3 Medial-Proximal	A-3-MP	P1
Adult 3 Medial-Distal	A-3-MD	P1
Adult 3 Lateral-Proximal	A-3-LP	P1
Adult 3 Lateral-Distal	A-3-LD	P1
13 Months Medial-Proximal	Y-13M-MP	P4
13 Months Medial-Distal	Y-13M-MD	P4
13 Months Lateral-Proximal	Y-13M-LP	P3
13 Months Lateral-Distal	Y-13M-LM	P2
7 Weeks Medial	Y-7W-M	P2
7 Weeks Lateral	Y-7W-L	P2
12 Days Medial	Y-12D-M	P2
12 Days Lateral	Y-12D-L	P2
9 Days Medial	Y-9D-M	P2
9 Days Lateral	Y-9D-L	P2

P1 = 249 N/m, 8.5 µm
P2 = 254 N/m, 9.5 µm
P3 = 261 N/m, 8 µm
P4 = 283 N/m, 9 µm

Figure 6.9: Probes used on every sample

Appendix III: Staining Protocols

Erasmus MC Orthopaedics/ENT lab

Erasmus Orthopaedic Research Lab Ee1614		
Title: **Hematoxylin Eosin staining on paraffin – MMA - and cryosections**		Page **1/1**
Protocol: **O-04**	Version: 3.0	Effective date: **05/10/213**
Author: **Nicole Kops**		Primary reviewer: **N.Kops**

Background:
The HE staining is the quickest and most commonly used staining to check cell and tissue morphology.

Eosin is an **acidic** dye: it is negatively charged (general formula for acidic dyes is: $Na^{+}dye^{-}$)**.** It stains basic (or acidophilic) structures red or pink. This is also sometimes termed 'eosinophilic'.
Thus the cytoplasm is stained pink by H&E staining.

Haematoxylin can be considered as a **basic** dye (general formula for basic dyes is:dye^{+} Cl^{-}). **Haemotoxylin** is actually a dye called hematein (obtained from the log-wood tree) used in combination with aluminium ions (Al^{3+}). It is used to stain acidic (or basophilic) structures a purplish blue. This colour shift (blueing) only happens when the red staining is passed on to a neutral or alkaline solution like hard tapwater. (Haematoxylin is not strictly a basic dye, but it is used with a 'mordant' that makes this stain act as a basic dye. The mordant (aluminium salts) binds to the tissue, and then haematoxylin binds to the mordant, forming a tissue-mordant-haematoxylin linkage.). Thus the nucleus is stained purple by H&E staining.

This means that the nucleus, and parts of the cytoplasm that contain RNA stain up in one colour (purple), and the rest of the cytoplasm stains up a different colour (pink).

General materials needed:

- Hellendahl jar or blue plastic container+rack
- Alcohol 70%,96%,100% (eg Boom #84901622)
- Acetone (eg Boom #A01C11X)
- O-Xylene (Sigma #X1040)
- Chloroform (Sigma #372978)
- Haematoxylin Gill's (ready-to-use, Sigma #GHS232 → **ALWAYS FILTER BEFORE USE, use the big filter papers on top of fridge!!)**
- Eosin Y (Merck, 1.15935), 2% in 50% EtOH, then add 0.5ml glacial acetic acid per 100 ml staining solution. Reuse until color changes from green fluorescent orange to orange.
- Entallan/Depex (Merck #1.07961.0500)
- Coverslips

Precautions and disposal:

O-Xylene **Acetone**		Read instruction cards: O-xylene Acetone
Chloroform		Read instruction card: Chloroform
Hematoxylin **Eosin**		Read instruction card: hematoxylin Eosin

Wear gloves when handling any of the above stated chemicals and work in the recirculation cabinet while using ethanol, acetone, chloroform, hematoxylin or xylene.

Ethanol, chloroform, acetone and xylene are to be disposed of in the white waste containers underneath the recirculation cabinet. Hematoxylin and eosin are to be reused as much as possible or to be disposed of in the white container underneath the histology sink.

Protocol:

Pre-treatment paraffin sections:

- Deparaffinize in Xylene 2x, 100% EtOH 2x, 96% EtOH 1x and 70% EtOH — 5' each
- Rinse with distilled water — 2 x 3'

Pre-treatment MMA sections:

- Remove plastic foil from the sections and place slides in xyleen/chloroform mixture (1:1) to get the MMA out of the sections. Check if it is completely gone, if you still see edges where the MMA has been prolong this step — 60' +
- Hydrate trough Xylene 2x, 100% EtOH 2x, 96% EtOH 1x and 70% EtOH — 5' each
- Rinse with distilled water — 2 x 3'

Pre-treatment cryosections/cytospins:

- Defrost sections under hairdryer for 60 minutes before opening box (to prevent ice crystals destroying the morphology of your sections)
- Place slides in a Hellendahl jar and add aceton to fix the tissue/cells — 10'
- Rinse with distilled water — 2 x 3'

Then for all types of samples:

1. hematoxylin — 5'
2. Tapwater to convert red staining into blue. Either running tapwater or refresh every minute — 5'-10'
3. Quick dip in distilled water
4. Eosin — +/- 45 sec

5. 70% EtOH 10 sec
6. dehydrate in 96% EtOH, 100% EtOH, 2x xylene 1' each
7. Mount with Entallan (Depex) while slides are still wet from xylene
8. Let slides dry in the recirculation cabinet for at least 60'.

Staining results

Blue:	Keratohyalin, nuclei, cytoplasmic RNA, calcium deposits, bacteria
Red:	muscle, keratin, elastic fibres, fibrin
Pink:	Collagen, reticulin, nerve fibres, amyloid
Orange:	red blood cells

Erasmus MC Orthopedics/ENT lab		
Title: **Safranin O staining for GAGs on paraffin, MMA - and cryosections**		Number of pages**: 3**
Protocol: **GAG-03**	Version: 3.0	Effective date: **27/10/2020**
Author: **Nicole Kops**		Primary reviewer: **N.Kops**

Background:
This method is used for the detection of cartilage, mucin, and mast cell granules on formalin-fixed, paraffin- or MMA embedded tissue sections, and may be used for frozen sections as well. The cartilage and mucin will be stained orange to red, and the nuclei will be stained black (when hematoxylin is used). The background is stained bluish green in case of Fast Green and bright green when Light Green is used.

In normal, not severely damaged cartilage the binding of Safranin O to GAGs in stoichiometric and is found to be very little nonspecific. Hence the intensity of Safranin O staining is directly proportional to the proteoglycan content in normal cartilage. Safranin 'O' has thus been used to demonstrate any changes that occur in articular diseases such as OA and is also widely used to grade the severity of OA in eg. the Mankin scoring system.

Note:

- The binding of Safranin O to cartilage GAG is only stoichiometric when the amount of GAG in the tissue is not too low. This is obviously not always the case in OA, and Safranin O may thus not be a sensitive indicator of GAG content in very severely diseased cartilage (ref: Histochemistry. 1988;89(2):185-8)
- **When staining decalcified tissue, decalcification with acid decalcifiers like formic acid is preferred as EDTA, used as a non-acidic decalcificier, breaks down GAGs. Area's that are low on GAGs will be more susceptible to this breakdown resulting in a possible underestimation of the amount of GAGs present in the tissue when using EDTA.**
  When wanting to perform immunohistochemical stainings on the same samples we do use EDTA as decalcifier taking the breakdown of GAGs for granted as IHC's are much more sensitive to the negative influence of acids than GAGs for EDTA.
- The haematoxylin nuclear stain is left out of the protocol as this might overrule the green and orange. The nuclei are well visible anyway.
- We prefer Light Green over Fast Green as the Light Green gives a brighter green staining result.

General materials needed:

- Hellendahl jar or blue plastic container+rack
- Alcohol 70%,96%,100% (eg Boom #84901622)
- Acetone (eg Boom #A01C11X)
- O-Xylene (Sigma #X1040)
- Chloroform (Sigma #372978)
- Light Green Yellowish (Fluka #62110), 0.1% in distilled water eg 100mg/100ml
  OR
  Fast Green (Sigma #861154), 0.05% in distilled water eg. 50mg/100ml
- Safranin O (= Safranin T, Fluka #84120) 0.1% in distilled water (eg 100mg/100ml)
- Acetic acid (Fluka #45730), 1% in distilled water (eg 1ml/100ml)
- Entallan/Depex (Merck #1.07961.0500)
- Coverslips

Precautions and disposal:

O-Xylene **Acetone**		Read instruction cards: O-xylene Acetone
Chloroform **Fast Green**		Read instruction card: Chloroform Fast Green
Safranin O		Read instruction card: Safranin O

Wear gloves when handling any of the above stated chemicals and work in the recirculation cabinet while using ethanol, acetone, chloroform, haematoxylin or xylene.

Ethanol, chloroform, acetone and xylene are to be disposed of in the white waste containers underneath the recirculation cabinet. Haematoxylin, Light Green, Fast Green and Safranin O are to be reused as much as possible or to be disposed of in the white container underneath the histology sink.

Protocol:

Pre-treatment paraffin sections:

- Deparaffinize in Xylene 2x, 100% EtOH 2x, 96% EtOH 1x and 70% EtOH — 5' each
- Rinse with distilled water — 2 x 3'

Pre-treatment MMA sections:

- Remove plastic foil from the sections and place slides in xyleen/chloroform mixture (1:1) to get the MMA out of the sections. Check if it is completely gone, if you still see edges where the MMA has been prolong this step — 60' +
- Hydrate trough Xylene 2x, 100% EtOH 2x, 96% EtOH 1x and 70% EtOH — 5' each
- Rinse with distilled water — 2 x 3'

Pre-treatment cryosections/cytospins:

- Defrost sections under hairdryer for 60 minutes before opening box (to prevent ice crystals destroying the morphology of your sections)
- Place slides in a Hellendahl jar and add aceton to fix the tissue/cells — 10'
- Rinse with distilled water — 2 x 3'

Then for all types of samples:

1. Light Green solution* (or Fast Green if preferred) — 8' (5-10')
2. quick rinse in 1% acetic acid — 2x10 sec
3. Safranin O solution — 12'
4. Rinse in 96% ethanol 2x. Duration of rinse step is depending on tissue type. In case of joint sections rinsing should commence until growth plate is visible as a bright orange/red line in a bright green (or bluish) background — +/- 30 sec
5. dehydrate in 100% EtOH (1x) and xylene (2x) — 1' each
6. Mount with Entallan (Depex) while slides are still wet from xylene

7. Let slides dry in the recirculation cabinet for at least 60'.

*: Light Green can cause tearing of bone when staining non-decalcified MMA sections so in case this happens, shorten this step.

Staining results

Cartilage:	orange/red
Nuclei:	dark red when haematoxylin is left out, otherwise dark blue/black
Cytoplasm/bone:	green (in case of Light Green) or blue (in case of Fast Green)

Erasmus MC Orthopedics/ENT lab		
Title: **RGB trichrome staining on (decalcified) paraffin sections**		Number of pages**: 3**
Protocol: **HIS-22**	Version: 1.0	Effective date: **27/10/2020**
Author: **Nicole Kops**		Primary reviewer: **N.Kops**

Background:
A novel RGB-trichrome staining method for routine histological analysis of musculoskeletal tissues.
Described in the link below is a novel staining method, the RGB trichrome, amenable for application to decalcified, paraffin embedded human musculoskeletal tissues. The acronym RGB corresponds to the three primary dyes used: picrosirius Red, fast Green, and alcian Blue. Although these individual pigments are commonly used either isolated, in binary combinations, or as part of more complex polychrome staining methods, when merged in the RGB trichrome staining produce high-quality/high-contrast images, permitting not only clear identification of different tissues (i.e., the different types of cartilage, bone and fibrous connective tissue), but also discrimination between calcified and uncalcified bone and cartilage, as well as an unexpected diversity of shades of color, while displaying singular properties among polychrome staining methods, such as the unveiling of the bone osteocyte dendritic/canalicular network.

The link**:**
https://www.nature.com/articles/s41598-020-74031-x

Novell to us is that we can stain osteoid in decalcified samples so there is no need to embed in MMA anymore. Besides this huge benefit there is also a better differentiation of tissue, even within the tissues itself.

Note:

- In the article from Nature 5% nitric acid is used as a decalcifying agent but as we mostly have EDTA decalcified samples this protocol has been tested on EDTA samples and works very well as well.
- Other types of sections but paraffin have not been tested yet.
- The thickness of the sections plays a key role in the outcome of the staining. Please pay attention that all sections are 6um in thickness. When in doubt while sectioning, discard the section that might be too thin as the intensity ratio between Fast Green and Picro Sirius Red is very delicate. Cutting thicker sections has been tested (Nicole, 23/10/2020) but that does not improve the staining either.

General materials needed:

- Hellendahl jar or blue plastic container+rack
- Alcohol 70%,96%,100% (eg Boom #84901622)
- O-Xylene (Sigma #X1040)
- Alcian Blue 8GX (Sigma, A5268), 1% w/v in 3% aqueous acetic acid solution (pH 2.5)
- Fast Green (Sigma #861154), 1% w/v in distilled water (eg. 1gram/100ml)
- Sirius Red (aka Direct Red 80) (Sigma, 365548), 1% w/v in a saturated aqueous solution of picric acid.
- Acetic acid (Fluka #45730), 1% in tap water (eg 1ml/100ml)
- Tapwater
- Entallan/Depex (Merck #1.07961.0500)
- Coverslips

Precautions and disposal:

O-Xylene **Acetone**		Read instruction cards: O-xylene Acetone
Chloroform **Fast Green**		Read instruction card: Chloroform Fast Green
Sirius Red/Direct Red 80		Read instruction card: Sirius Red

Wear gloves when handling any of the above stated chemicals and work in the recirculation cabinet while using ethanol, acetone or xylene.

Ethanol, chloroform, acetone and xylene are to be disposed of in the white waste containers underneath the recirculation cabinet. Fast Green and Alcian blue can be re/used many times but when to be disposed of, please discard in the white waste containers underneath the recirculation cabinet.
The Sirius Red solution can be reused many times and can be kept for up to 3 years. **When it needs disposal be very careful not to use any metal lids/containers. Picric acid crystals can be explosive !! Collect PSR solution in a waste container in the yellow safety cabinet.**

Protocol:

1.	Deparaffinize in Xylene 2x, 100% EtOH 2x, 96% EtOH 1x and 70% EtOH	5' each
2.	Rinse with distilled water	2 x 3'
3.	Alcian Blue solution (check pH before staining)	20'
4.	Rinse in tap water	5'
5.	Fast Green solution	20'
6.	Rinse in tap water	5'
7.	Picro Sirius Red solution	30'
8.	Rinse in 1% acetic acid solution	2 x 3' *
9.	Dehydrate in 100% EtOH (not in recirculation cabinet)	1'
10.	dehydrate in 100% EtOH (1x) and xylene (2x) (in recirculation cabinet)	1' each
11.	Mount with Entallan (Depex) while slides are still wet from xylene	
12.	Let slides dry in the recirculation cabinet for at least 60'.	

*: duration may vary, depending on type of tissue.

Staining results (in sections generally stained in the lab, for the full range of results, see Nature article)

Osteoid	bright red
Calcified bone	green
Uncalcified bone	red
Proteoglycans (GAGs)	bright blue
Collagen fibers	red

Appendix IV: Results Histology and Mechanical Tests

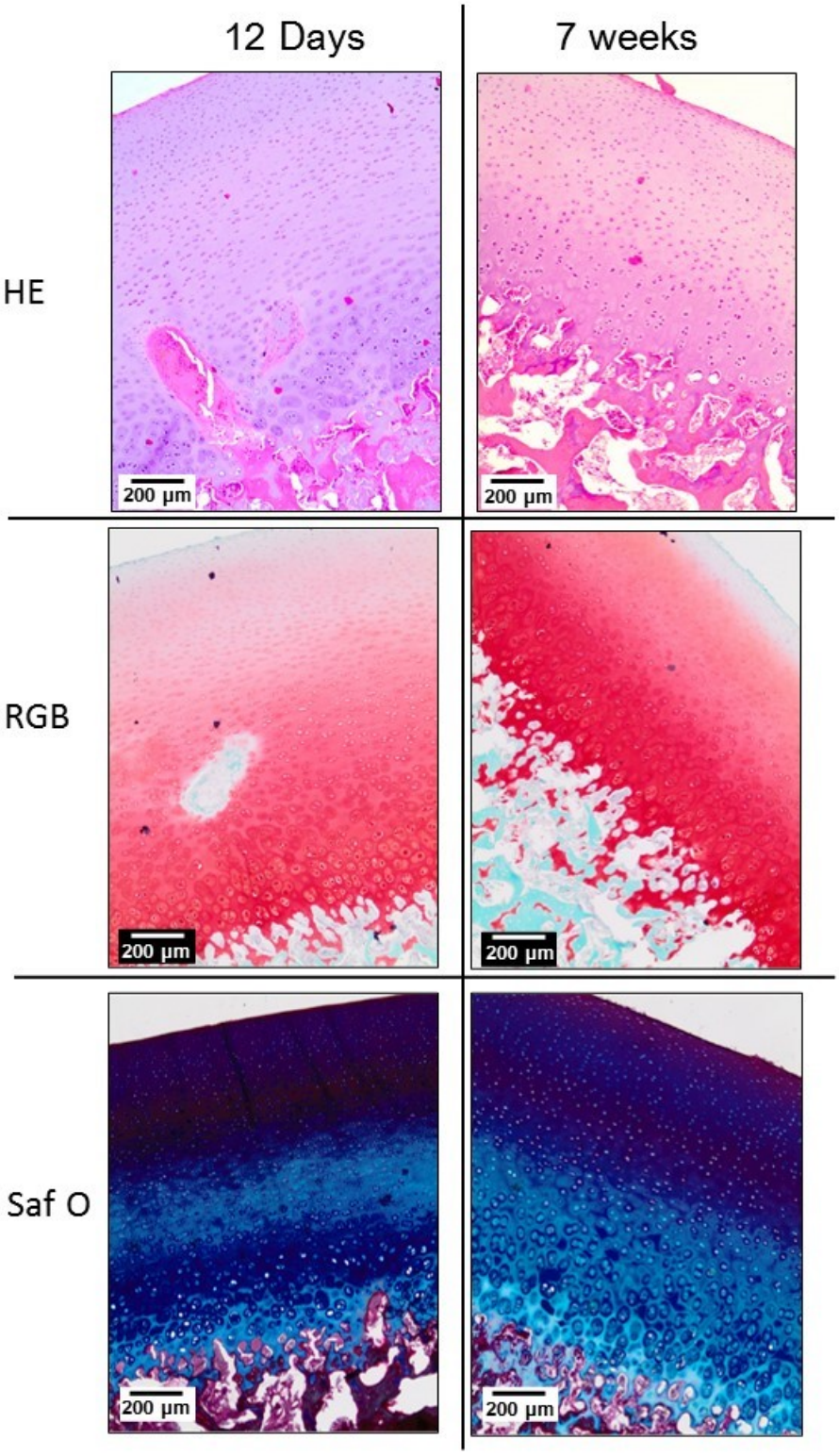

Figure 6.10: Histology images of the 12 days and 7 weeks old interface samples. HE, RGB and Saf O stainings were performed on these samples.

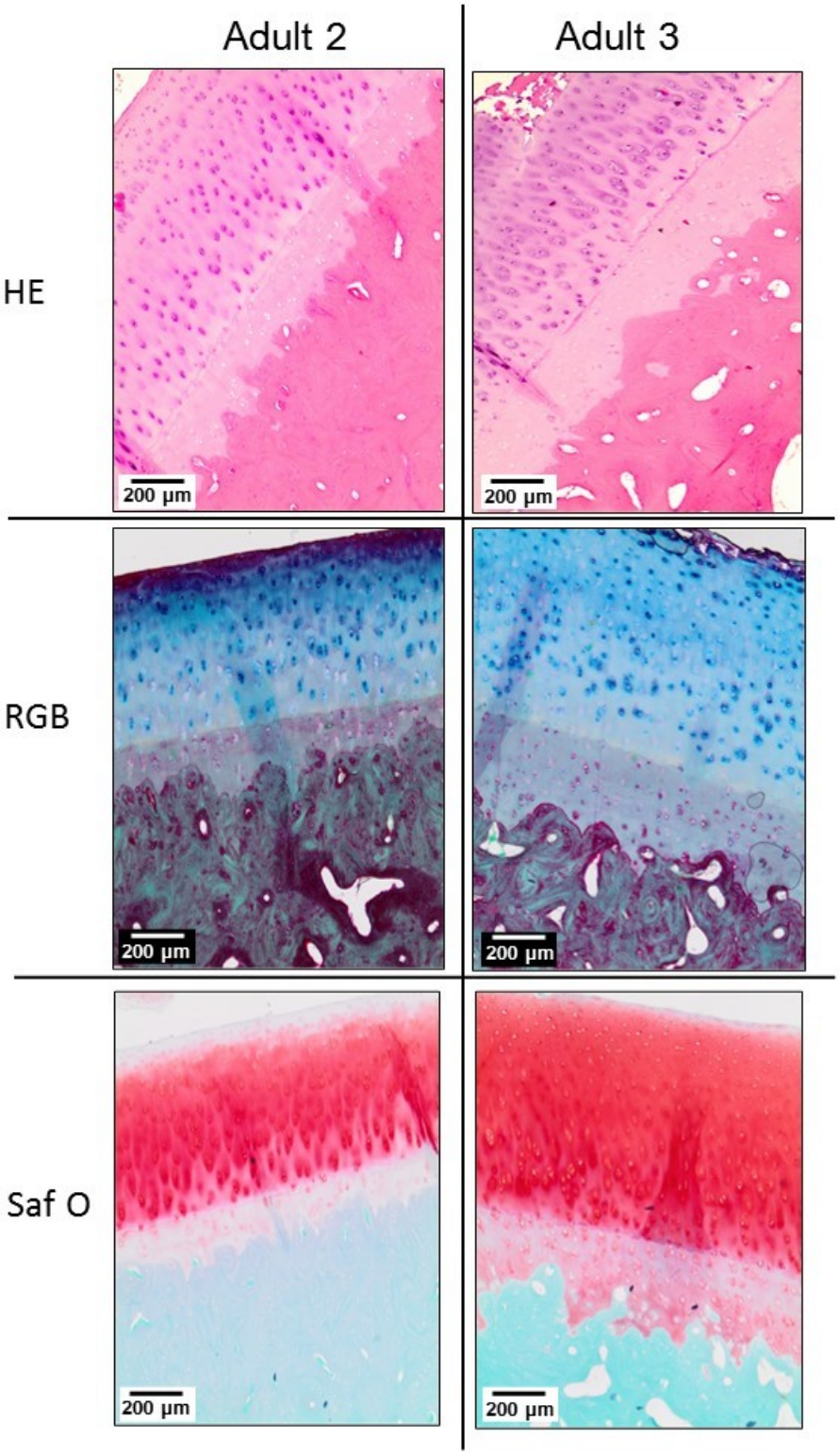

Figure 6.11: Histology images of the Adult 2 and Adult 3 interface samples. HE, RGB and Saf O stainings were performed on these samples.

Nanoindentation Heatmaps of all Samples

In this section, the heatmaps of all the samples are presented. Each sample was indented three times in the same location according to the nanonidenter machine. After the Oliver-Pharr data analysis, the data was filtered with a Gaussian filter, where σ was set as 0.5. This value was chosen in order to avoid the values of the calcified cartilage to be blurred out. The values in the heatmaps represent the elastic modulus in MPa, indicated with a scale bar on the right side of the matrices. The black boxes are data points which were eliminated from further data analysis due to an indentation error.

Adult 1 : Lateral-Distal

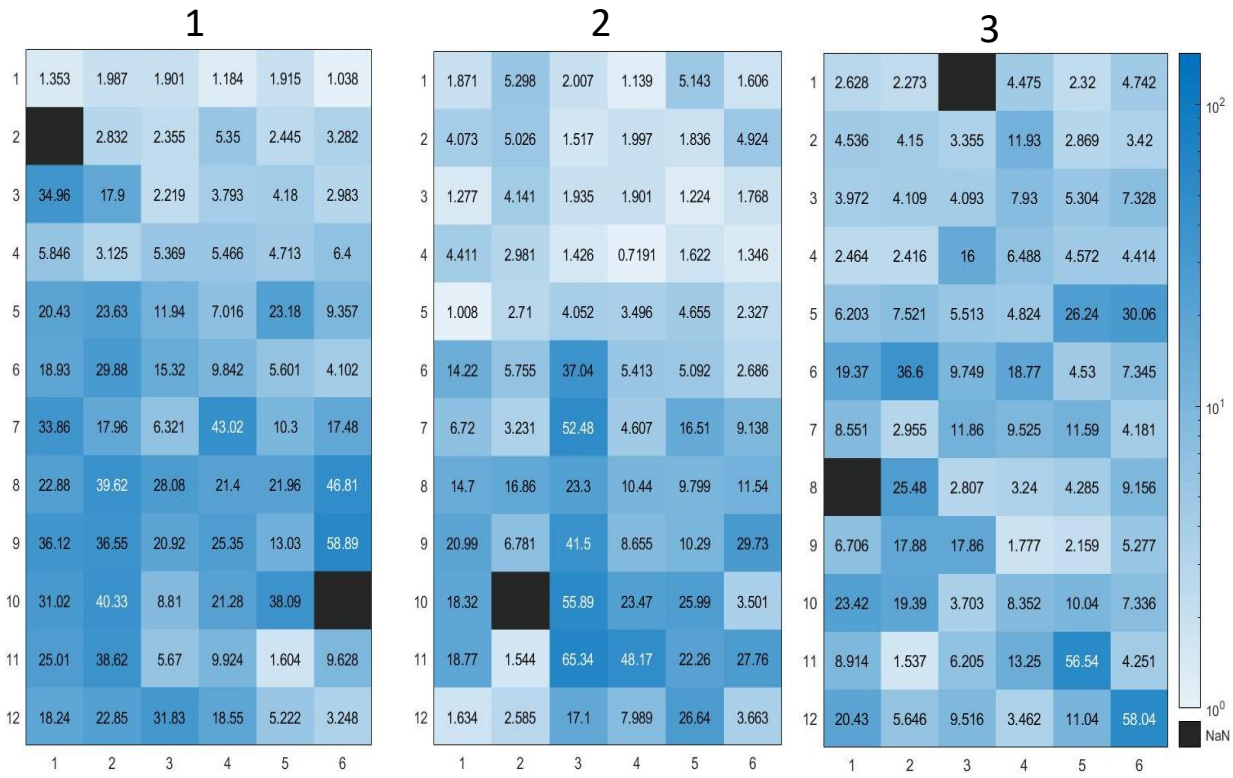

Gaussian Filter

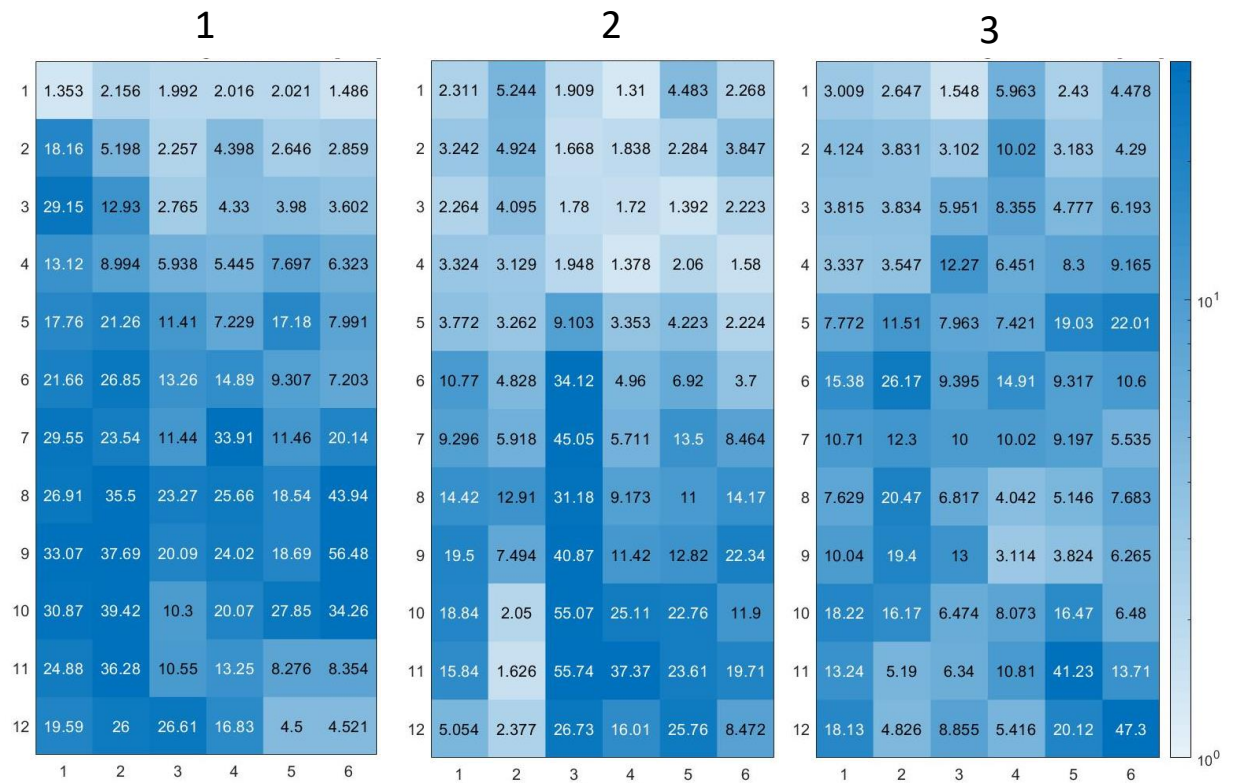

Adult 1 : Lateral-Proximal

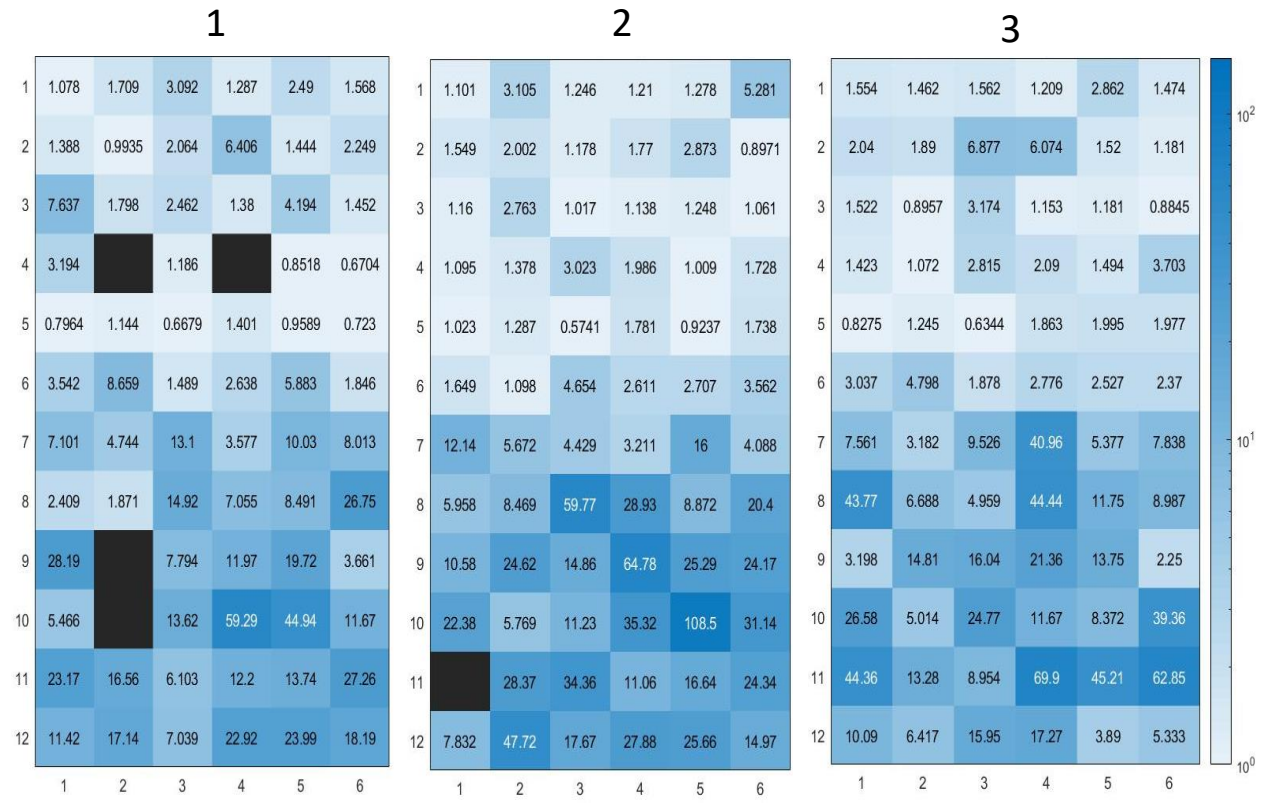

Gaussian Filter

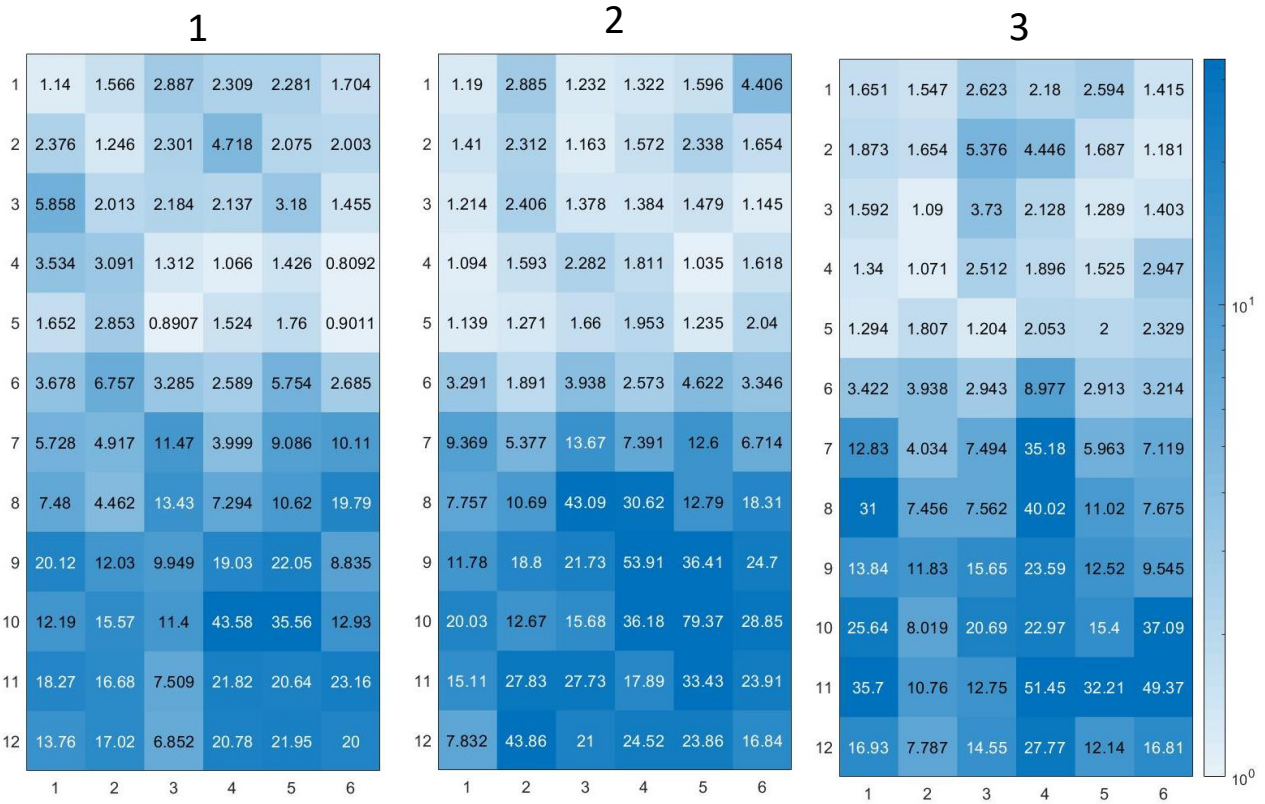

Adult 1 : Medial-Proximal

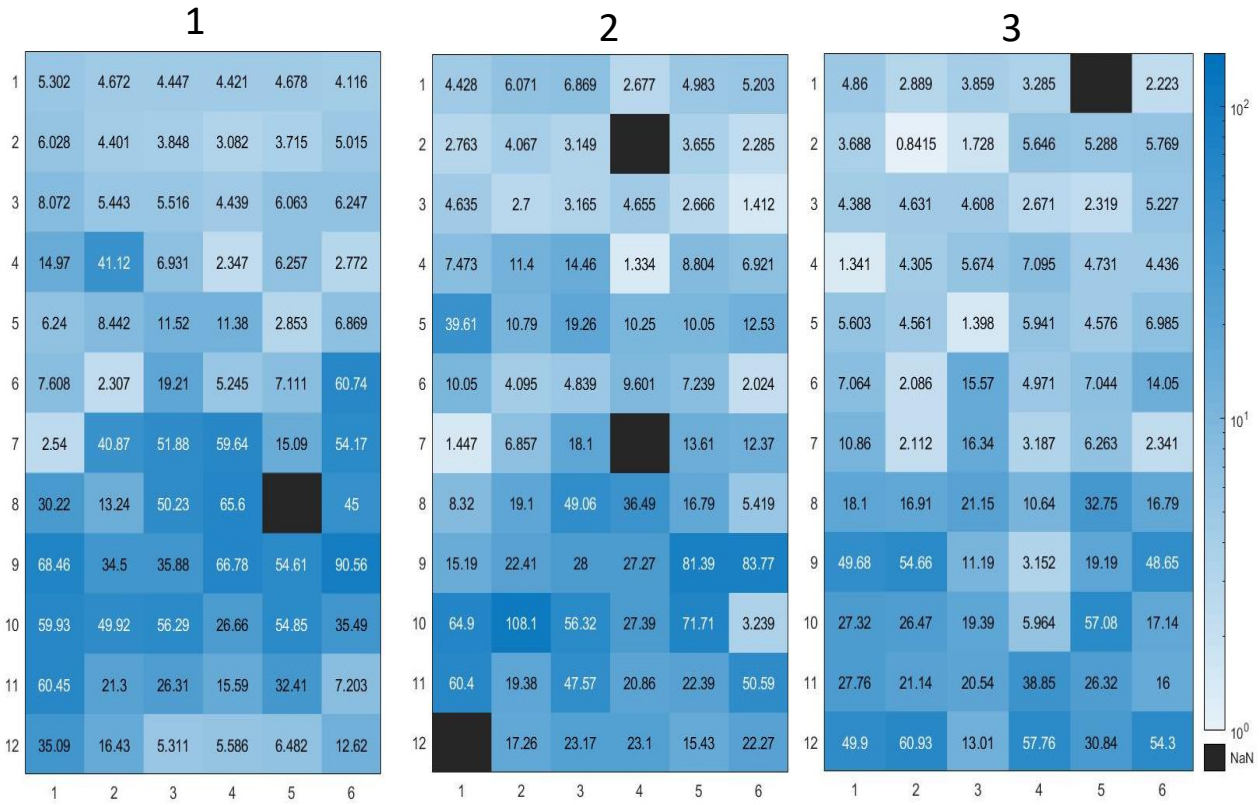

Gaussian Filter

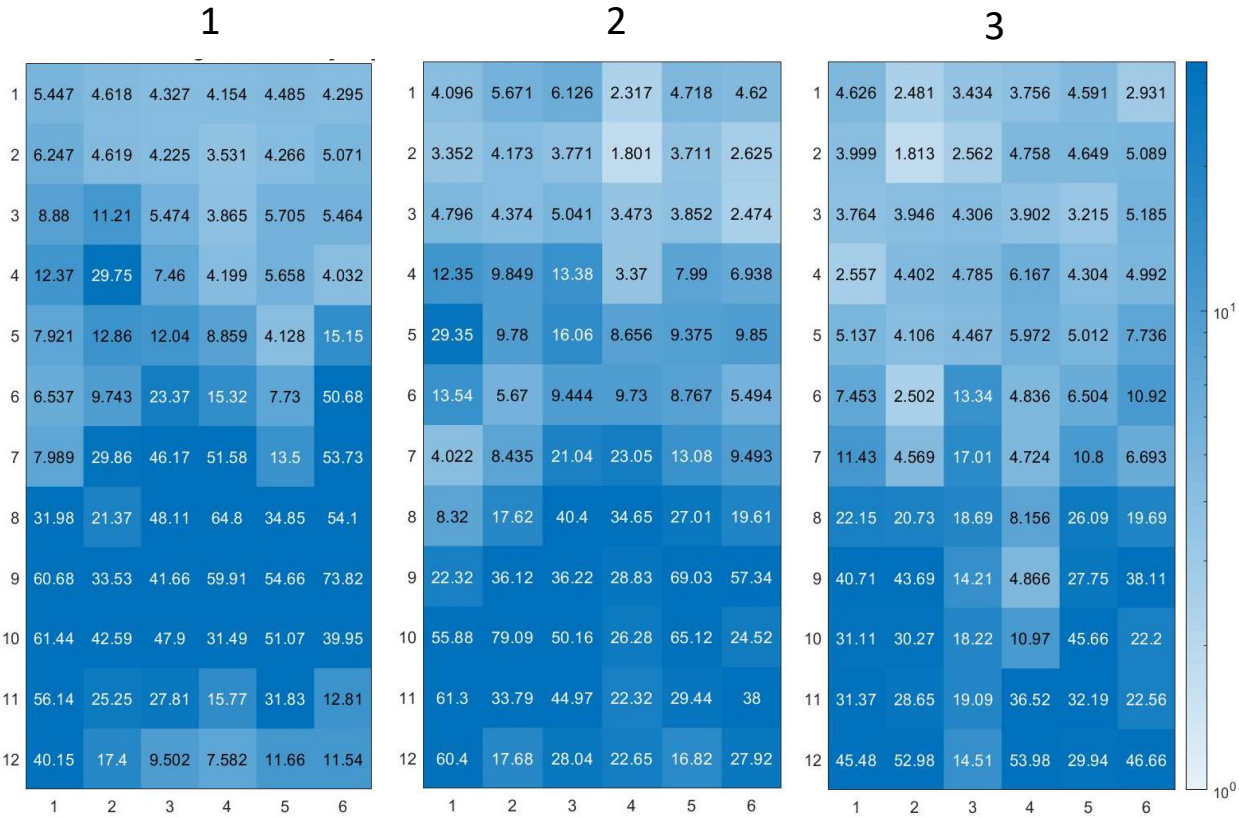

Adult 1 : Medial-Distal

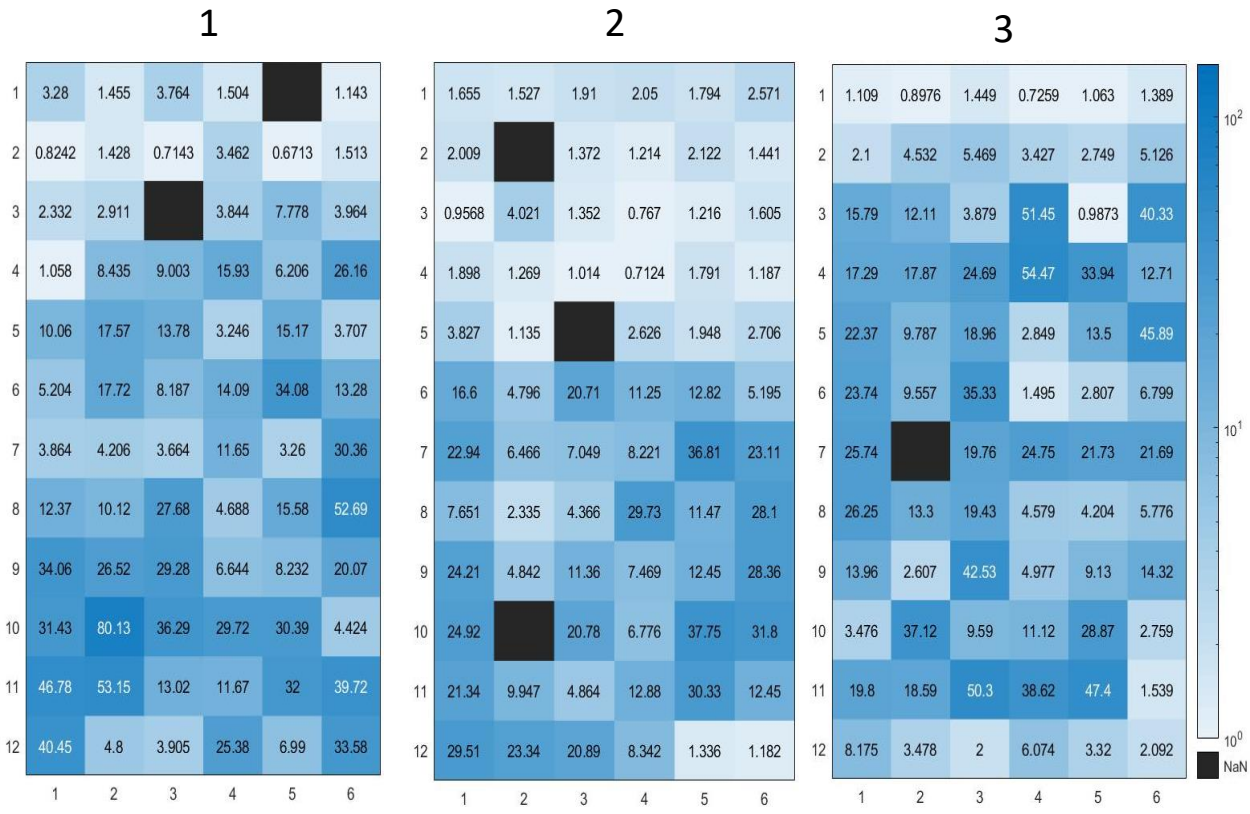

Gaussian Filter

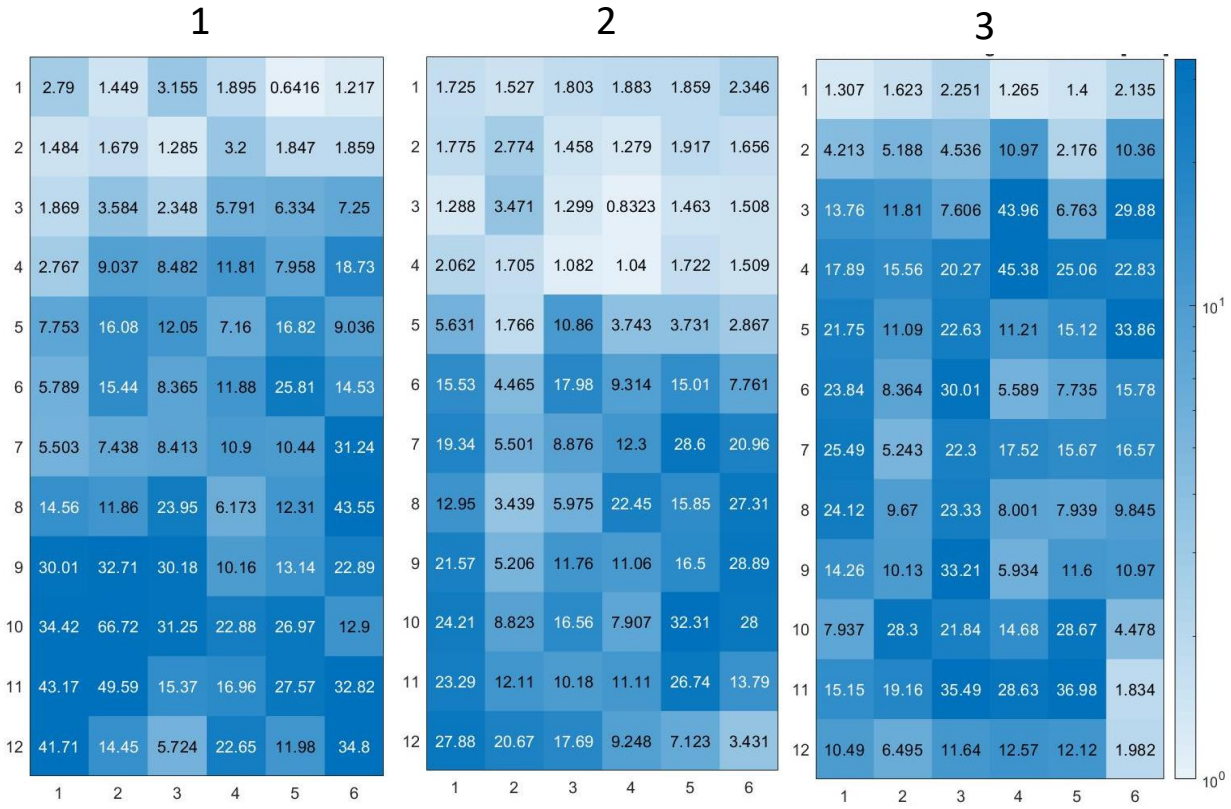

Adult 2 : Lateral

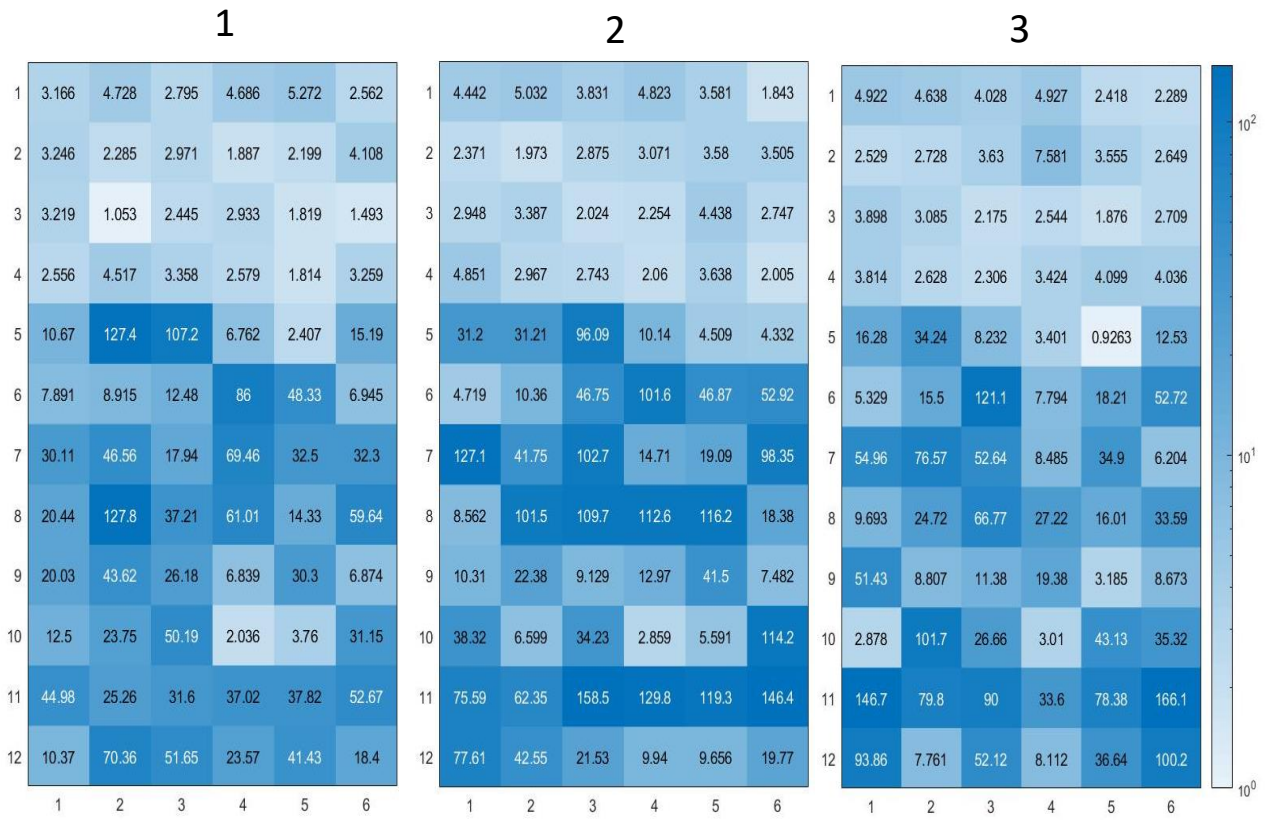

Gaussian Filter

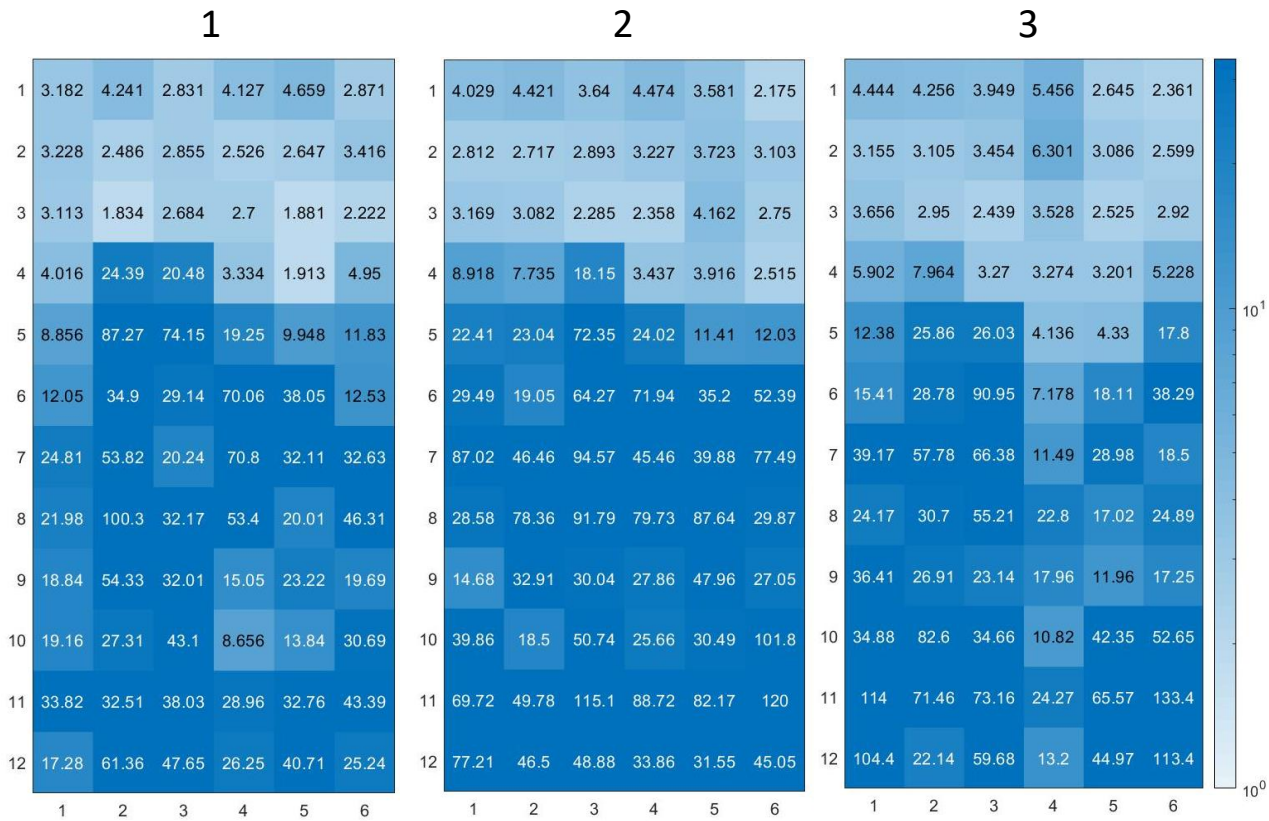

Adult 2 : Medial-Distal

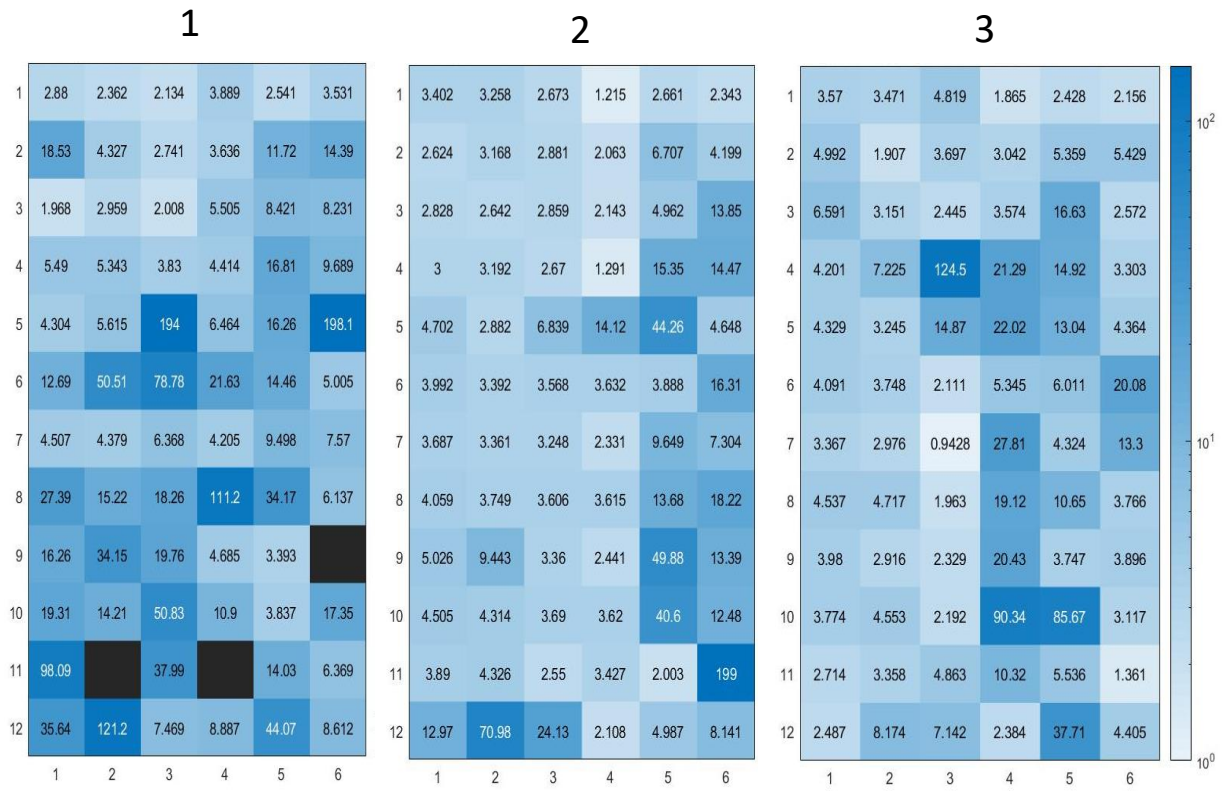

Gaussian Filter

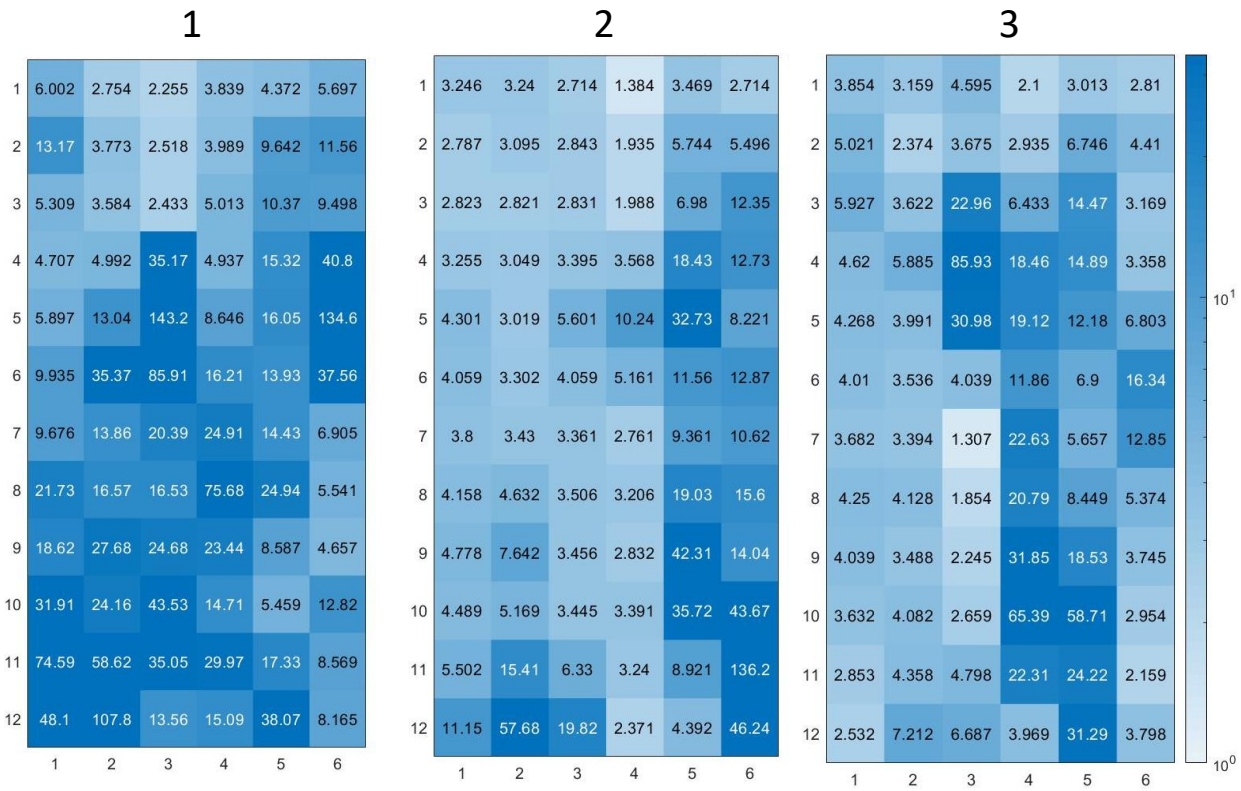

Adult 2 : Medial-Proximal

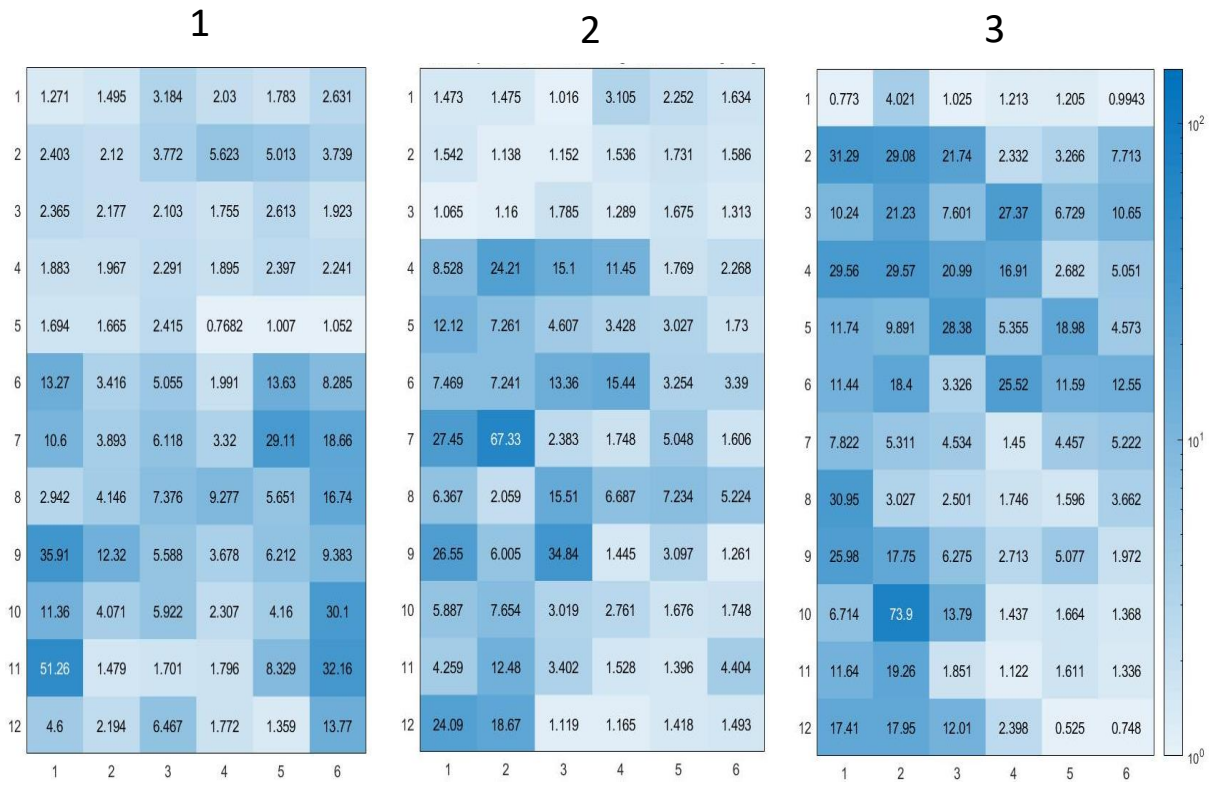

Gaussian Filter

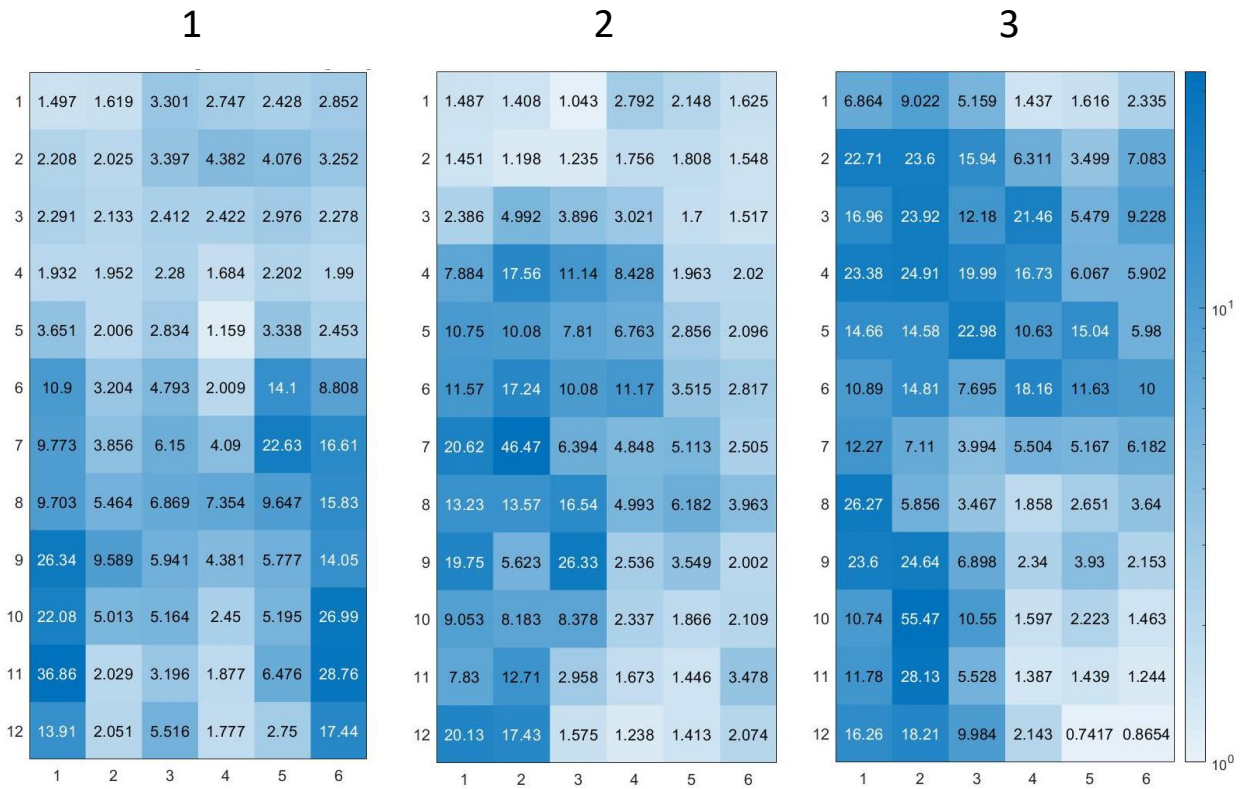

Adult 3 : Lateral-Distal

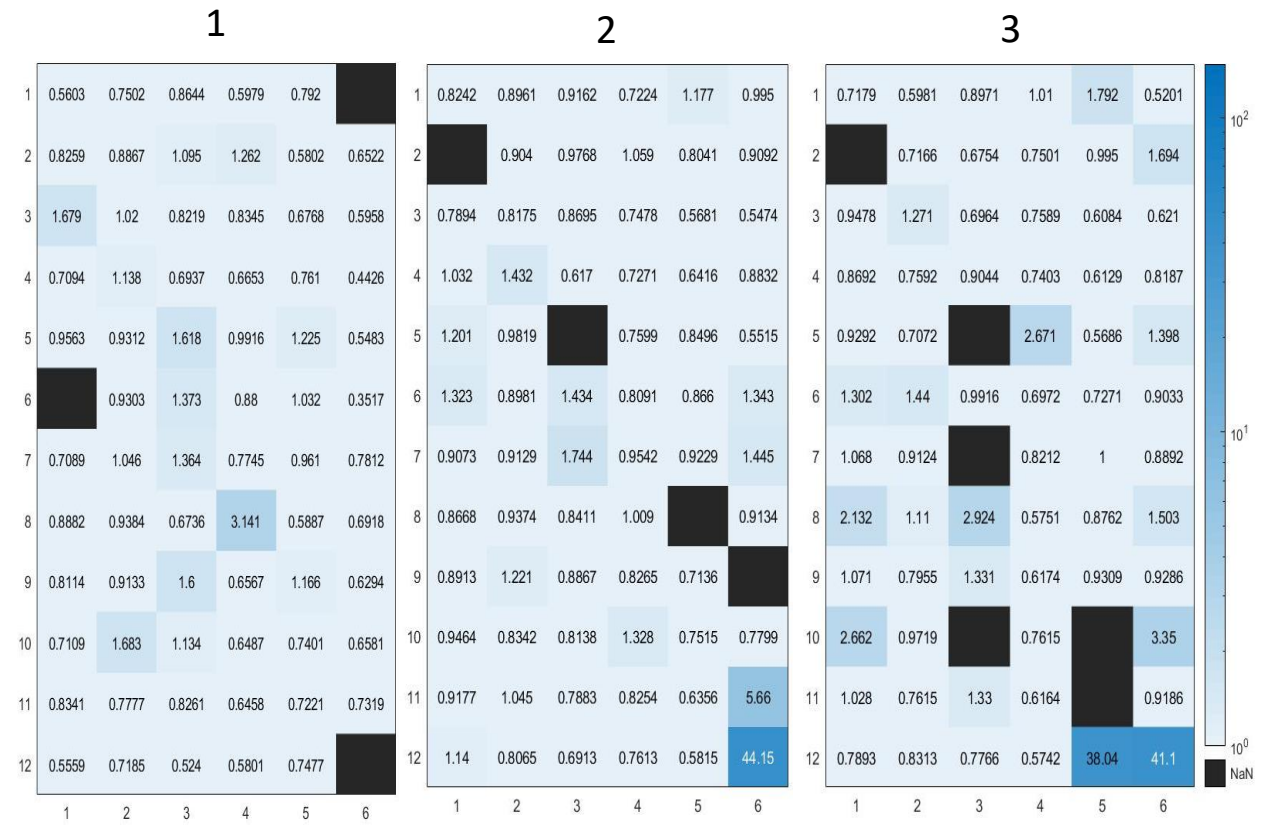

Gaussian Filter

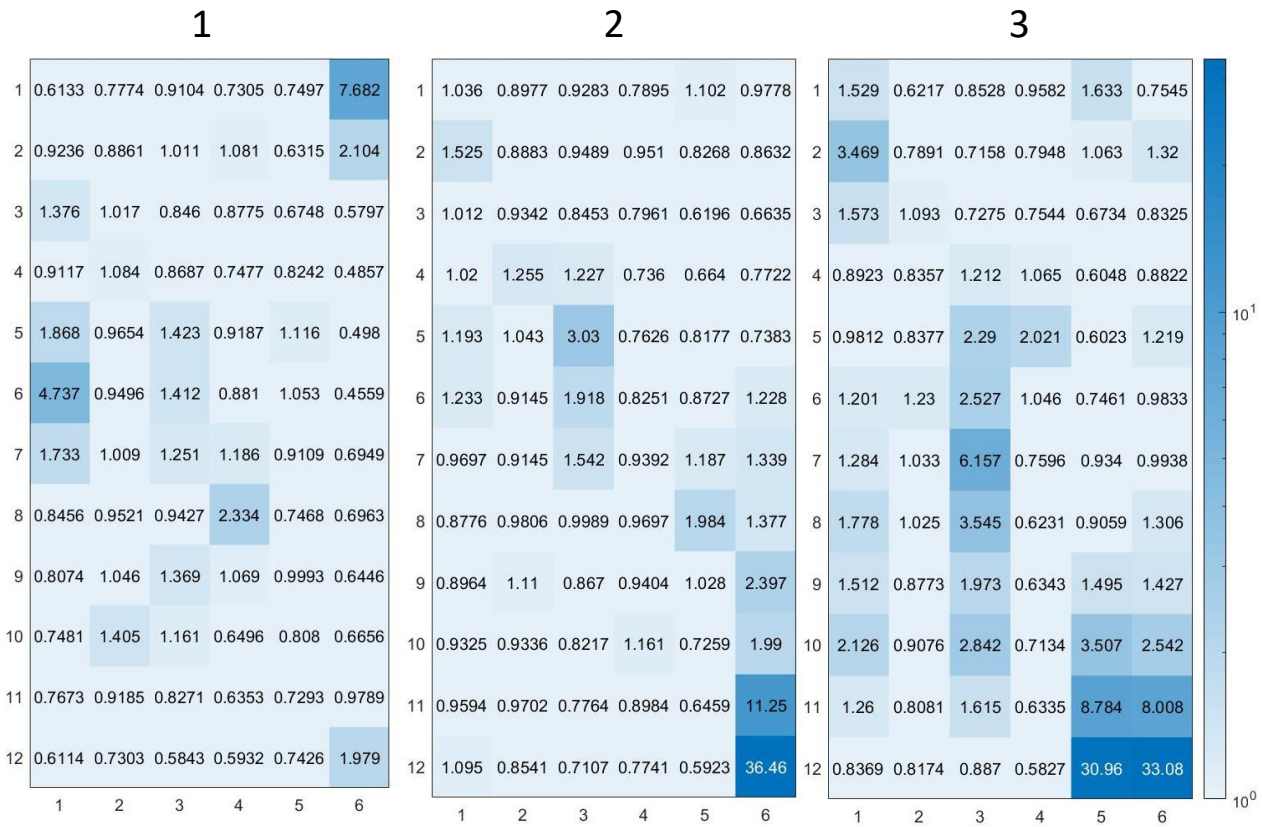

Adult 3 : Lateral-Proximal

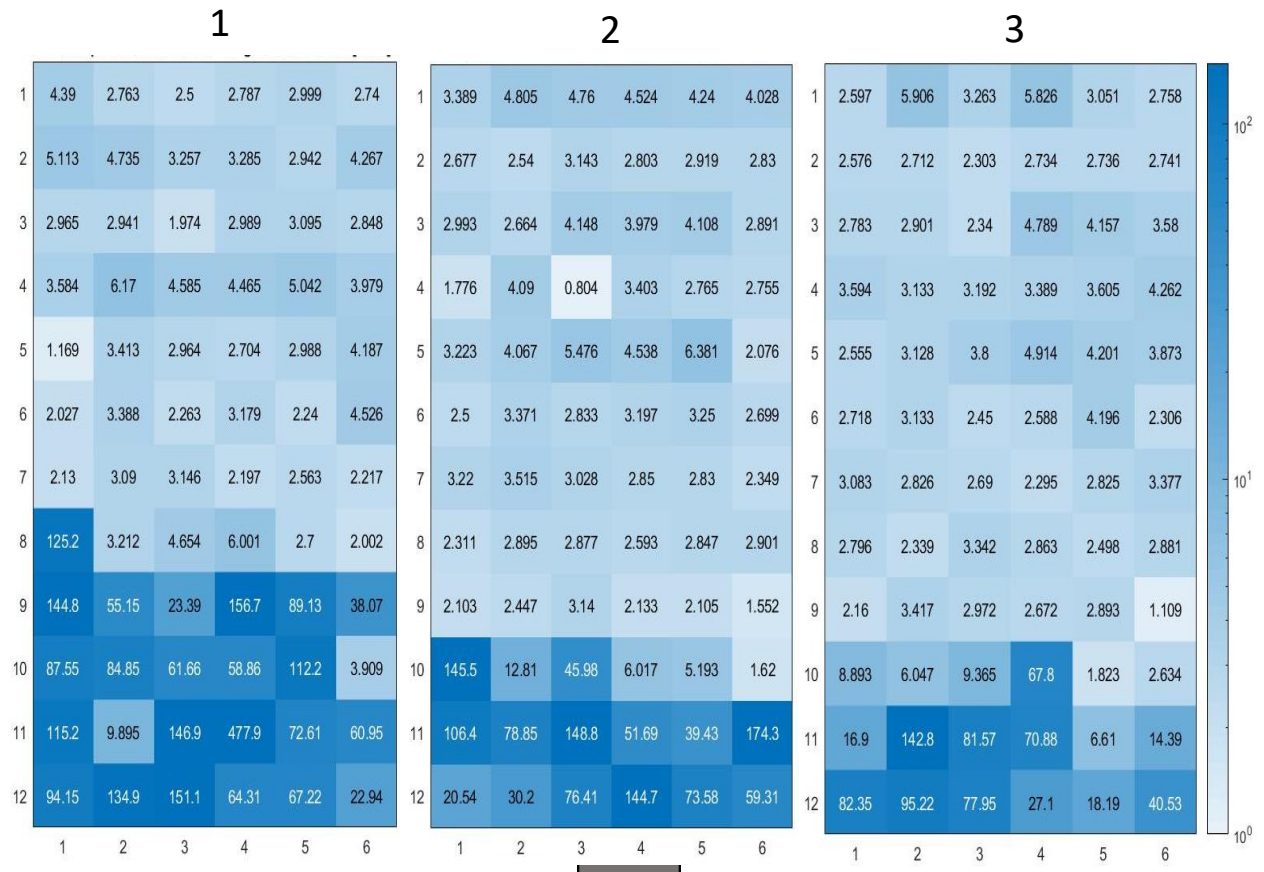

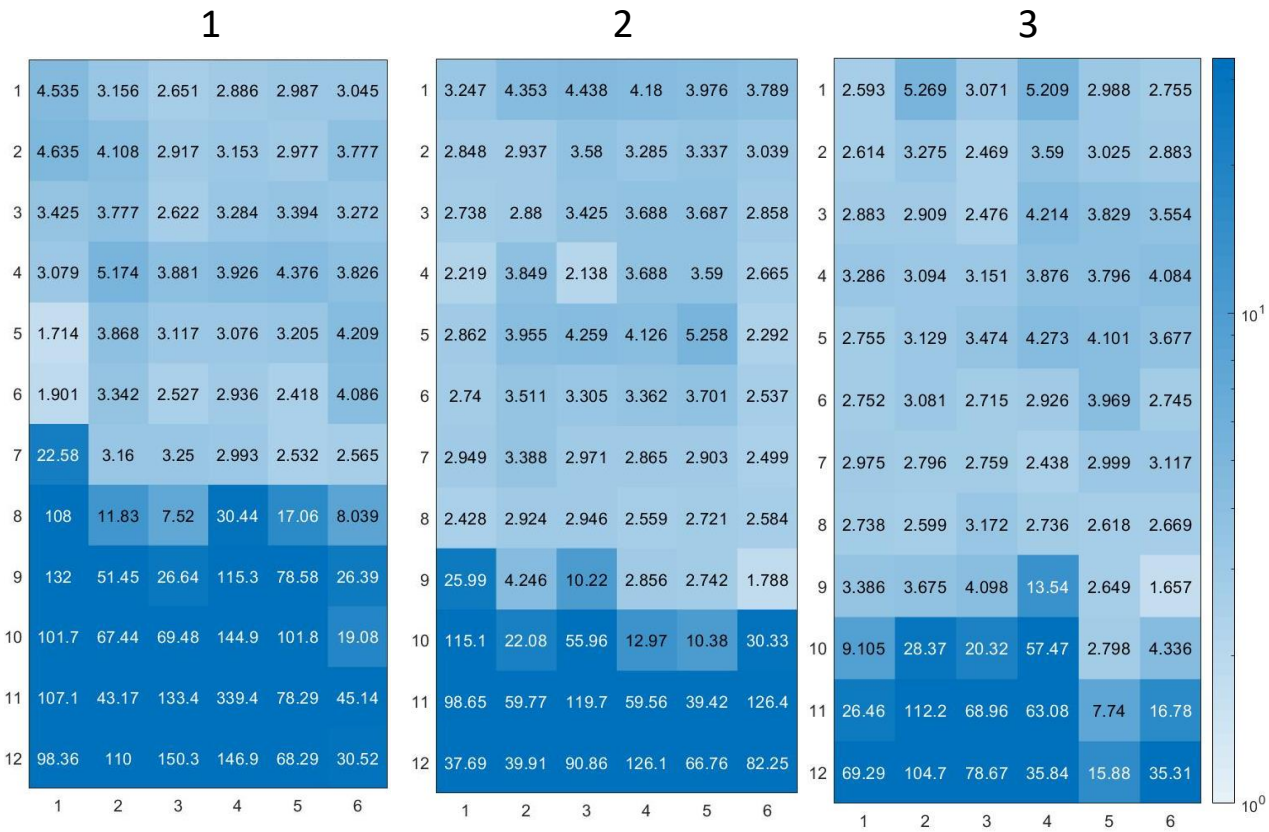

Adult 3 : Medial-Distal

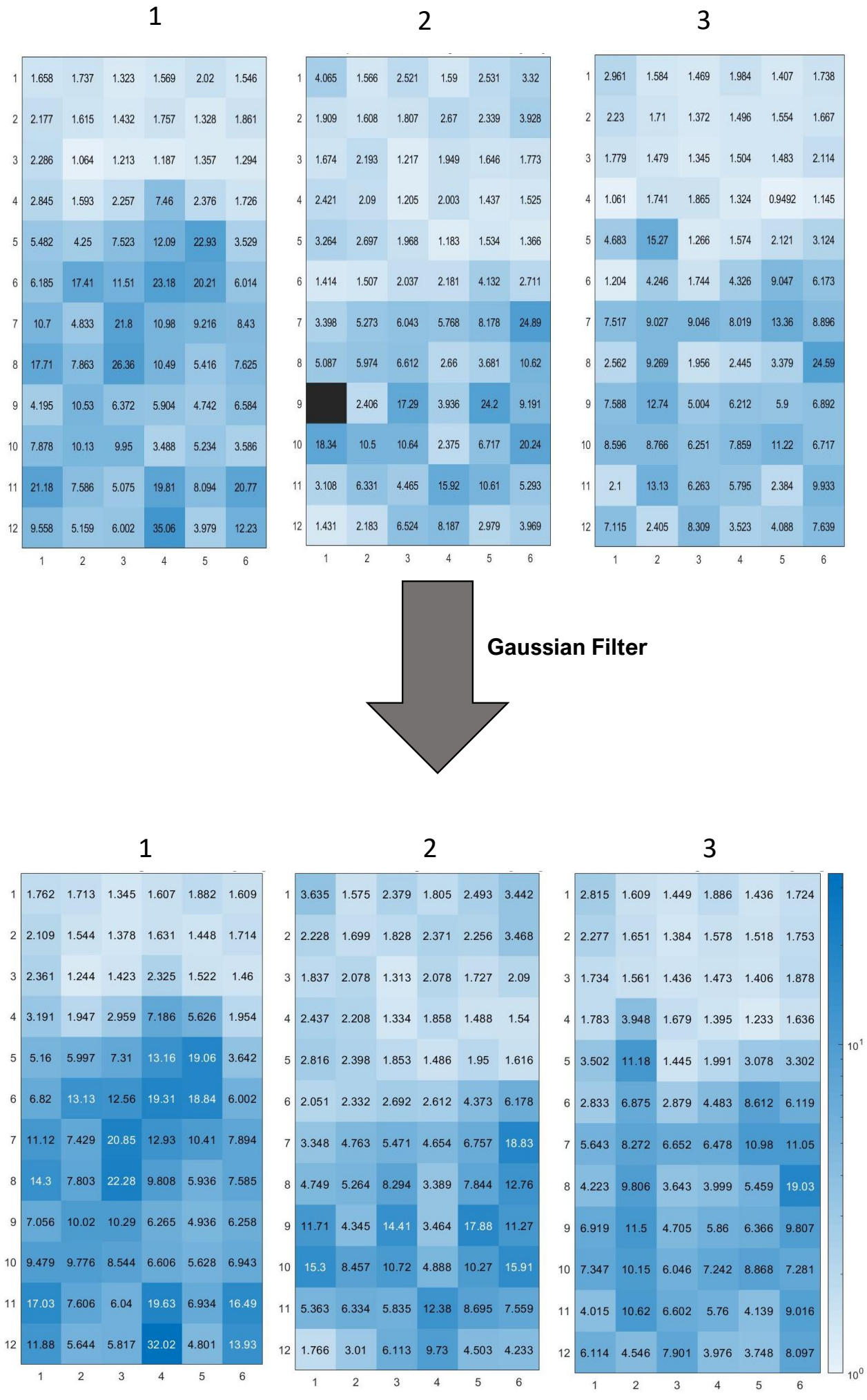

Adult 3 : Medial-Proximal

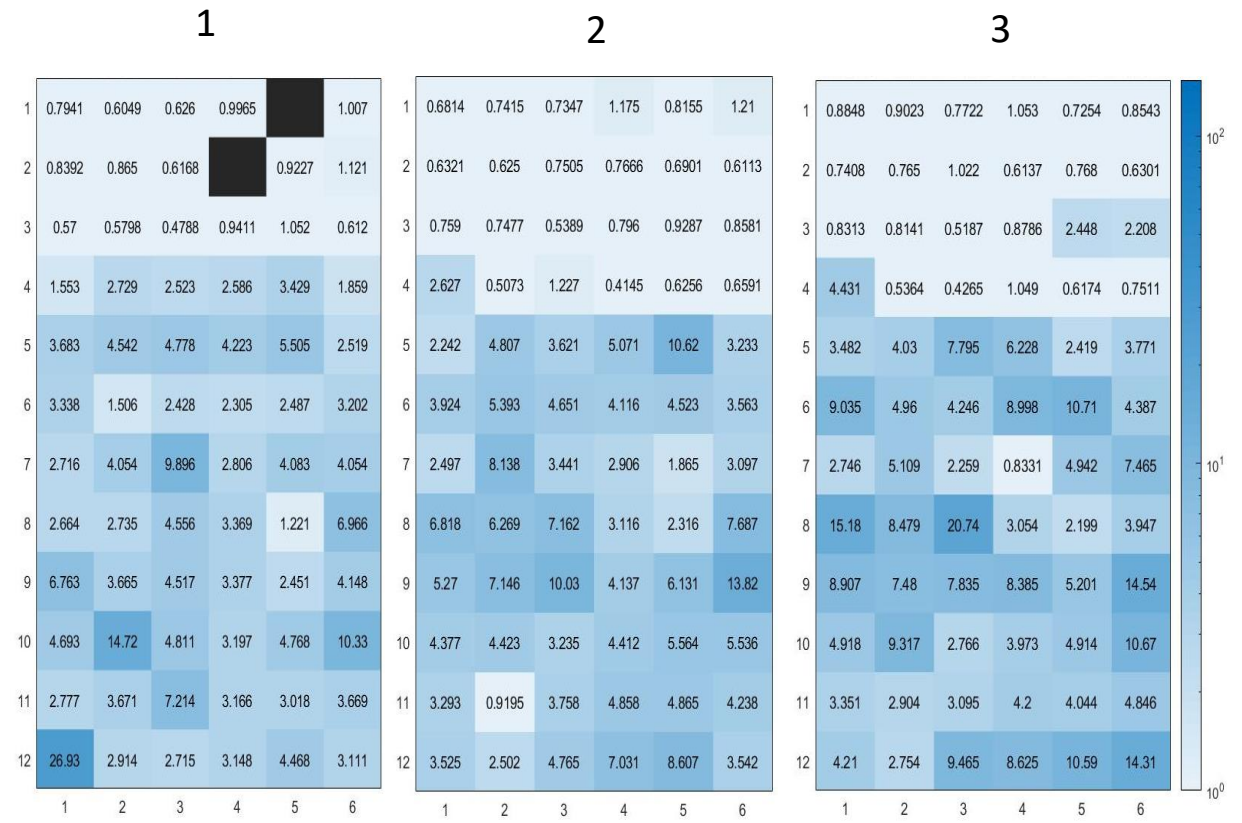

Gaussian Filter

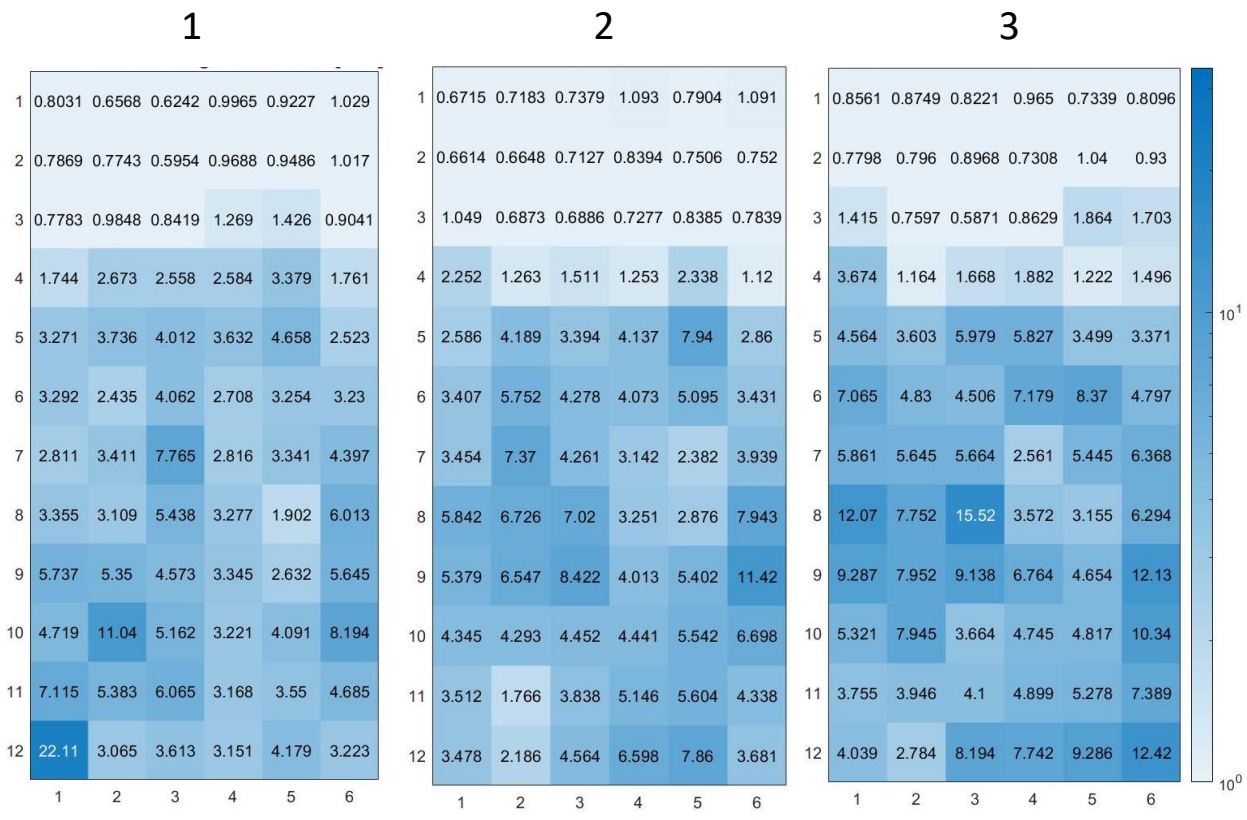

13 Months: Lateral-Distal

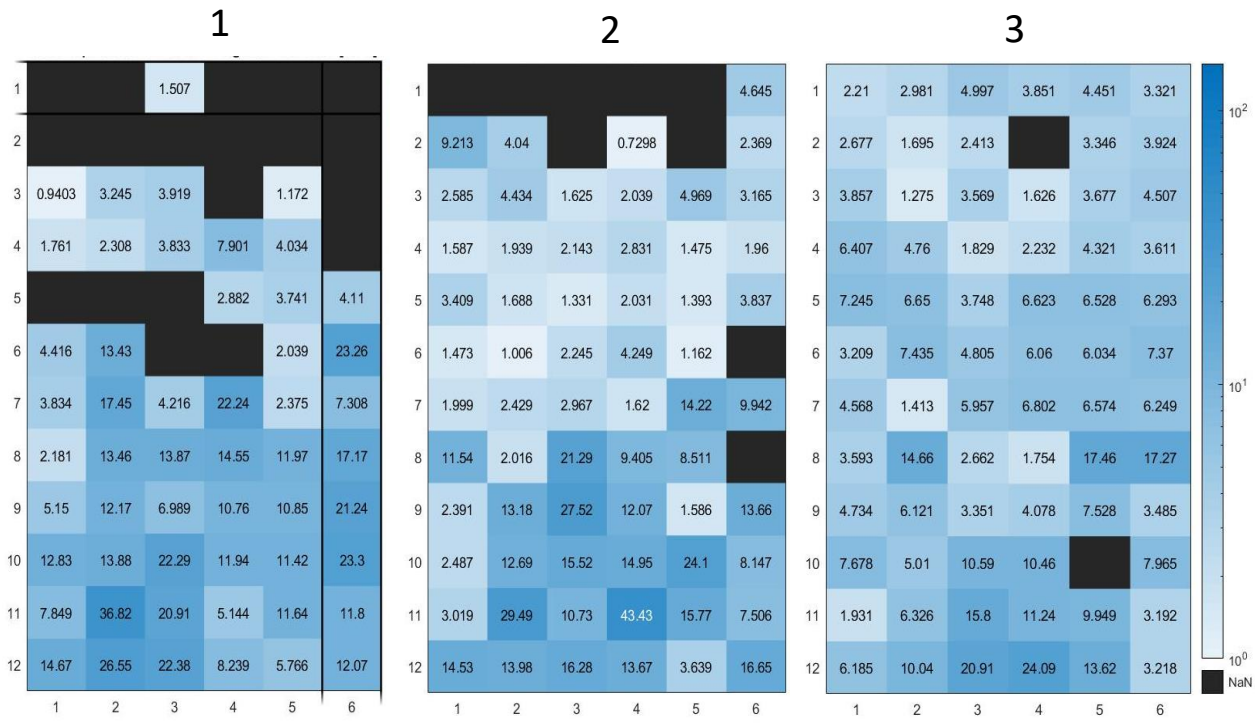

Gaussian Filter

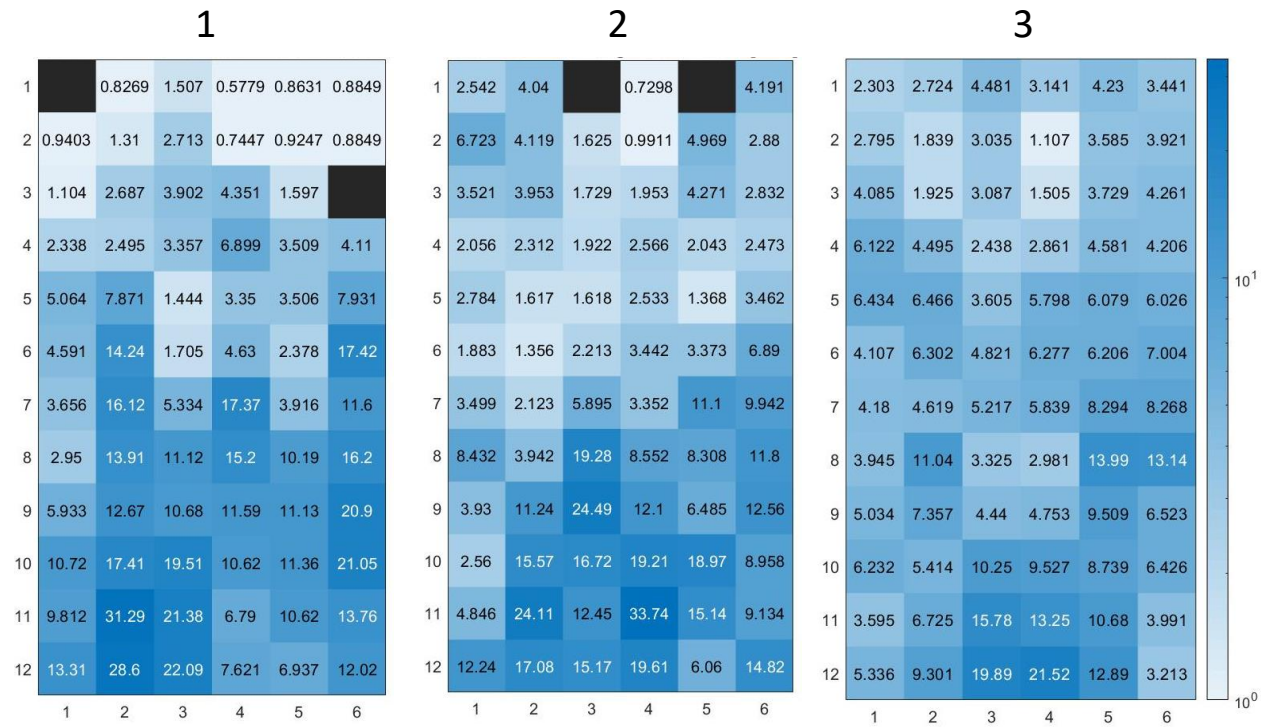

13 Months: Lateral-Proximal

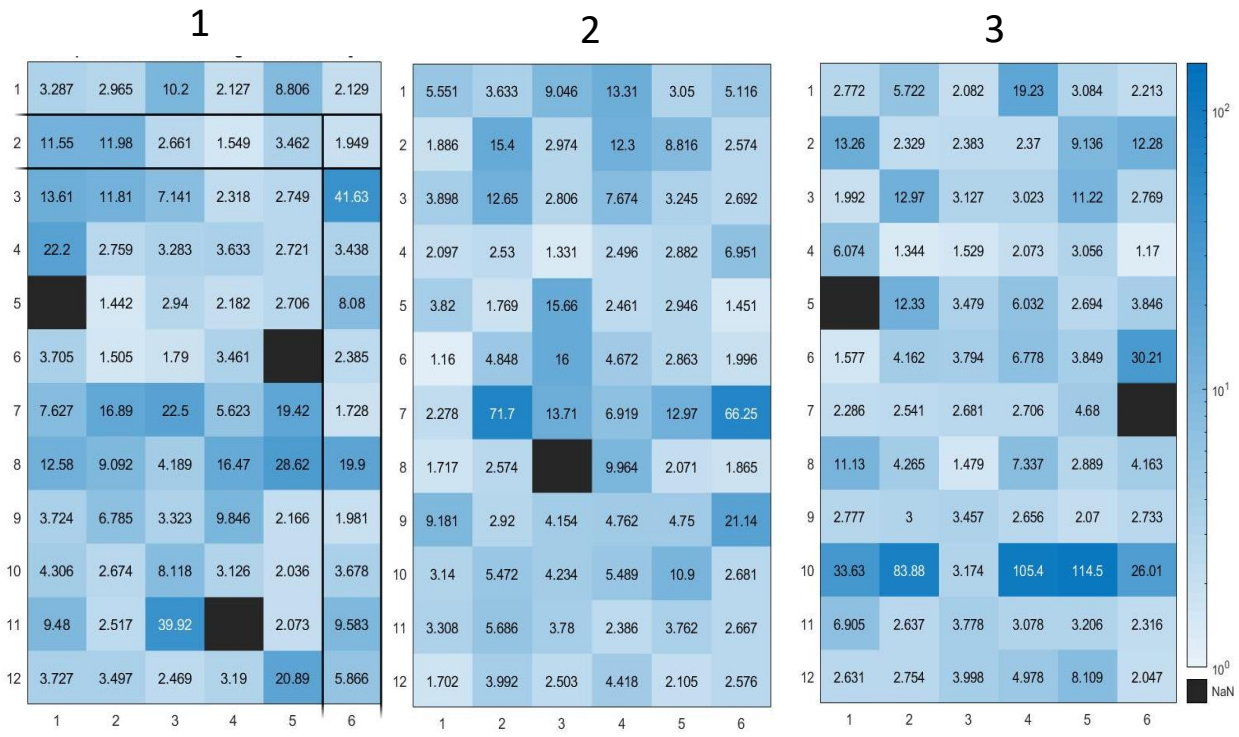

Gaussian Filter

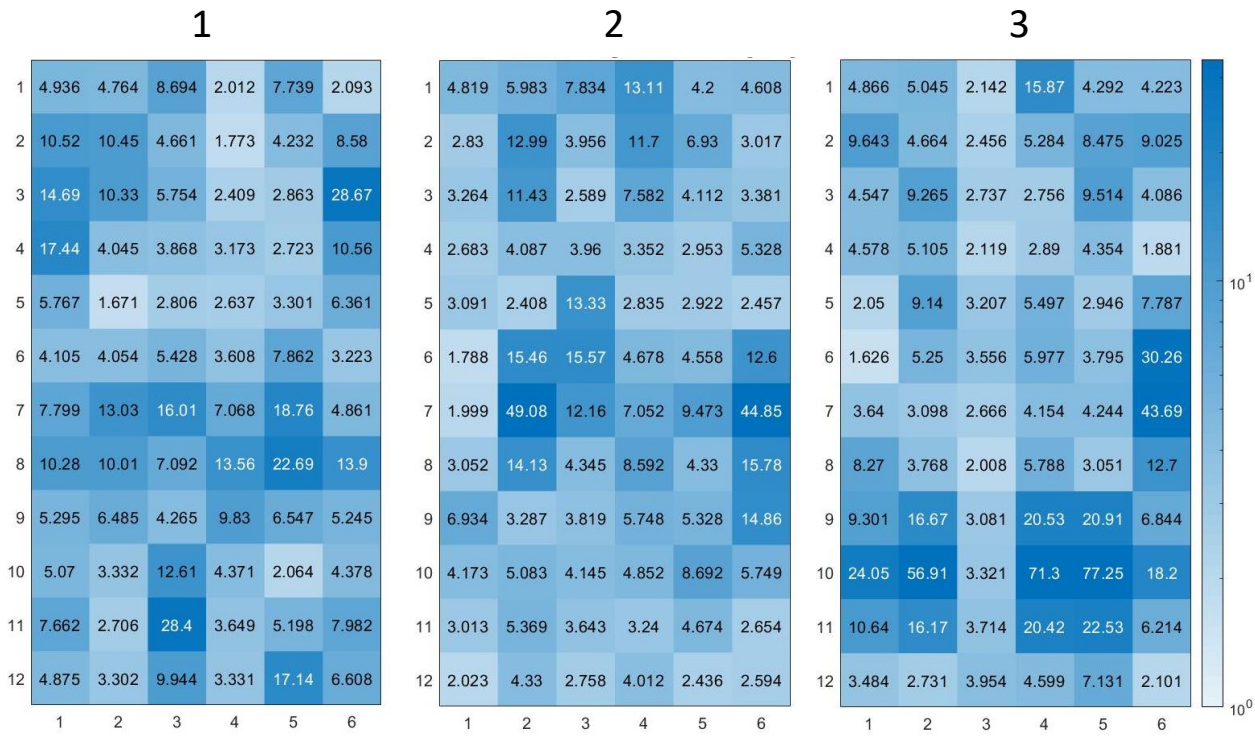

13 Months: Medial-Distal

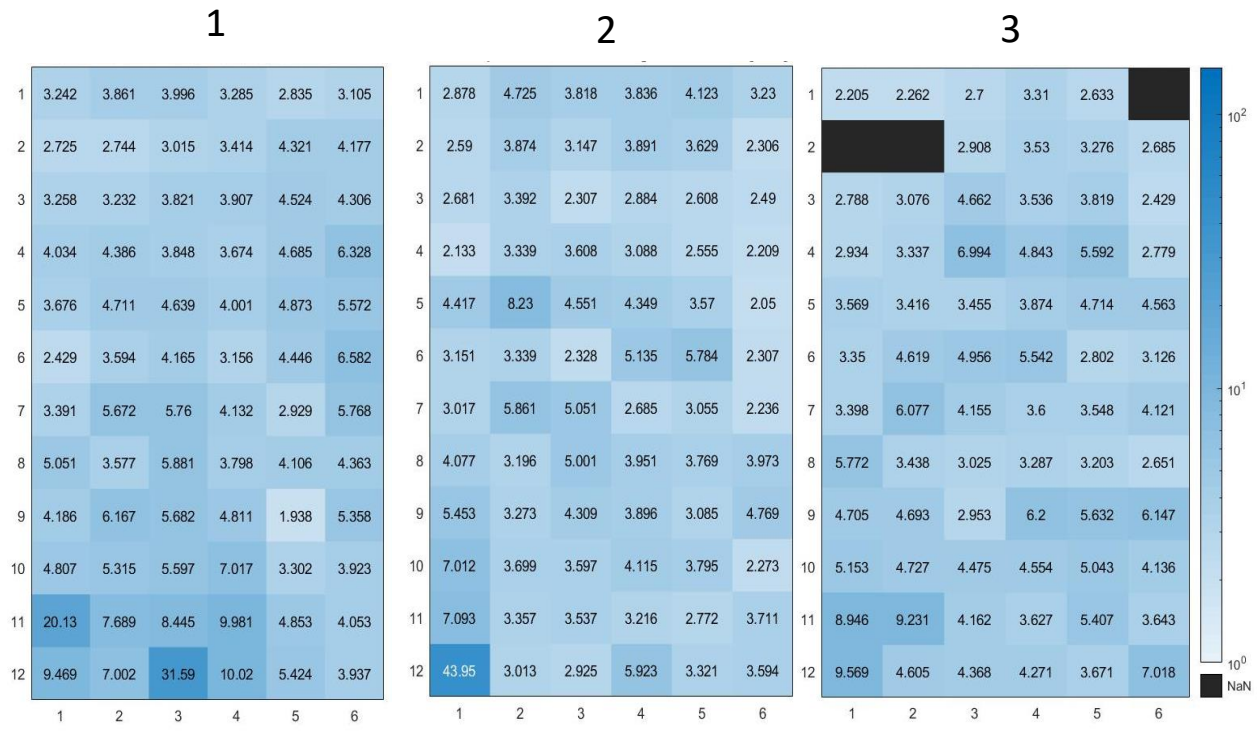

Gaussian Filter

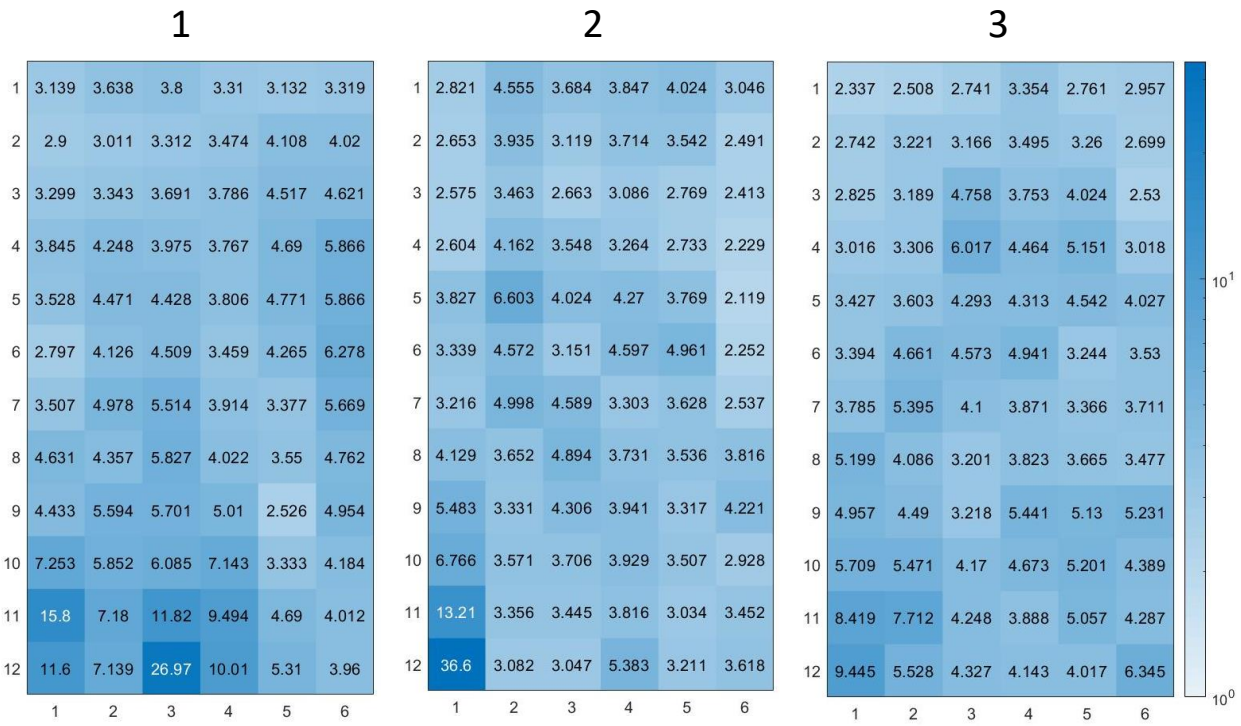

13 Months: Medial-Proximal

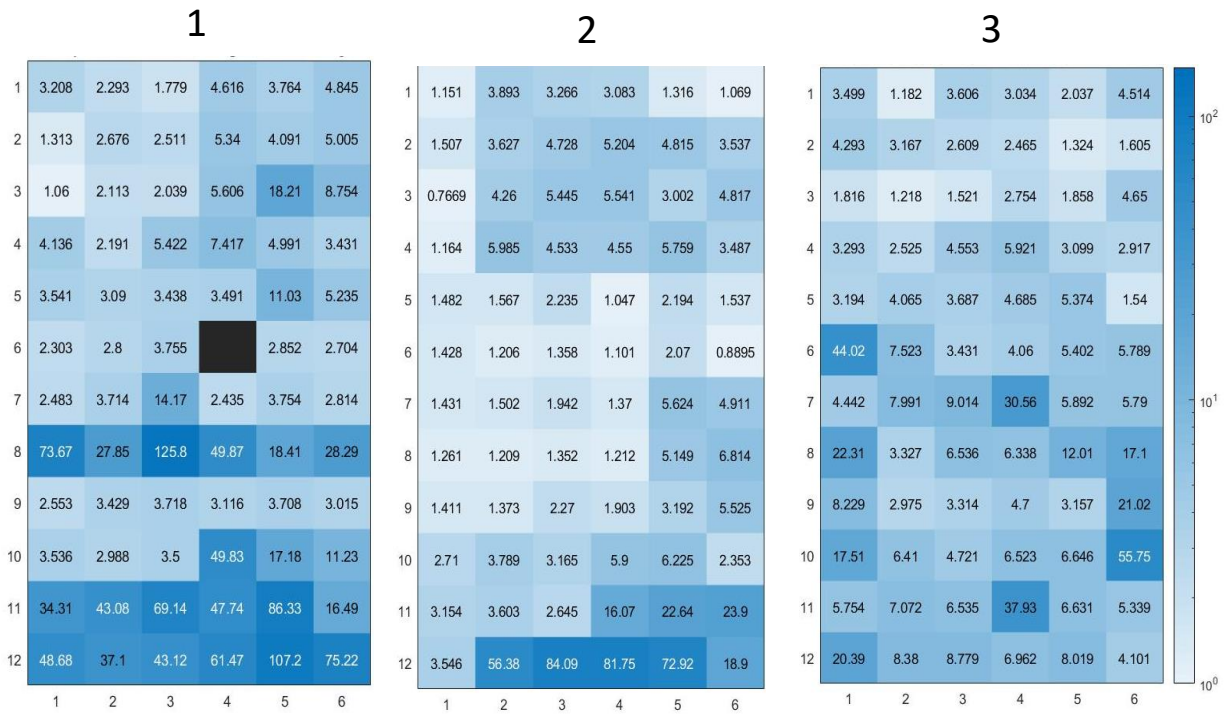

Gaussian Filter

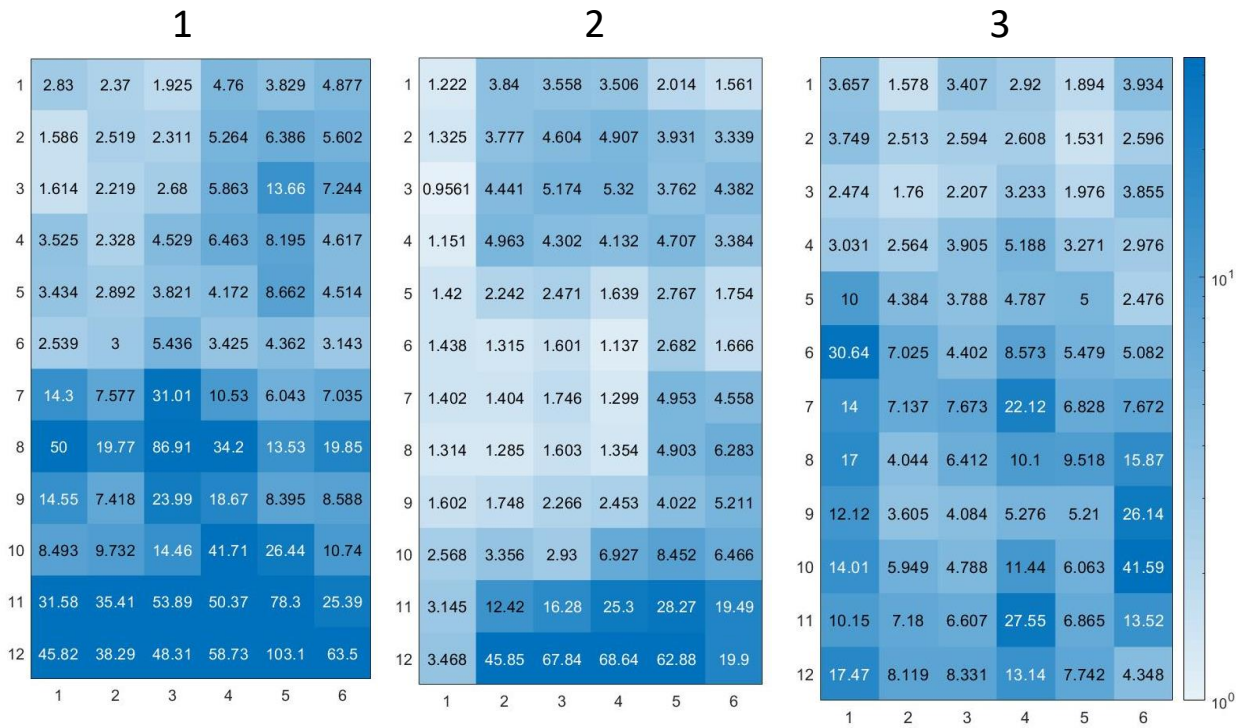

7 Weeks: Lateral

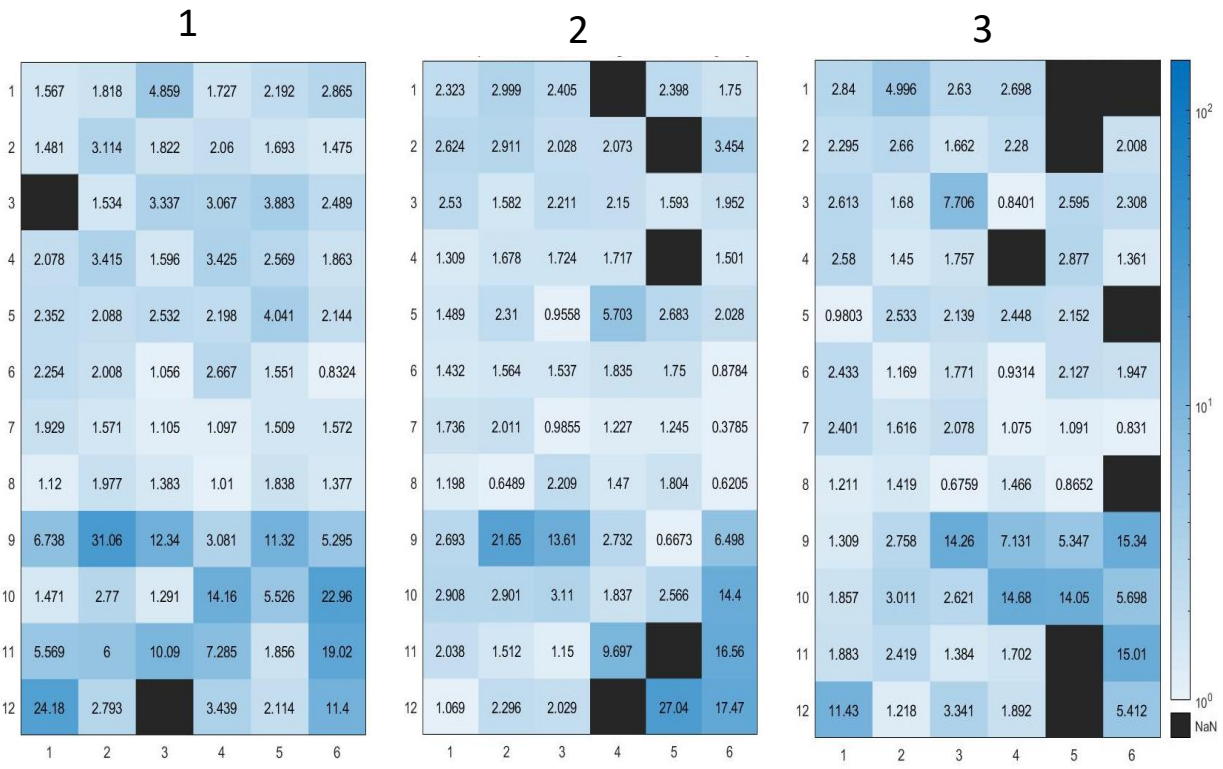

Gaussian Filter

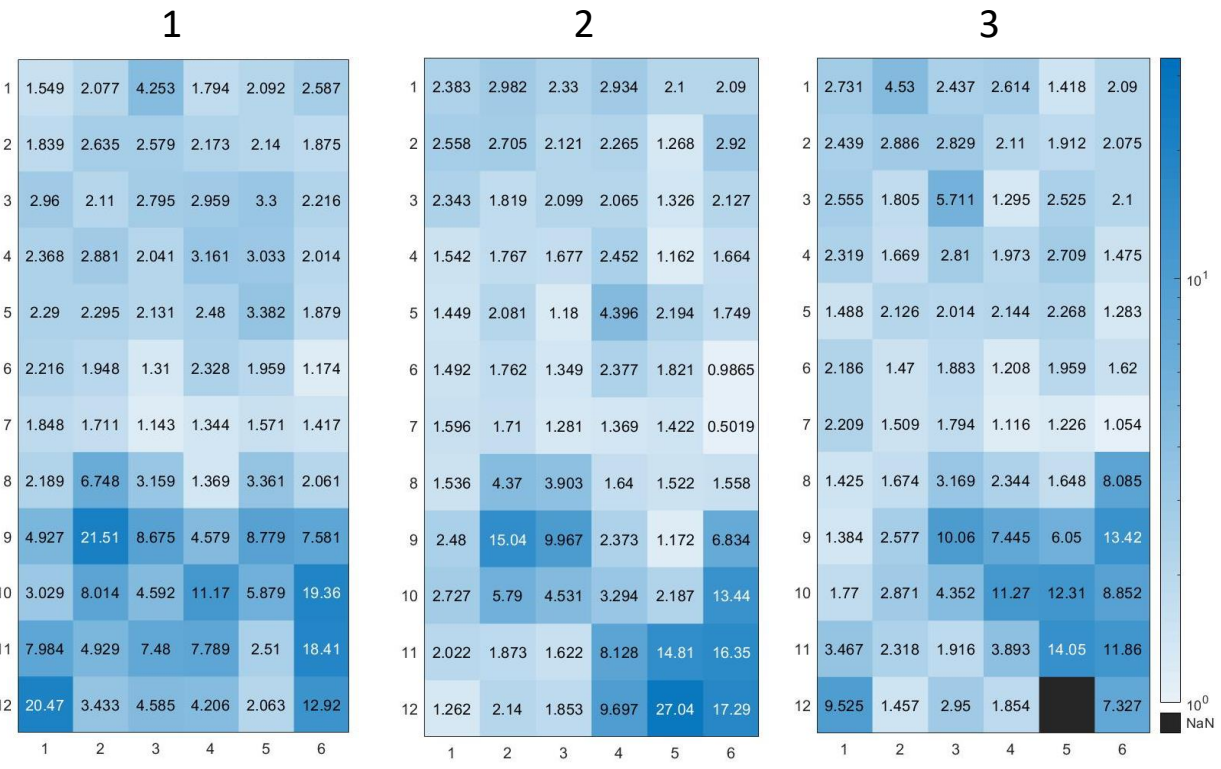

7 Weeks: Medial

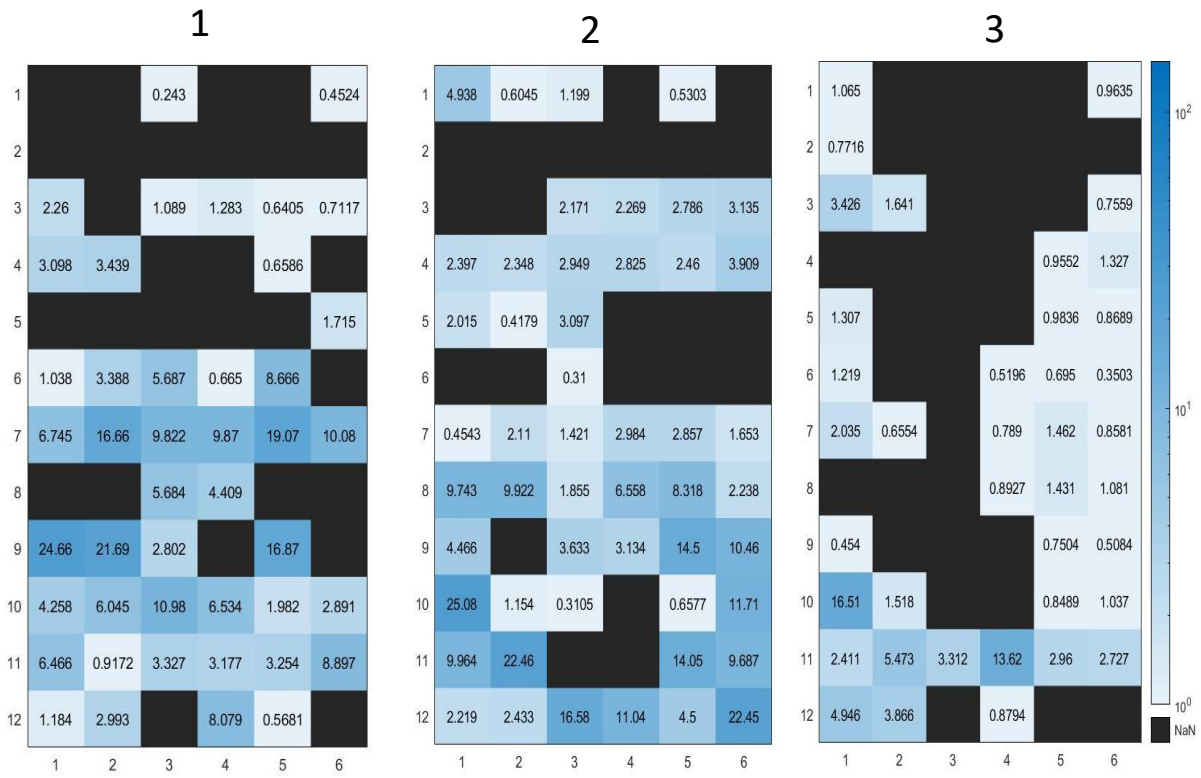

Gaussian Filter

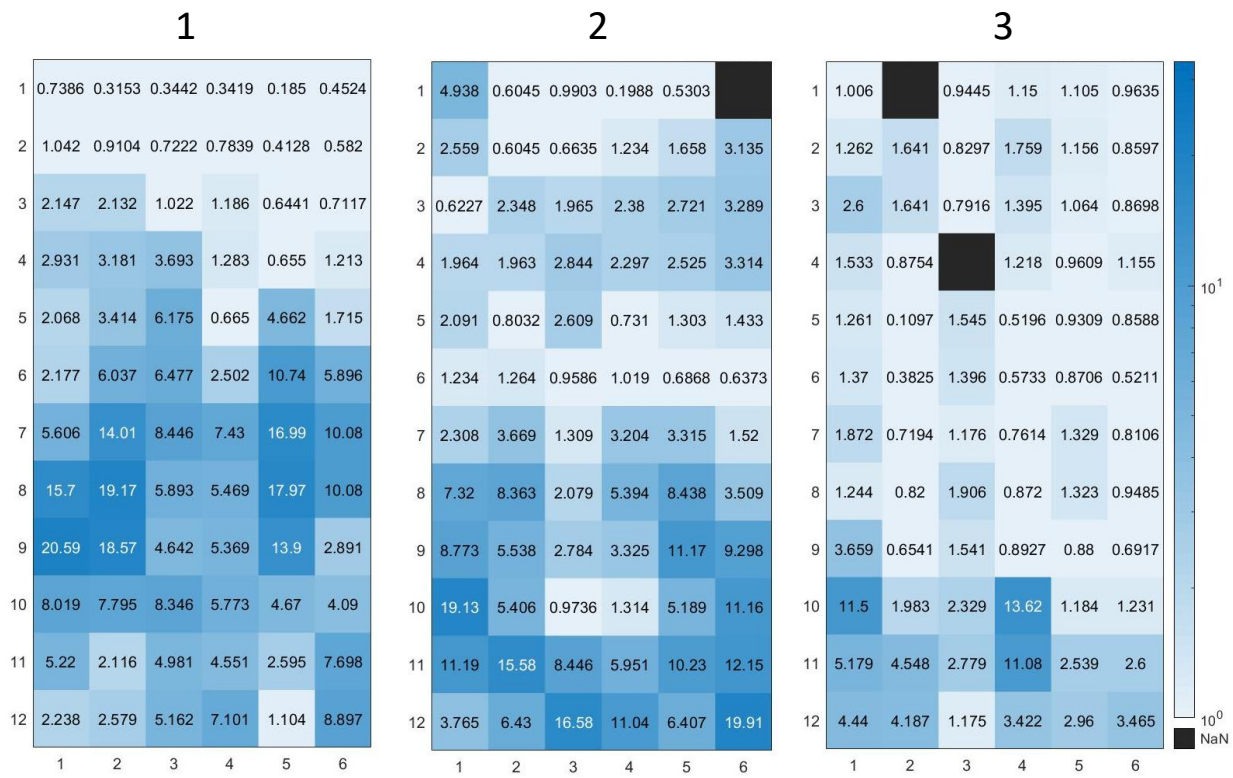

12 Days: Lateral

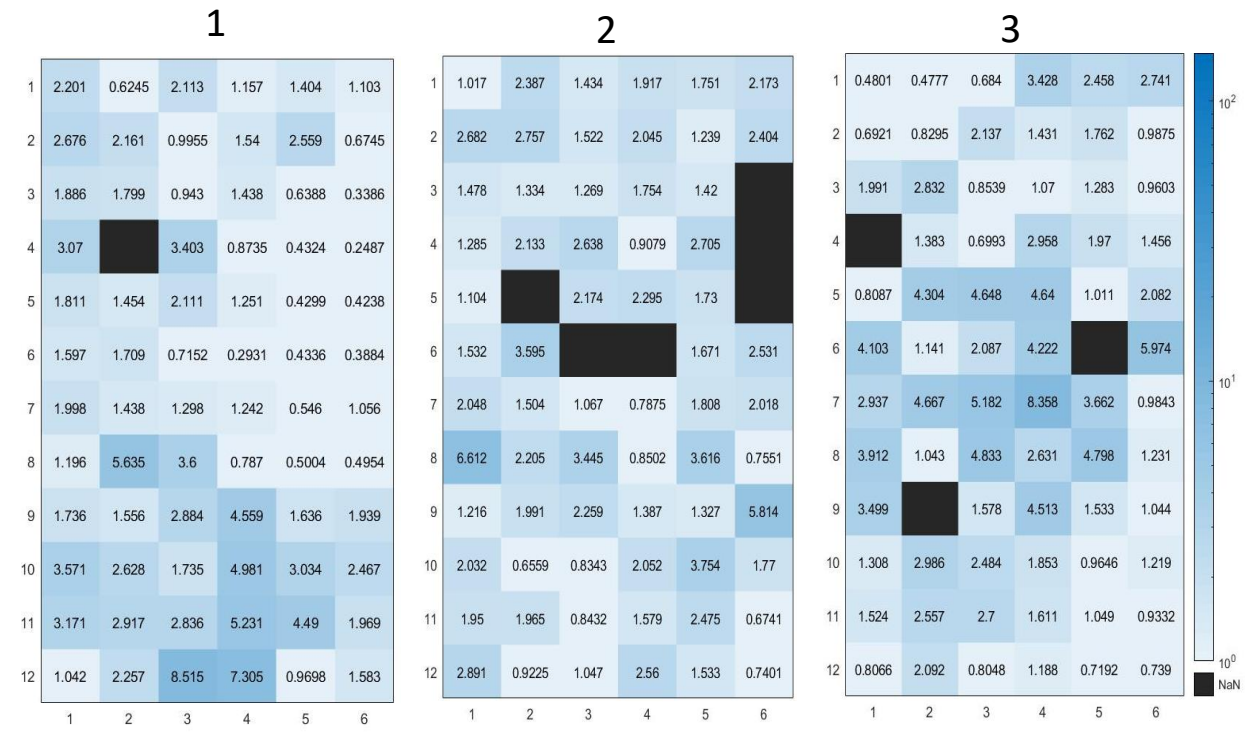

Gaussian Filter

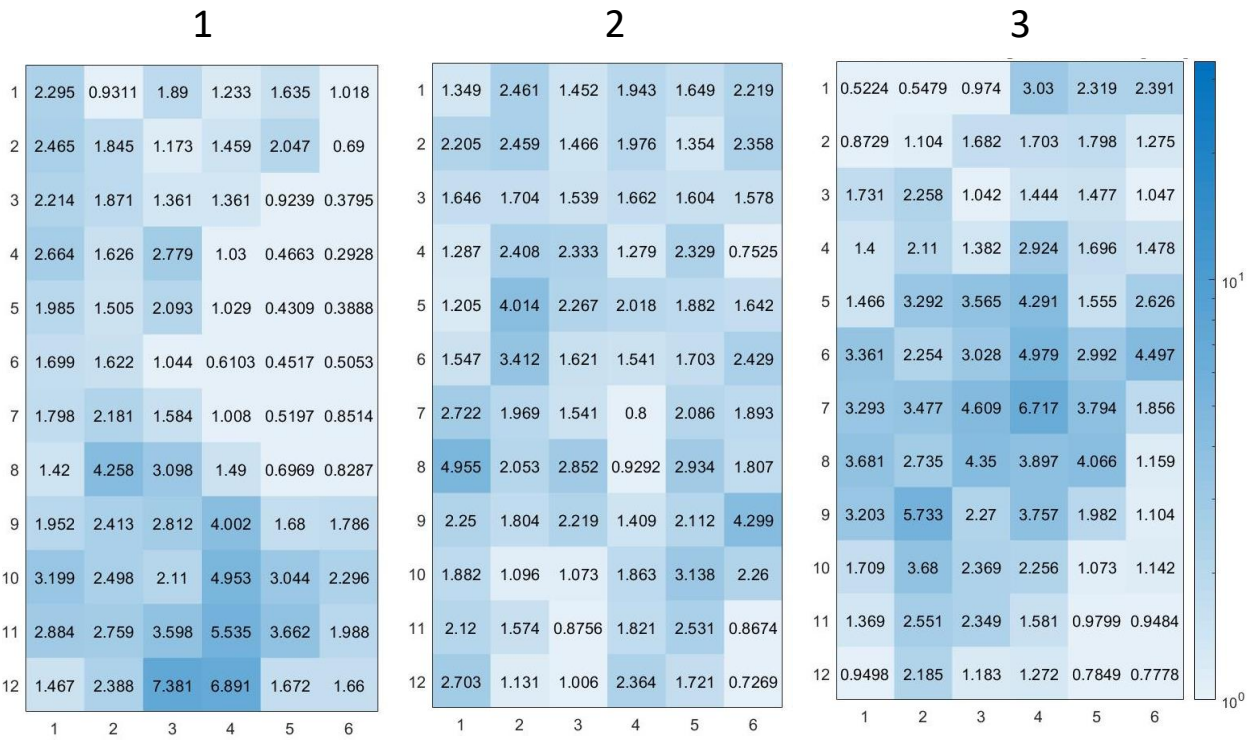

12 Days: Medial

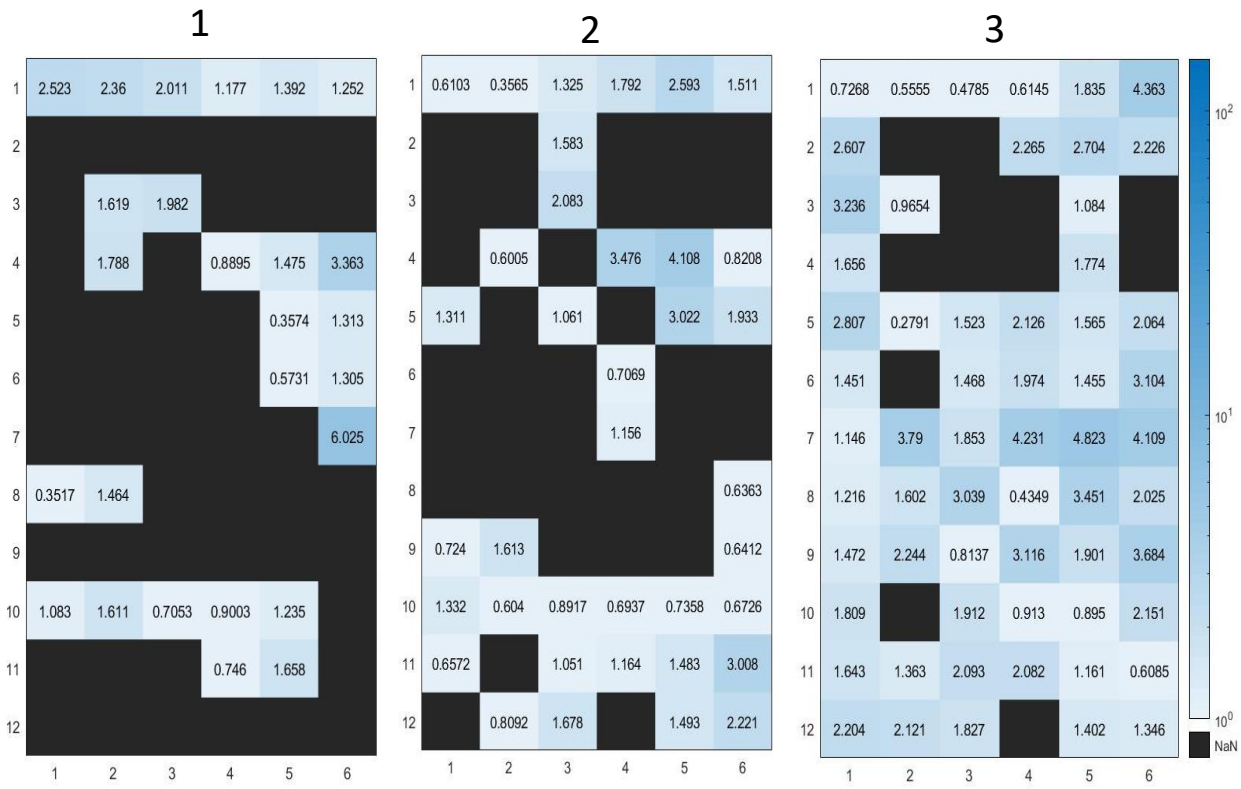

Gaussian Filter

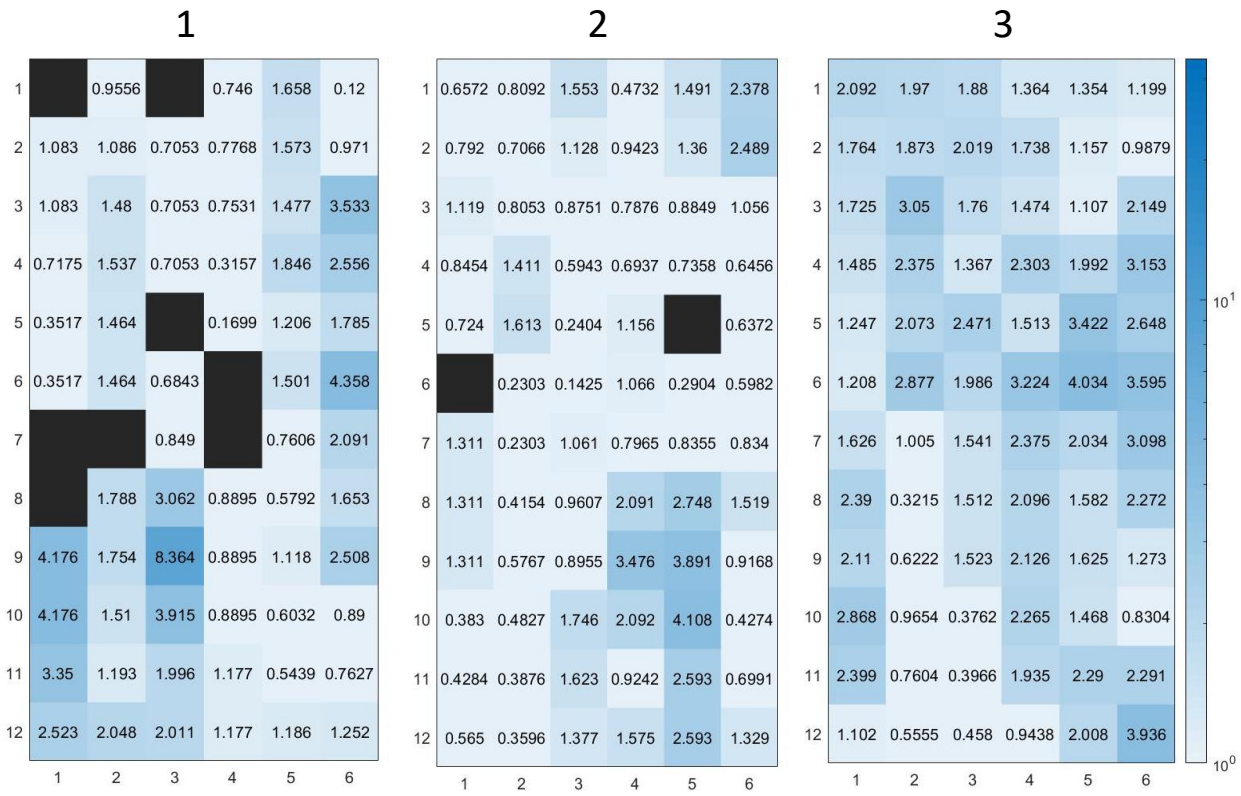

9 Days: Lateral

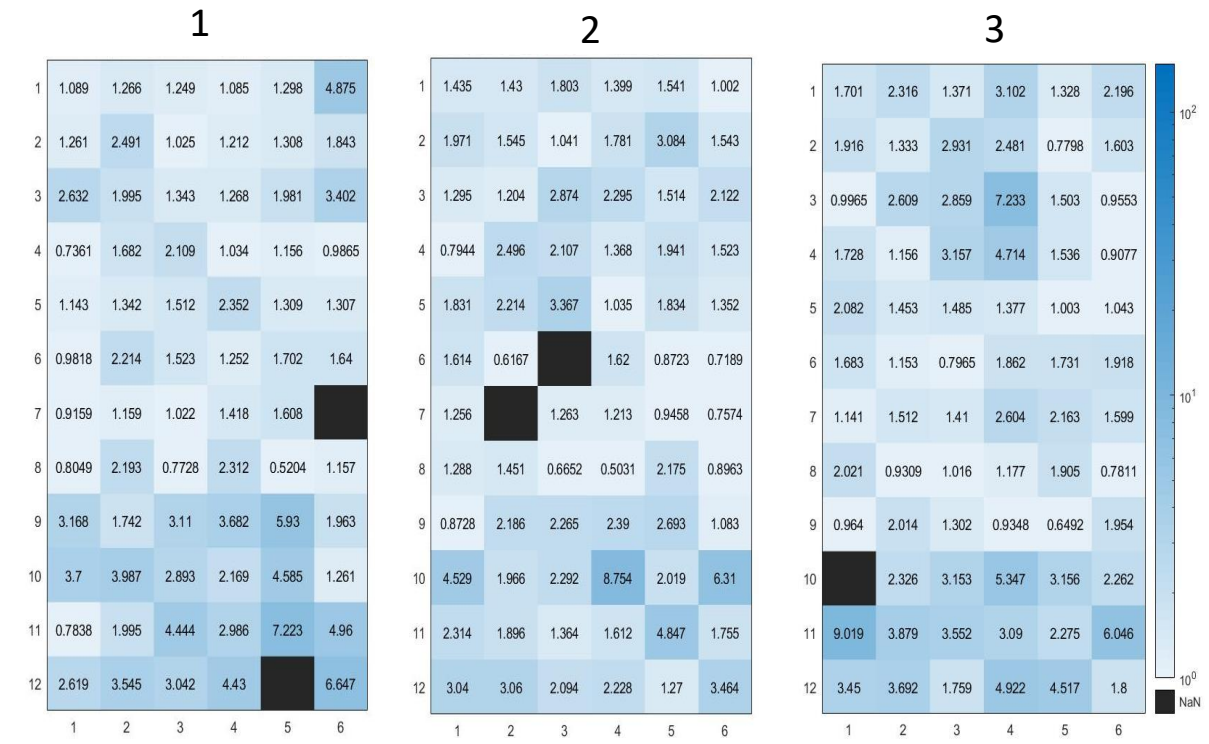

Gaussian Filter

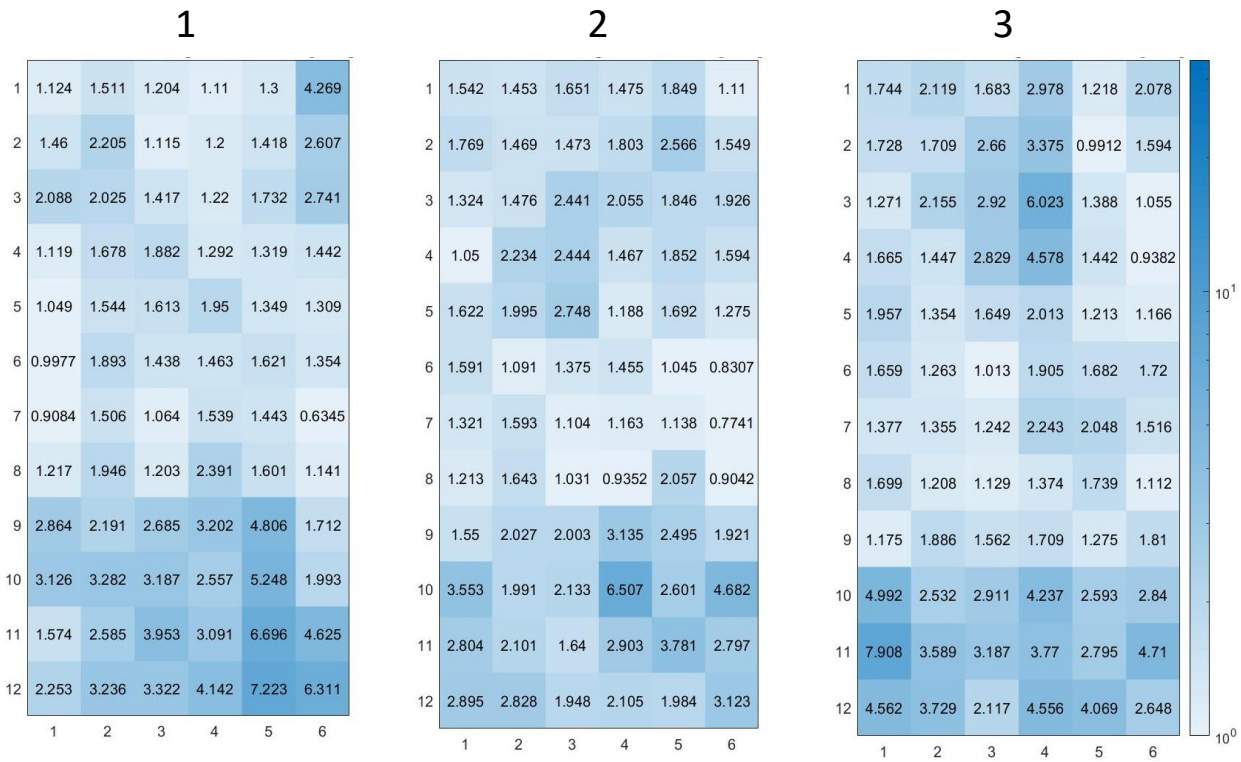

9 Days: Medial

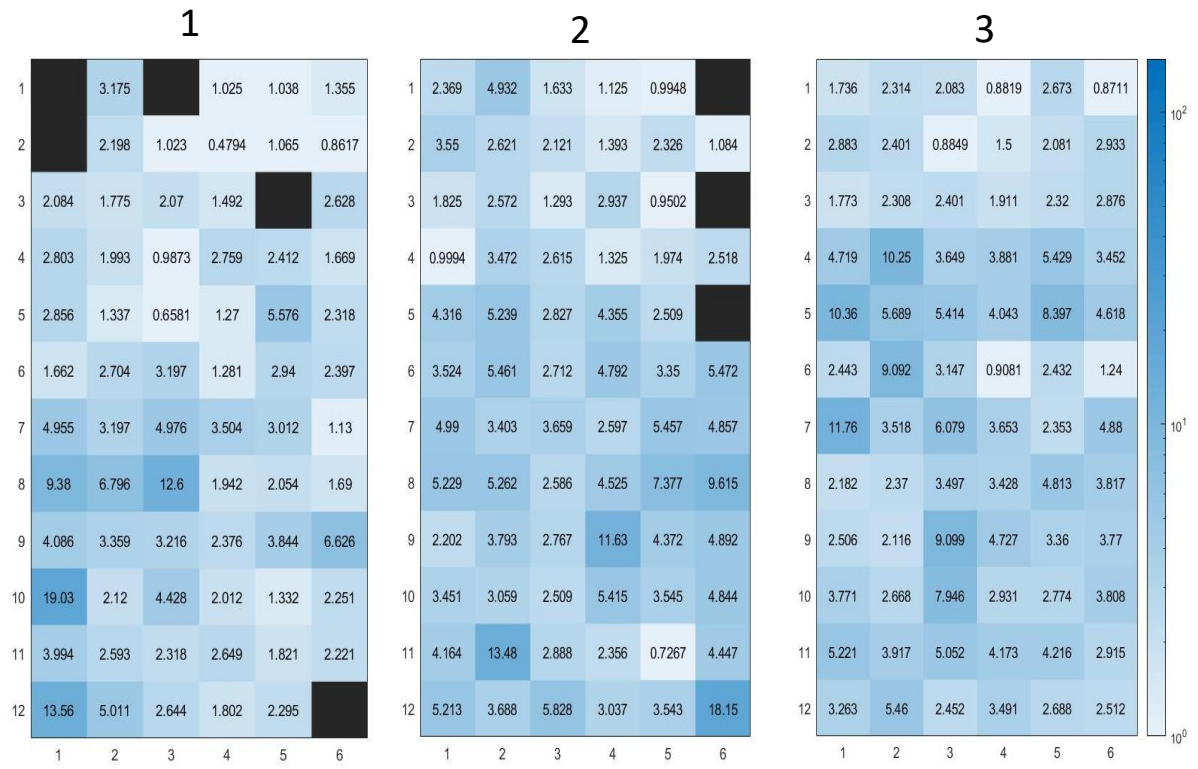

Gaussian Filter

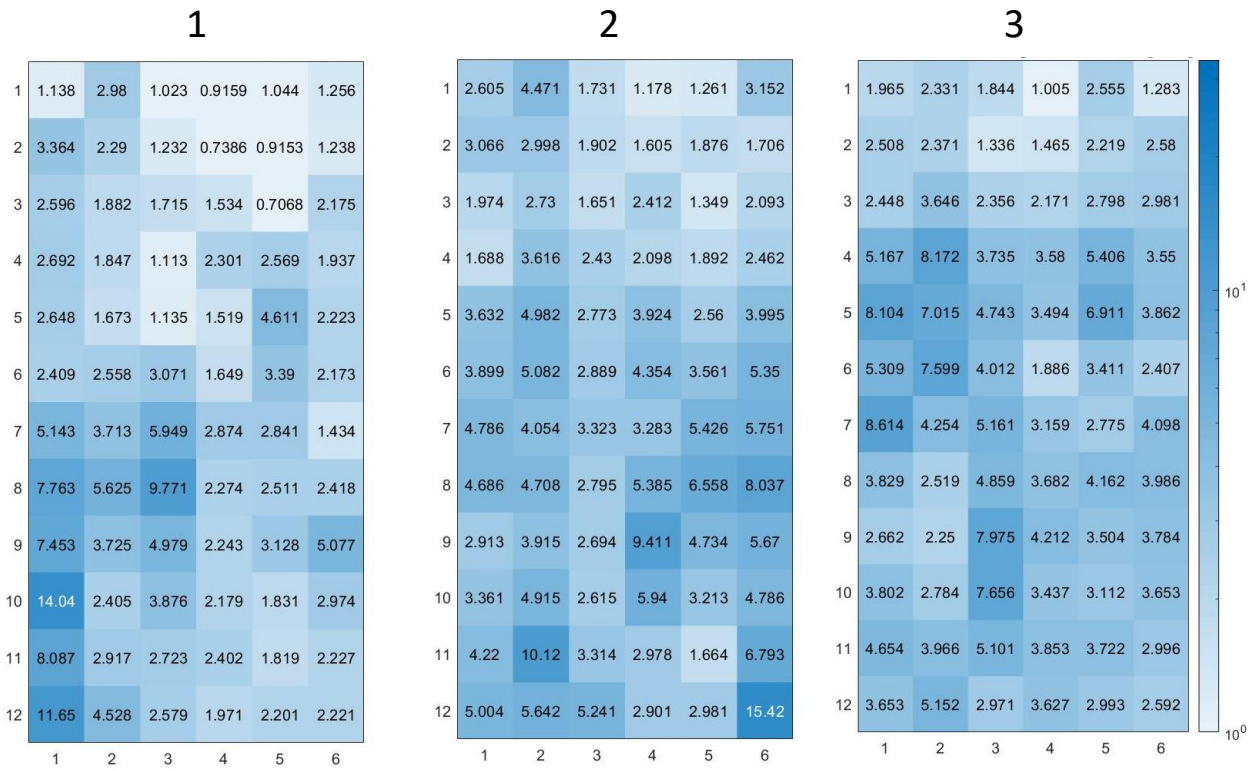

Digital Image Correlation Force Curves and Images at Selected Time Point

Adult 1: Lateral-Proximal

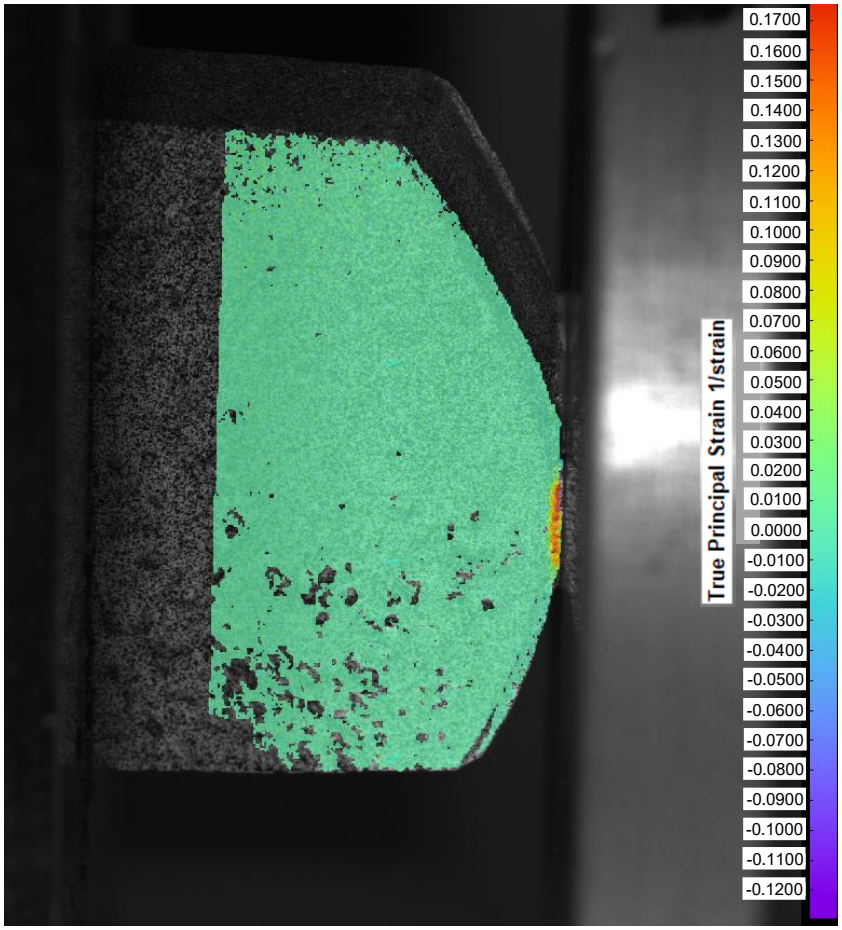

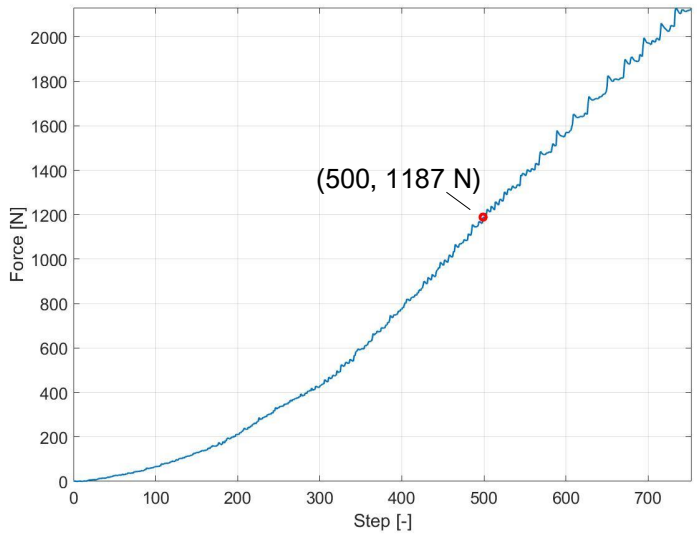

Adult 2: Lateral

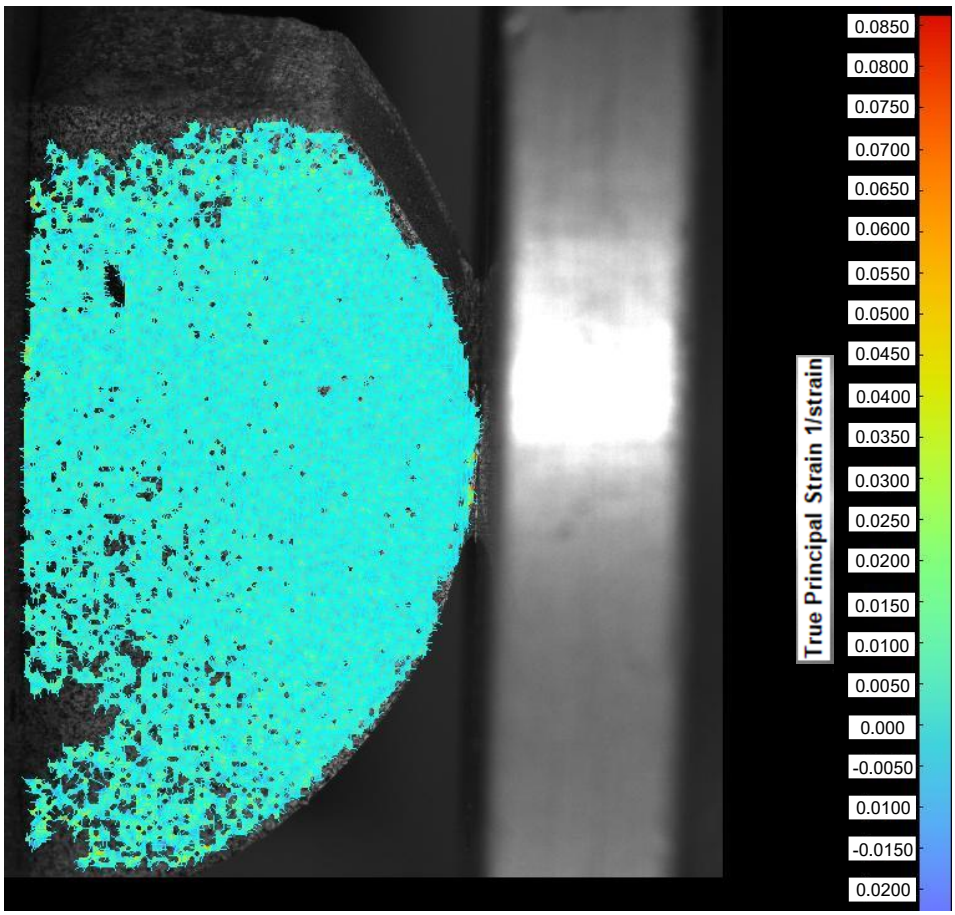

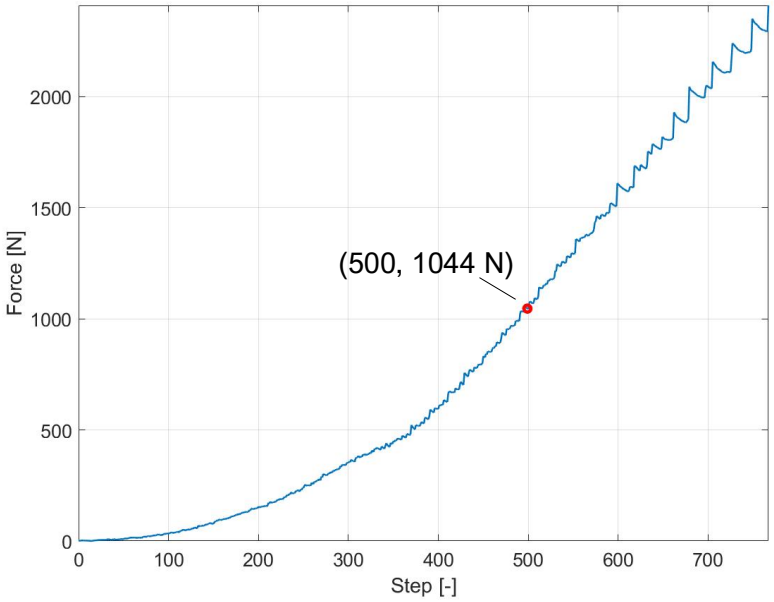

Adult 3: Medial-Distal

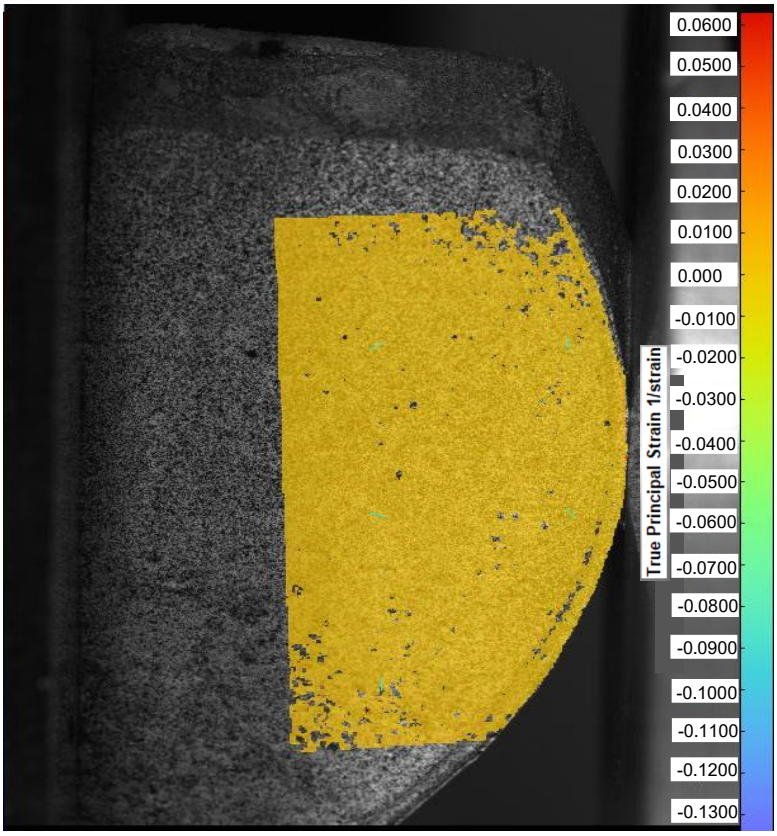

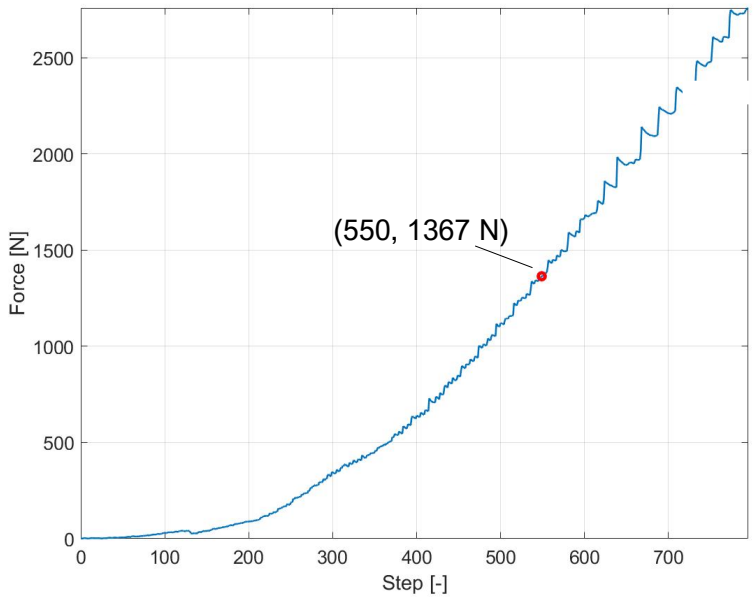

13 Months: Lateral-Distal

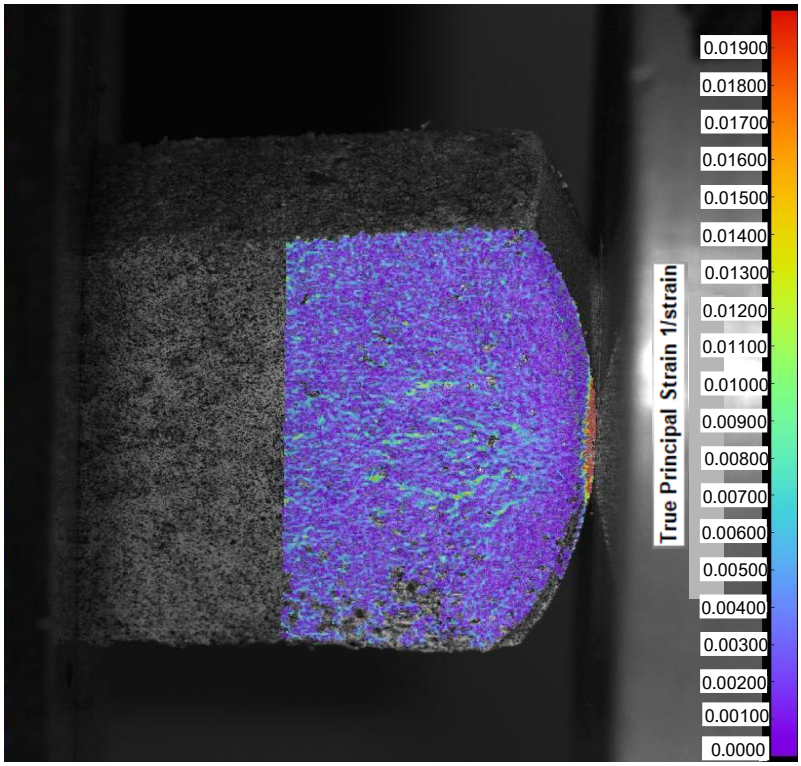

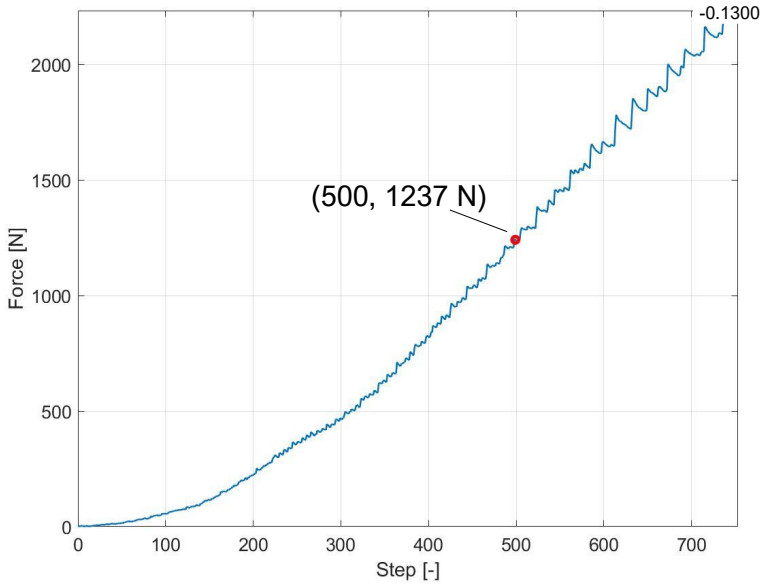

13 Months: Medial-Proximal

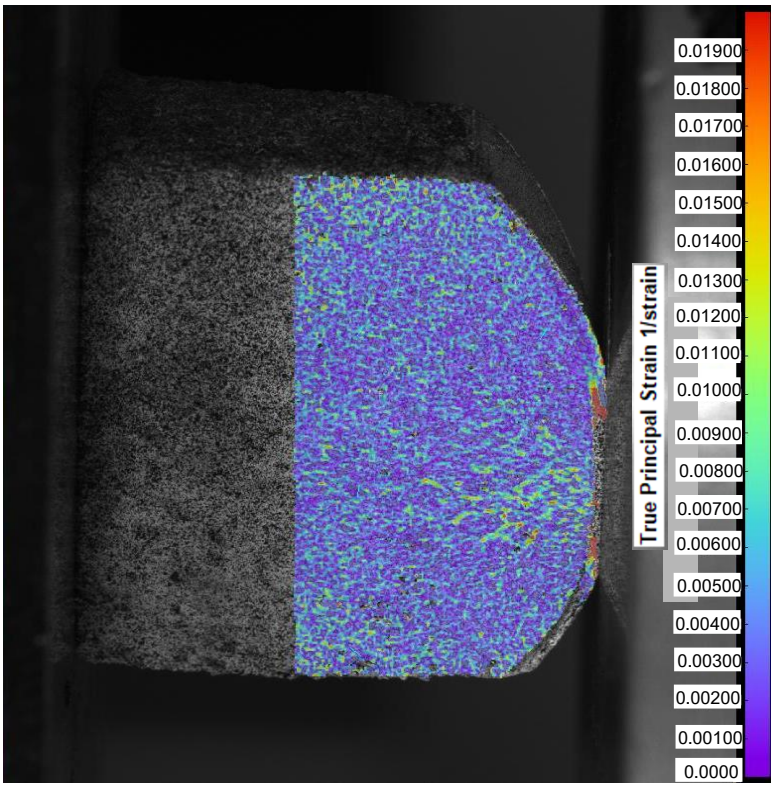

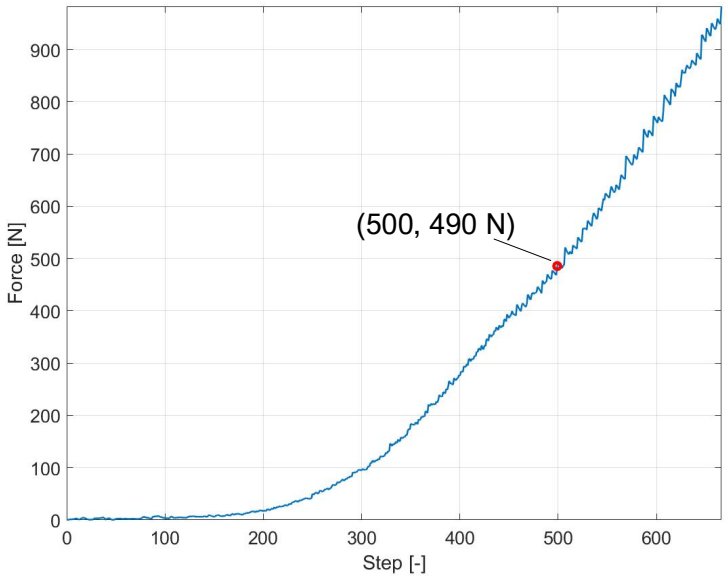

7 Weeks: Lateral

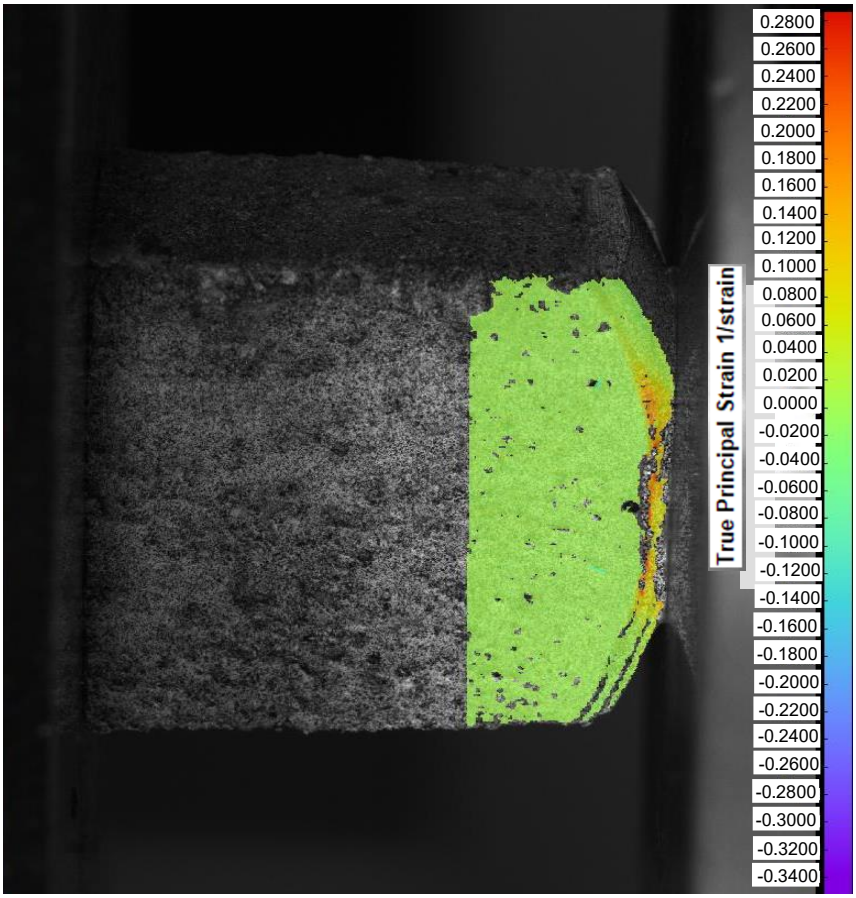

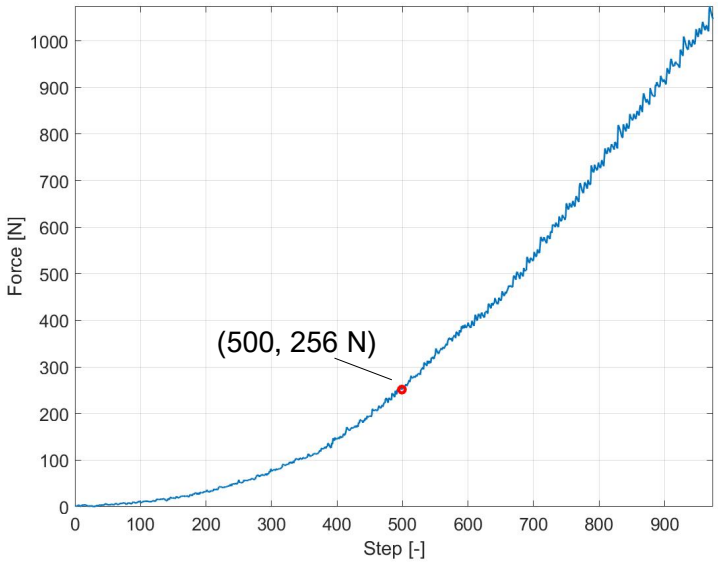

12 Days: Lateral

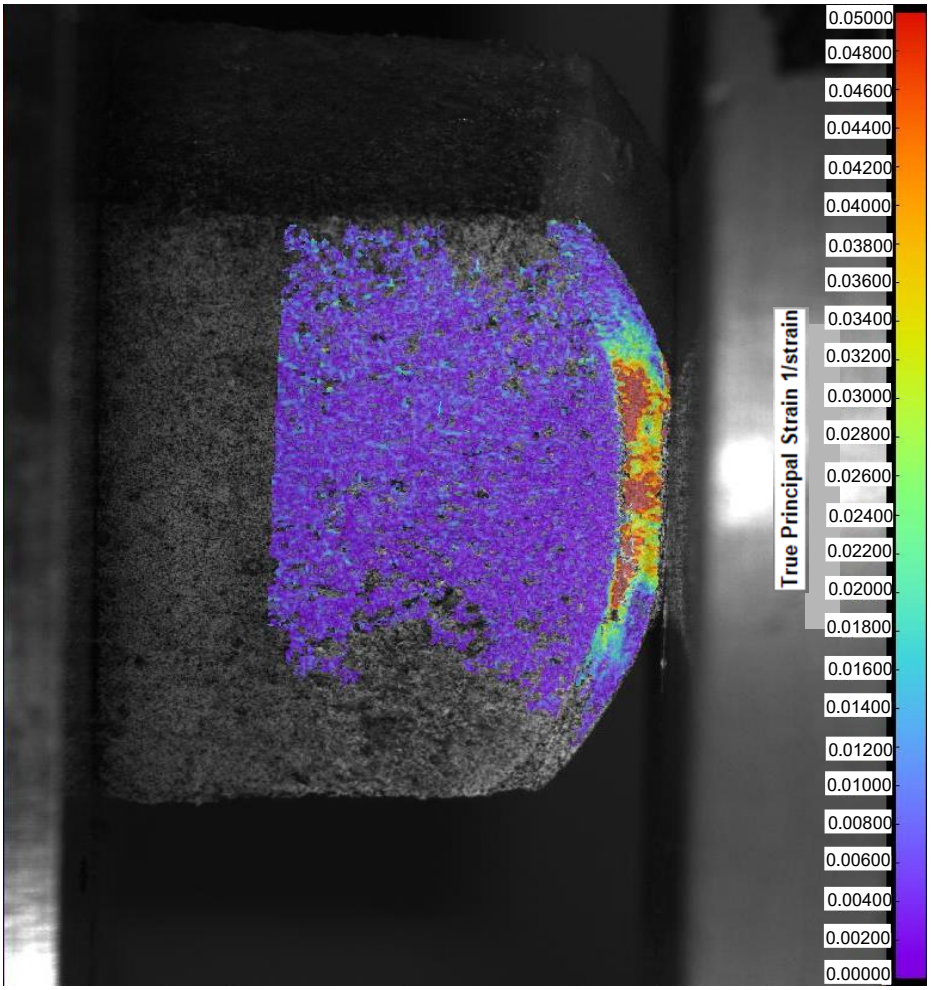

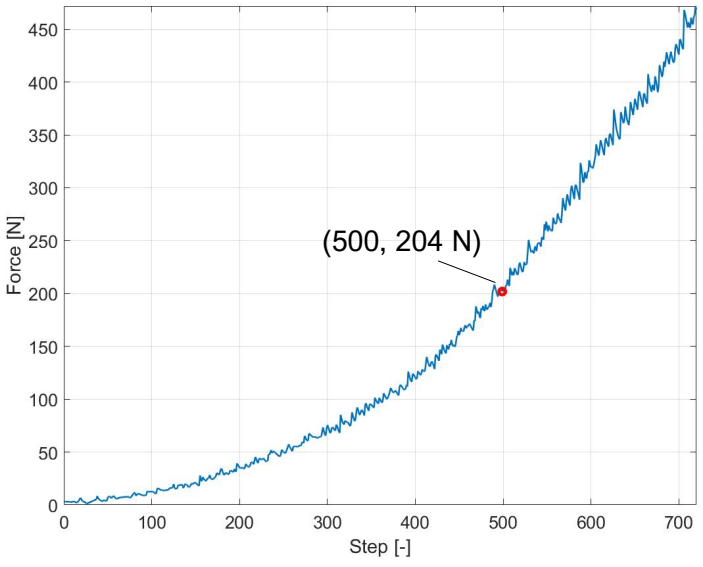

Appendix V: Mechanical Testing Protocol for Nanoindentation and Compression Tests with DIC

Sample	Label	Probe
Adult 1 Medial-Proximal	A-1-MP	P3
Adult 1 Medial-Distal	A-1-MD	P3
Adult 1 Lateral-Proximal	A-1-LP	P3
Adult 1 Lateral-Distal	A-1-LD	P3
Adult 2 Medial-Proximal	A-2-MP	P3
Adult 2 Medial-Distal	A-2-MD	P3
Adult 2 Lateral	A-2-L	P1
Adult 3 Medial-Proximal	A-3-MP	P1
Adult 3 Medial-Distal	A-3-MD	P1
Adult 3 Lateral-Proximal	A-3-LP	P1
Adult 3 Lateral-Distal	A-3-LD	P1
13 Months Medial-Proximal	Y-13M-MP	P4
13 Months Medial-Distal	Y-13M-MD	P4
13 Months Lateral-Proximal	Y-13M-LP	P3
13 Months Lateral-Distal	Y-13M-LM	P2
7 Weeks Medial	Y-7W-M	P2
7 Weeks Lateral	Y-7W-L	P2
12 Days Medial	Y-12D-M	P2
12 Days Lateral	Y-12D-L	P2
9 Days Medial	Y-9D-M	P2
9 Days Lateral	Y-9D-L	P2

P1 = 249 N/m, 8.5 µm
P2 = 254 N/m, 9.5 µm
P3 = 261 N/m, 8 µm
P4 = 283 N/m, 9 µm

Figure 6.12: Probes used on every sample for the nanoindentation tests

Nanoindentation

The aim for this experiment was to map the local stiffness gradient of biological hard-soft interfaces by performing nanoindentation on the equine osteochondral interface. Results from this nanoindentation experiment were analysed and the procedure was optimised to create a complete stiffness matrix.

1. Requirements

1.1 Equipment

- Piuma Nanoindenter
    - Nanoindenter Head
    - Optics11 OP1550 Interferometer
    - Piuma Controller
    - Attached PC with Piuma Nanoindenter software
    - Nanoindenter Probes
- Glass Petri-dish
- Plastic Petri-dish
- Pasteur pipettes
- BenchKote
- Tweezer
- Spatula
- Super glue

1.3 Specimen

- Equine metacarpophalangeal joint
    - Equine metacarpophalangeal joints are provided by The Faculty of Veterinary Medicine (Utrecht, Netherlands). The specimens will have a tissue statement from the relevant University. They will be cut at Erasmus Medical Centre into rectangular blocks of approximately 2 cm^3. Thereafter, they will be frozen in a -20°C freezer. Then they will be placed in a cool box with icepacks and transported to the ML-1 Laboratory 34-J-0-440-B Faculty 3mE TU Delft by car, where they will immediately be stored in a -20°C freezer till the time of the experiment.

1.4 Consumables

- PPE: Nitrile gloves
- Tissue paper

1.5 Reagents

- Distilled water
- Complete protease inhibitor cocktail
- Isopropanol
- 1x TBS (Tris-Buffered Saline)
- 70% Ethanol Disinfectant
- Chlorine tablet

2. Procedure

2.1 Work-space preparation

- Cover the workspace with BenchKote to prevent contact with the biological material.
- Wrap all the surfaces exposed to the sample with clingfilm to protects from any spillage or spatters

2.2 Sample preparation

- Prepare 100 mL 1x TBS and add 1 tablet of protease inhibitor cocktail
- Take the sample from the -20°C freezer and let it thaw in a dish fully immersed in 1x TBS with protease inhibitors in a fridge the night before testing.
- Fixate the specimen to the plastic petri dish with super glue only touching the bone end.
    - Be sure to only use a minimal amount of glue, so that the specimen can be pulled of the dish after measurements.
- Let the glue stiffen up.
- When ready pour in a volume of buffer/solution, 1x TBS + protease inhibitors, into the petri-dish on top of the samples till fully immersed. The buffer solution will be the solution into which the test is going to be performed.

2.3 Nanoindentation

- Set up nanoindenter with required probe based on stiffness and tip size from manufacturer
- Calibrate Piuma nanoindenter according to manufacturer instructions
- Find your sample and perform ‘surface finding protocol’ of Piuma nanoindenter according to manufacturer specifications
- Program the nanoindentation procedure into the Piuma software
    - Set required grid
    - Set nanoindentation displacement-time protocol
- Begin nanoindentation
    - Note that the table and equipment should not be touched during the process as any external perturbations will affect results

2.4 Cleaning Procedure

- Pull the specimen off the petri-dish and store the specimen in the -20°C freezer correctly labelled, as described in Appendix 2.5 of the Handbook.
- Clean nanoindenter tips using distilled water - isopropanol - distilled water, in that order.
    - Apply the liquids using a dropper carefully on the nanoindenter tip directly over a petri dish to catch any falling liquid

        - Ensure distance between tip and petri dish is not to great as to prevent splatter of cleaning liquids
- Dispose the excess cleaning fluid collected in a petri-dish and the buffer solution with the protease inhibitors in a small, clean bucket. Add a chlorine tablet and let it sit for a few minutes. After, the fluid will be disposed in the 'Organic with Halogen' chemical disposal.
- Dry the nanoindenter tip using the fibers of a paper towel
    - Tear a paper towel in its corner to expose the underlying fibers
    - Use the individual fibres to carefully wipe off any excess cleaning liquids remaining on the tips.
    - Dispose the tissue paper used for cleaning in the WIVA-vat.
- Dispose the surface protection paper and the plastic petri dish in the WIVA-vat.
- Clean everything in the workspace with 70% ethanol and a paper towel.
- Dispose the paper towels and nitril gloves in the WIVA-vat.

Compression Tests with DIC

The purpose this experiment was to use Digital Image Correlation (DIC) for full-field measurement of (3D surface) strains during compression testing over the equine metacarpophalangeal osteochondral interfaces.

1. Requirements

1.1 Specimen

- Equine metacarpophalangeal joint
    - Equine metacarpophalangeal joints are provided by The Faculty of Veterinary Medicine (Utrecht, Netherlands). The specimens will have a tissue statement from the relevant University. They will be cut at Erasmus Medical Centre into rectangular blocks of approximately 2 cm^3. Thereafter, they will be frozen in a -20°C freezer. Then they will be placed in a cool box with icepacks and transported to the ML-1 Laboratory 34-J-0-440-B Faculty 3mE TU Delft by car, where they will immediately be stored in a -20°C freezer till the time of the experiment.

1.2 Reagents

- 1x TBS (Tris-Buffered Saline)
- Complete Protease Inhibitors Cocktail
- 70% Ethanol disinfectant
- Chlorine tablet

1.3 Equipment

- Lloyd LR5K machine
    - Equipped with a data acquisition unit consisting of two cameras with tripods, a lighting system and a laptop.
- Airbrush
- White primer paint (acrylic)
- Black paint (acrylic)
- Clingfilm
- BenchKote
- Masking tape

1.4 Trial Preparation

- The Lloyd LR5K and all the equipment will be placed in the ML-1 Laboratory 34-J-0-440-B to perform the measurements.
- All excess parts will be removed for the tests.
- All working surfaces must be covered with BenchKote, all other surfaces that could get in touch with specimen material must be wrapped in clingfilm.

➢ Inside the lab a spill kit (see App. 3.1) is present including:

- 70% ethanol disinfectant
- A package or roll of paper towels
- Autoclavable bags
- Nitril gloves
- Forceps

- Inside the lab one must wear:
- safety glasses
- Lab coat
- Nitril gloves

2. Procedure

2.1 Specimen preparation (Lab 34-J-0-440-B)

- Remove the specimens from the -20°C freezer
- Unpack the specimens
- Let specimens thaw in a petri dish fully immersed in 1x TBS with protease inhibitors in the fridge the night before testing.

2.2 Trials (Lab 34-J-0-440-B)

Any contact of the specimen with the Lloyd LR5K other than the holder will be avoided during the trial.

- The containment area as described in §1.3 is fully prepared
- Mount the specimen in the Lloyd LR5K
- Perform trials
- Remove sample and refreeze it in the -20°C freezer.

2.3 Disinfecting and Disposal

- Remove all BenchKote and place it in the WIVA-vat.
- Remove all the clingfilm from the surfaces and place it in the WIVA-vat
- Wipe the surfaces with 70% ethanol and dispose them in the WIVA-vat
- The 1x TBS with protease inhibitors will be disinfected by adding a chlorine tablet. After a few minutes, pour the liquid in the ‘Organic with Halogen’ chemical disposal.

2.4 Storage

- Before trials the specimens are stored in a -20°C freezer.
- After trials the specimens will be refrozen in a -20°C freezer.
- After completing all the trials, all the frozen specimens will be transported back to Erasmus Medical Centre following all the appropriate regulations, where they will be further processed.

Appendix VI: Matlab code

```
%-------------------------------------------------------------------------/
%   File:   Final_Code_EB.m
%
%   Description: Fit the force [uN] - displacement [nm] curve using  ...
    the traditional Oliver-Pharr method to obtain the elastic modulus [MPa]
%   [Kohn and Ebenstein, JMBBM 2013, 20:316-326]
%   [Oliver and Pharr, J Materials Research, 7(6):1564-1583]
%
%   Input:  Nanoindenation file
%   Output: Heatmap Elastic Modulus
%   Author : Emma Boersma

%   Date : 20-12-2021
%   This code is adapted from code written by Prof. Davide          ...
    Ruffoni at the University of Liege and modified by Robin Veeger from ...
    TU Delft. It was adapted by Edwin Tay and Emma Boersma to be used ...
    within TU Delft for the Piuma nanoindenters available within the labs.
% ...
    ------------------------------------------------------------------------ ...
    /

%%% This code was written for data output from the Piuma Nanoindenter %%%


clearvars   ;
close all   ;
clc         ;


%%% PARAMETERS TO SET %%%

path        = '\Users\Emma     ...
    Boersma\Documents\BME\Thesis\Equine\Nanoindentation\Equine ...
    A2\011021_EquineA2_L\Matrix_3\matrix_scan03\'
filename1   = '011021_EquineA2_L S-1 X-';
filename2   = ' Y-';
file_struct     = ' I-1.txt';

R               = 8.5*10^-6;     % Nanoindenter tip radius [m]
Fit_per         = 0.95;
MeasurePointsX  = 6   ;          % Number of measurement points along ...
    x-axis
MeasurePointsY  = 12   ;         % Number of measurement points along ...
    y-axis


%% Open File & Fit Data %%

% For loop to iterate over folder containing nanoindentation files

for x = 1 : MeasurePointsX

   for y = 1 : MeasurePointsY

    xstr = num2str(x);
    ystr = num2str(y);

```

```
48
49      % Combines path and file names into a single string to iteratively
50      % open every file in the dataset folder.
51      input_file = [path filename1 xstr filename2 ystr file_struct];
52      fid = fopen(input_file,'r');
53
54
55      % Extract the relevant nanoindentation data, skipping the unneccesary
56      % heading data
57
58      maxdepth = textscan(fid,'%s %s %f',1,'HeaderLines',29);
59      data     = textscan(fid, '%f %f %f %f %f', 'HeaderLines', 37);
60      fclose(fid);
61
62
63      % Assign data to variables
64      depth    = data{1,3};
65      load     = data{1,2};
66      time     = data{1,1};
67      peak_disp = maxdepth{1,3};
68      k = 1 ;
69
70      depth(isnan(depth))=0;          %plot NaN values in graph
71
72
73      % Plot load-depth data
74      h=figure(k);
75      plot(depth,load,'o');
76      grid on; xlabel('Depth [nm]');ylabel('Load [uN]');k=k+1;
77      title(['Original P-D Data ',filename1 xstr filename2 ...
            ystr],'Interpreter','none');
78      saveas(h,sprintf('Load-Depth%d.jpg',x,y));
79
80
81      %Plot load-time data
82      h=figure(k);
83      plot(time, load,'o');
84      grid on; xlabel('Time [s]');ylabel('Load [uN]'); k=k+1;
85      title(['Original P-T Data', filename1 xstr filename2 ...
            ystr],'Interpreter','none');
86      saveas(h,sprintf('Time-Load%d.jpg',x,y))
87
88      %Plot indentation-time data
89      h=figure(k);
90      plot(time,depth,'o');
91      grid on; xlabel('Time [s]');ylabel('Depth [nm]'); k=k+1;
92      title(['Original D-T Data', filename1 xstr filename2 ...
            ystr],'Interpreter','none');
93      saveas(h, sprintf('Time-Depth%d.jpg',x,y))
94
95
96
97  if depth(6922)==0;                  %Eliminate faulty curves which did ...
        not indent at all, by this step the indenter should have indented ...
        looking at the timing set up
98      E_OP=NaN
99  else
100
101
102     % Calculating time_peak_disp, the time of peak displacement
```

```
103     depth_round = round(depth,-1);
104     peak_disp_round = round(peak_disp,-1);
105     idx_1 = find(depth_round == peak_disp_round,1);
106     time_peak_disp = time(idx_1);
107
108     %Calculating value load when start unloading
109     load_round = round(load,-1);
110     load_unloading= load(idx_1);
111
112
113
114     % Calculating time_first, the 'starting time' of unloading
115     upper_load = Fit_per * load_unloading ;             %95% of the ...
            curve to    make sure it is the unloading part
116     I_t_first = find(load > upper_load);I_t_first=I_t_first(end);
117     time_first = time(I_t_first);
118     upper_disp = depth(I_t_first);
119
120
121 %%%%%%%%%%%%%%%%%%%%%%%%% Oliver Pharr %%%%%%%%%%%%%%%%%%%%%%%%%%%%%%%%%%%%
122
123         % Calculating lower_disp to define the unloading part for ...
                analysis and its associated time_last
124         lower_load = 0.7 * upper_load;          %Analyzing the ...
                unloading curve from 95% to 70% of the curve
125         lower_load_round = round(lower_load);
126         idx = find(load_round > lower_load_round); idx=idx(end);
127         time_last = time(idx);
128
129
130         % Showing fit range for Oliver-Pharr
131         fit_range = find(time < time_last & time > time_first);
132         u_depth = depth(fit_range);                             %[nm]
133         u_load = load(fit_range);                               %[uN]
134
135
136         % Plotting the Oliver-Pharr fit range to check
137         h=figure(k);
138         plot(depth,load,'o',u_depth,u_load,'+r');
139         grid on; xlabel('Depth [nm]');ylabel('Load [uN]');k=k+1;
140         title(['Unloading Region OP ',filename1 xstr filename2 ...
                ystr],'Interpreter','none');
141         legend('Original Data','Unloading Region')
142         saveas(h,sprintf('OP-Range%d.jpg',x,y))
143
144
145         %find h where load is zero for the power-law fit
146         idx_load=find(load > 25);                %load keeps ...
                fluctuating around this number near the end of indentation
147         idx_load=idx_load(end);
148         h_loadzero = depth(idx_load);
149
150         % Define OP function and fit
151         OP_fit = @(p) ((p(1)*((abs(u_depth-p(2)))).^p(3)) - (u_load)); ...
                  %u_depth [nm], u_load [uN]
152         OP_fun = @(p) (p(1)*((abs(u_depth-p(2)))).^p(3)); ...
                                  %u_depth [nm]
153         p0 = [1.56*10^-4 h_loadzero  1.5]; ...
                                                  %[aplha h m] the alpha ...
```

```
            is based in the fit, m based on Oliver-Pharr paper and h the ...
            displacement when the load is zero
154
155
156         % Curve fitting step
157         options = ...
                optimset('TolFun',1e-10,'MaxIter',1000,'MaxFunEvals',10000);
158         P_fit_OP = lsqnonlin(OP_fit,p0,[],[],options);
159
160
161         % Plotting results to check fit on own data
162         h= figure(k);
163         plot(depth,load,'o',u_depth,(OP_fun(P_fit_OP)),'+');
164         grid on; xlabel('Depth [nm]');ylabel('Load [uN]');k=k+1;
165         title(['Oliver-Pharr FIT', filename1 xstr filename2 ...
                ystr],'Interpreter','none');
166         saveas(h,sprintf('OP-Fit%d.jpg',x,y))
167
168         S_OP    = P_fit_OP(3)*(P_fit_OP(1))*(((upper_disp)) - ...
                P_fit_OP(2))^(P_fit_OP(3)-1);
169         %Unloading stiffness at upper peak disp [uN/nm]
170         A_hc    = 2*pi*R*10^9*((upper_disp)) - pi*((upper_disp))^2;      ...
                %[nm^2]
171         E_r_OP = S_OP*sqrt(pi)/(2*sqrt(A_hc))*10^12;                     ...
                % [Pa]
172         E_OP = E_r_OP *(1-(0.3)^2)*10^-6;        % [MPa] Poisson rate ...
                is 0.3
173
174
175
176        %pause
177
178 end
179
180
181
182 if E_OP<0.1                      %All the curves with a lower Elastic ...
        Modulus value have shown to be curves with a non-fit.
183             E_OP = NaN
184         else
185             E_OP=E_OP
186 end
187
188
189   E_r_OP_matrix(x,y) = abs((E_OP));
190
191    end
192 end
193
194 %% Creating Heatmaps and Figures %%
195
196
197 % Defining Elastic Modulus Matrix
198 Er_total_matrix_1 = E_r_OP_matrix';         %Translate cartilage-bone ...
        indentations from left-to-right to top-to-bottom
199 Er_total_matrix_1 = smoothdata(Er_total_matrix_1,'gaussian',3, ...
        'omitnan');  %Gaussian with NaN excluded, window size three because ...
        want a standard deviation of 0.5 (so times 6)
200 Er_total_matrix = flip(Er_total_matrix_1); ...
                                            %Activate this line if the ...
```

```
      measurements are performed from bone to cartilage instead of ...
      cartilage to bone.

% Creating Heatmaps
figure
Fig1 = figure;
heatmap(Er_total_matrix,'GridVisible','off')
title("Heatmap Elastic Modulus Values[MPa]")
caxis([0 30]);
saveas(Fig1,'EMatrix_normal.jpg');          %Save figure in folder opened

figure
Fig2 = figure;
heatmap(Er_total_matrix,'ColorScaling','log','GridVisible','off')
title('Heatmap Elastic Modulus Values - Logarithmic scale [MPa]')
caxis([0 3.5]);
saveas(Fig2,'EMatrix_log.jpg');             %Save figure in folder opened

figure
Fig3 = figure;
heatmap(Er_total_matrix,'ColorScaling','log','GridVisible','off',
'CellLabelColor','none')
title('Heatmap Elastic Modulus Distribution - Logarithmic scale [MPa]')
caxis([0 3.5]);
saveas(Fig3,'EMatrixdis_log.jpg');          %Save figure in folder opened
```